ISTerre PhD Congress

2026 edition

June, 22 & 23

Le Sappey-en-Chartreuse

IPhDC 2026 ISTerre PhD Congress

ISTerre

Institut des Sciences de la Terre

Front page photo: Laureen Maury

ISTerre PhD Students and their thesis subjects

Interesting statistics

Distribution of PhD students by thesis year:

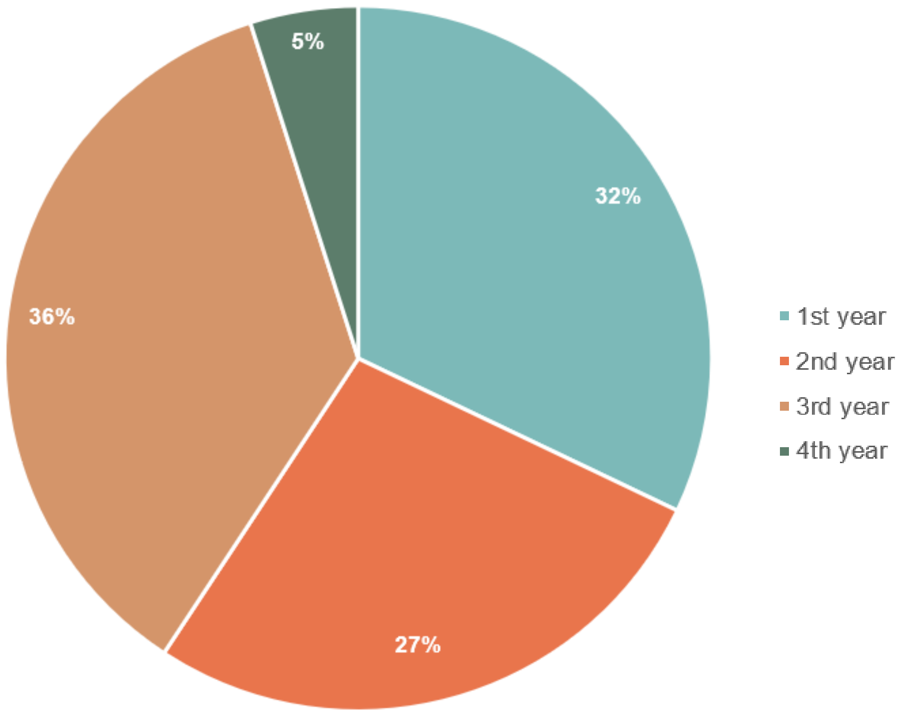

Distribution of PhD students by team:

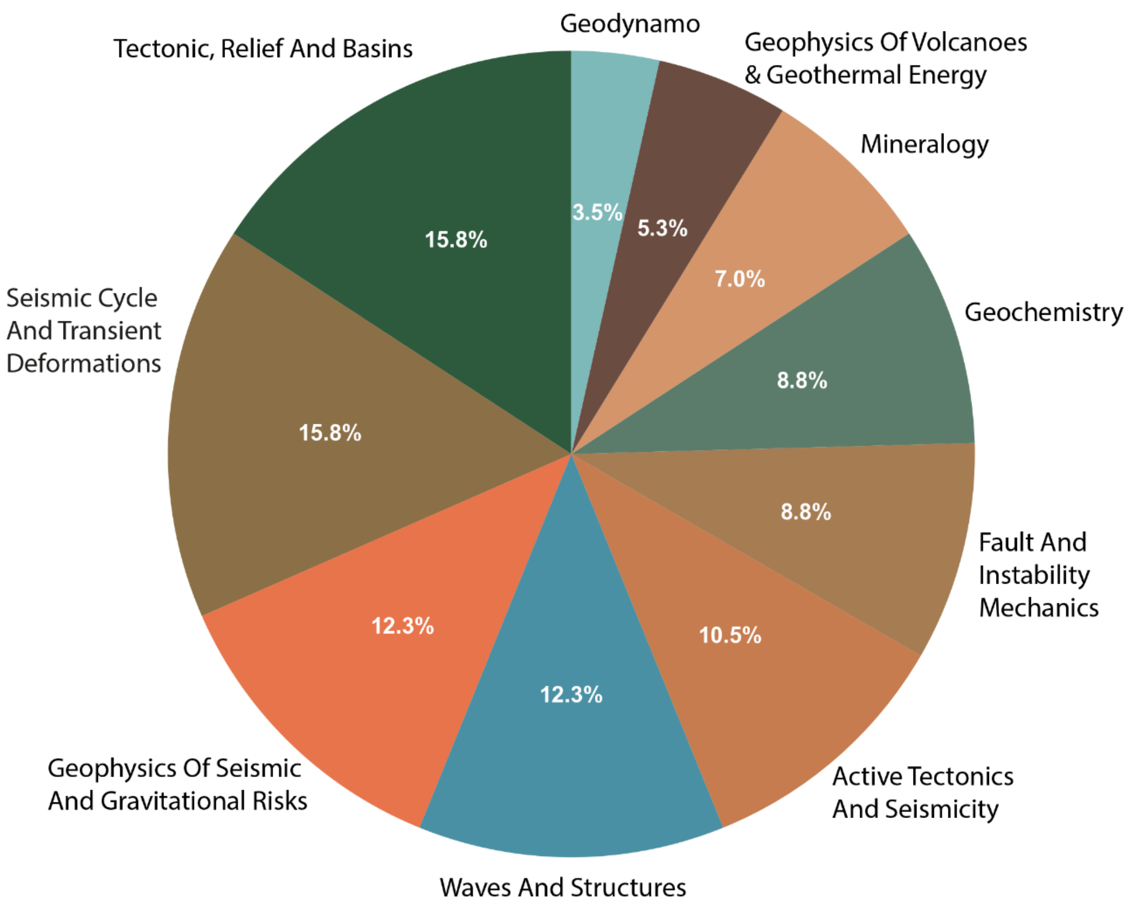

Distribution of favorite rock of students of ISTerre:

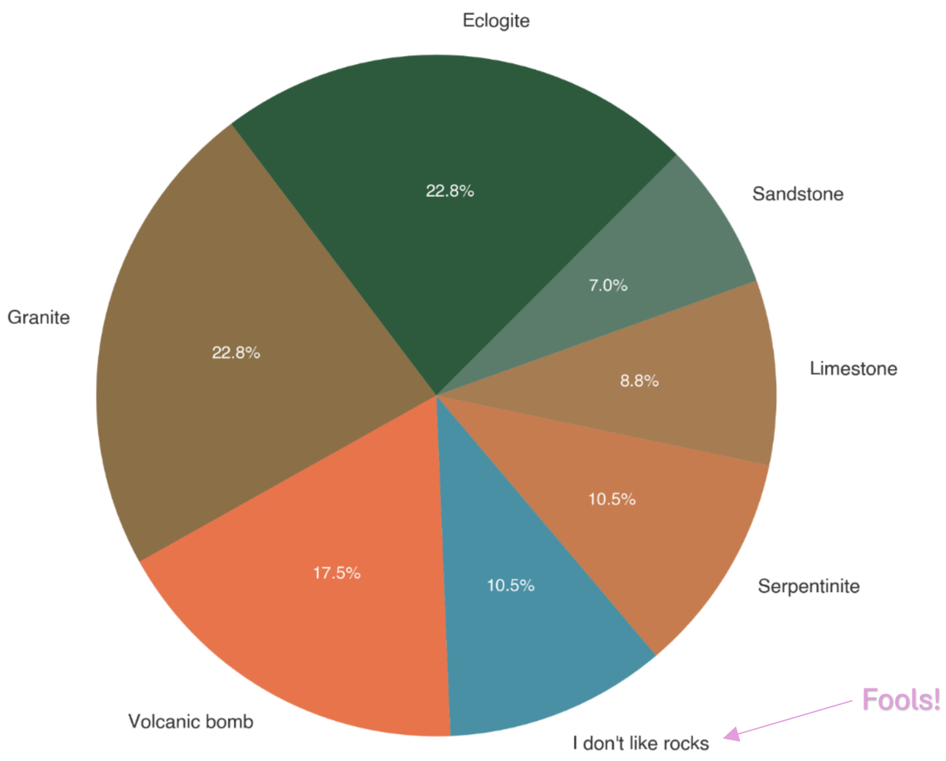

Distribution of favorite geological time periods of students of ISTerre:

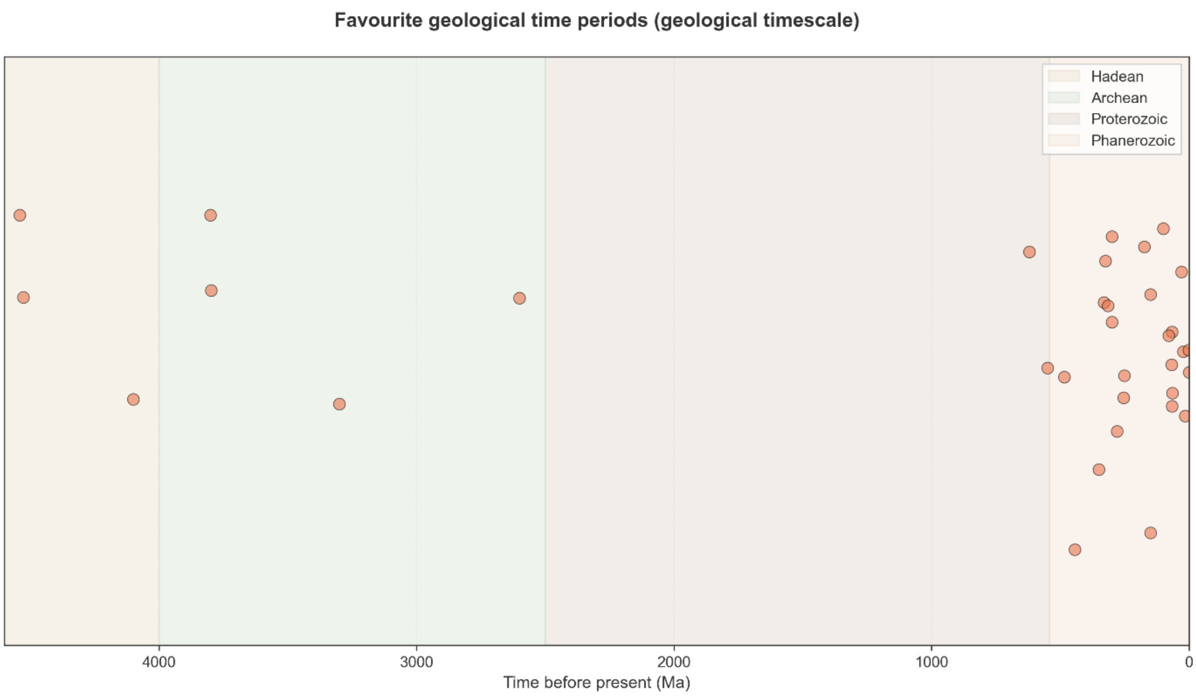

Distribution of language spoken by ISTerre students:

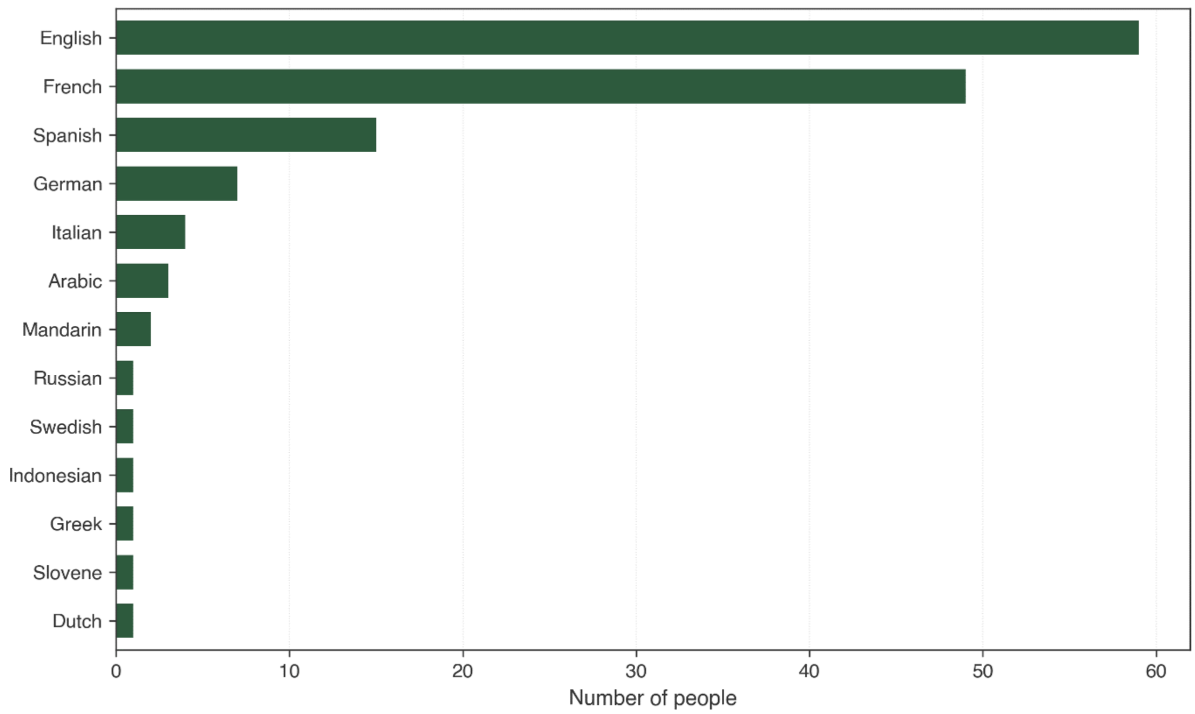

Distribution of Master subjects of ISTerre students:

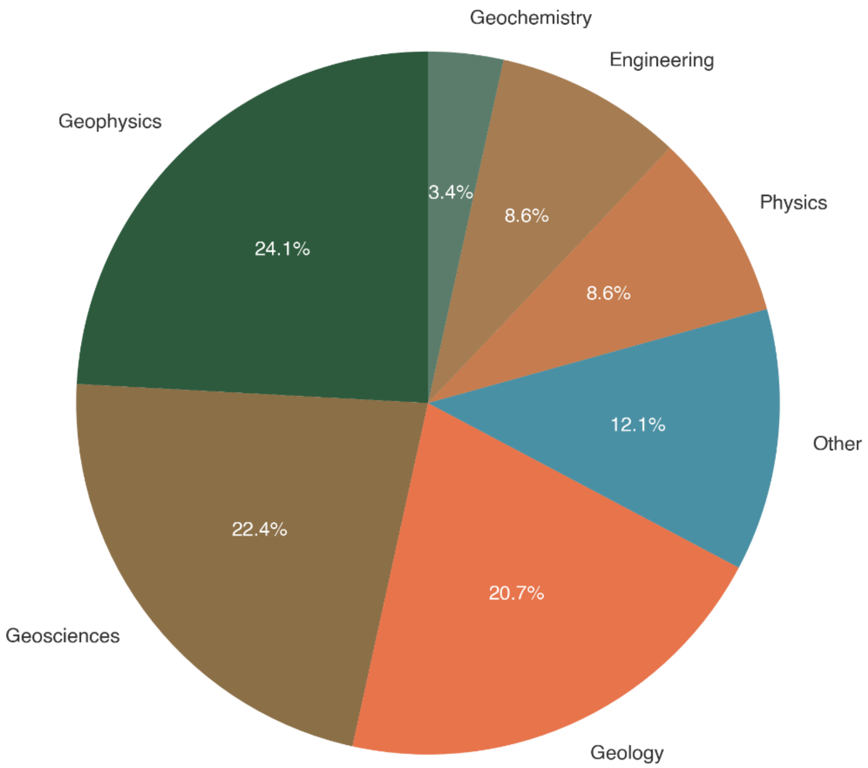

Distribution of the student population in offices as a function of time:

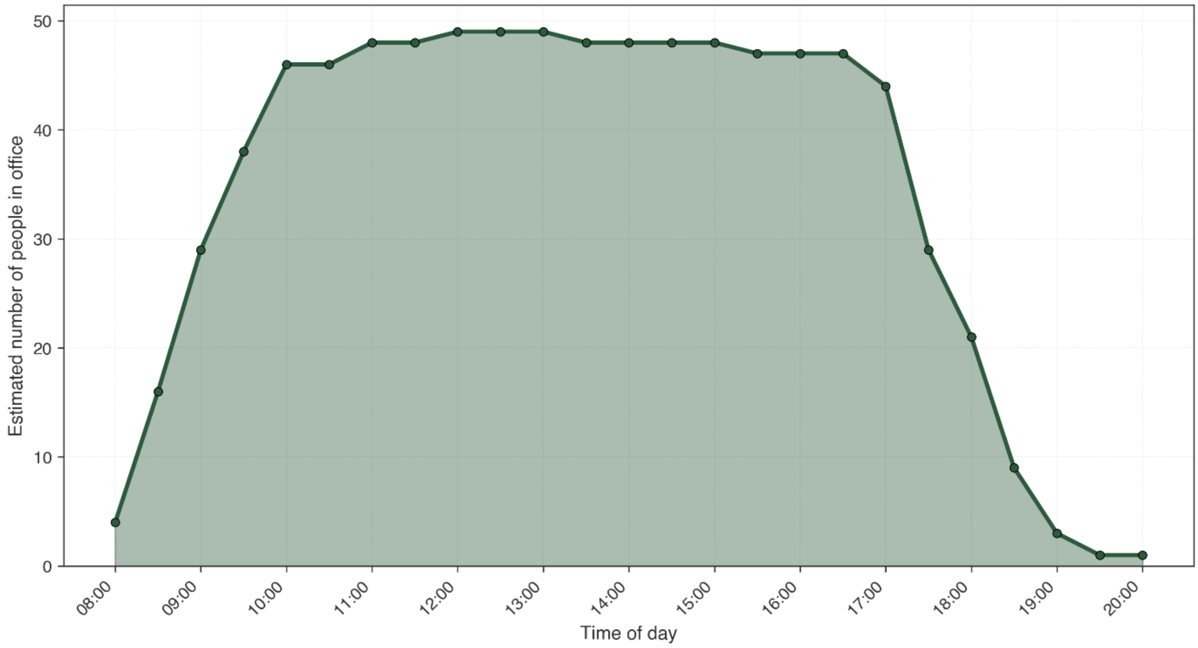

Distribution of teams by office hour:

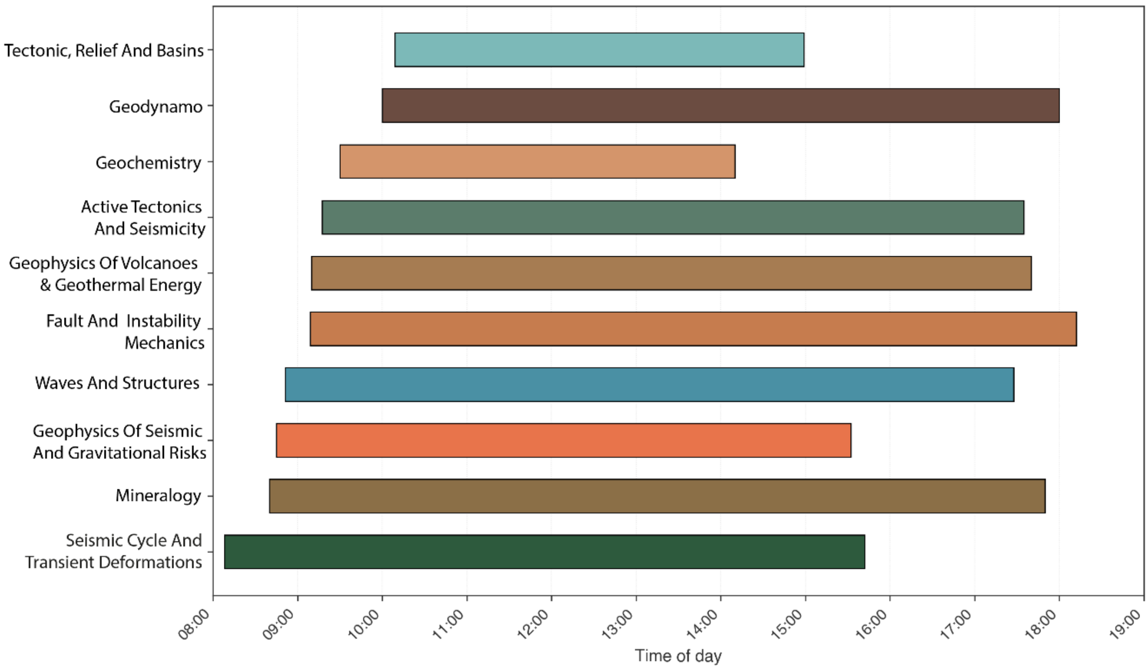

Why is TRB so bad ? It's because Anna only joins us for lunch and Yannick is a night owl.

Distribution of thesis topics by team and time spent at work:

Active Tectonics And Seismicity

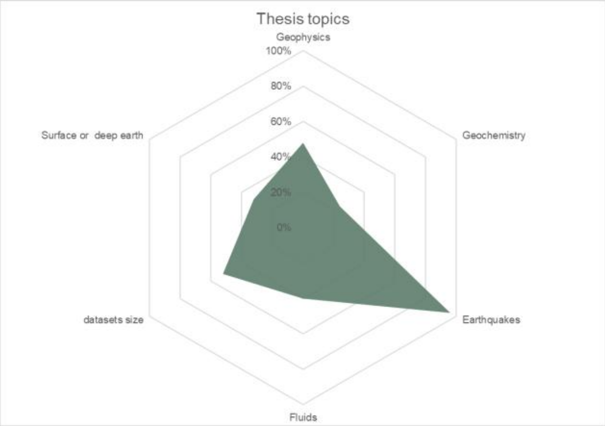

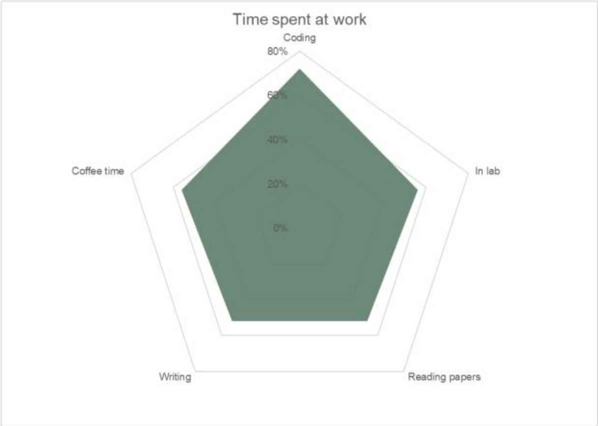

Fault And Instability Mechanics

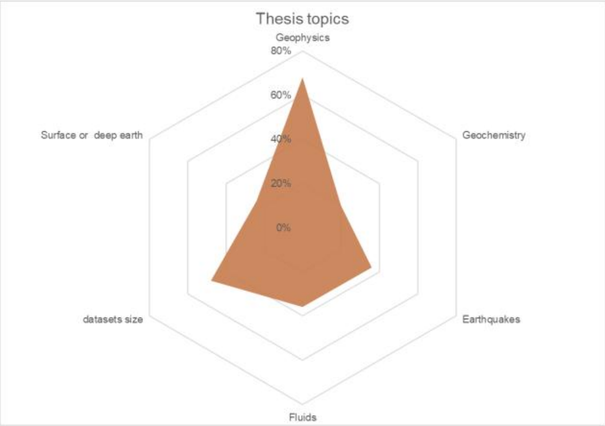

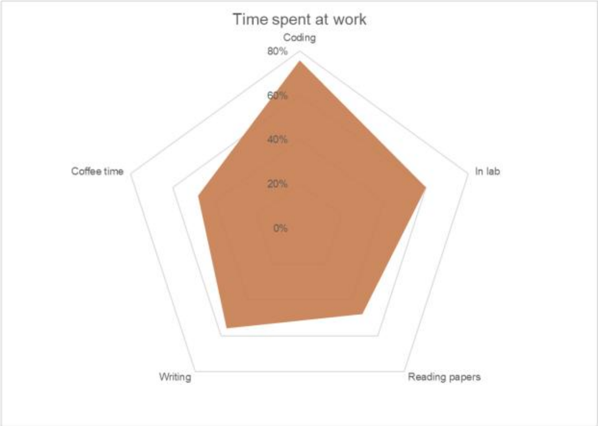

Geochemistry

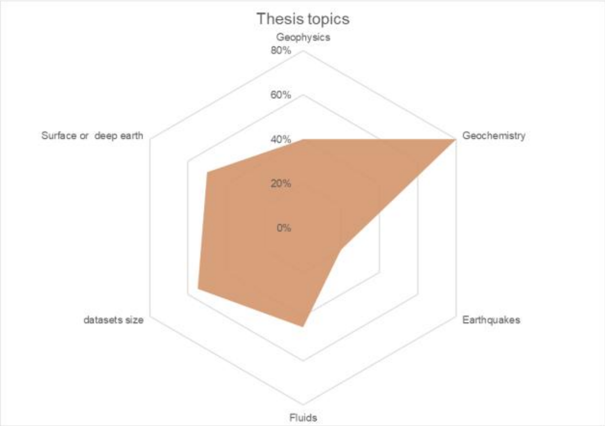

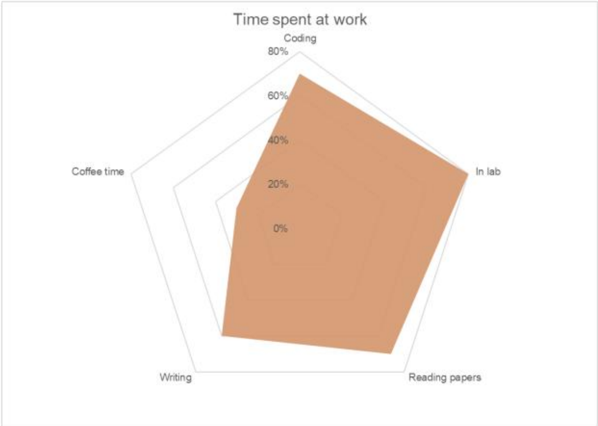

Geodynamo

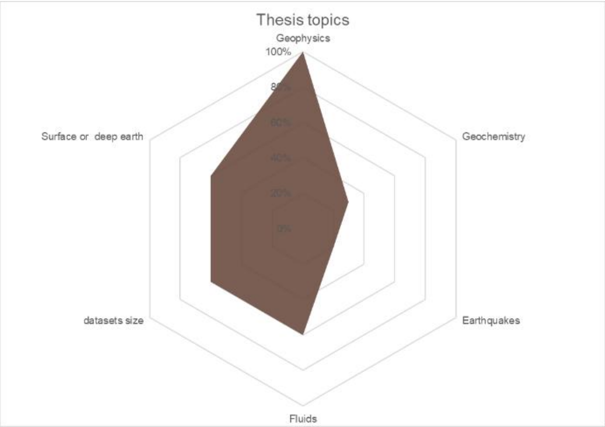

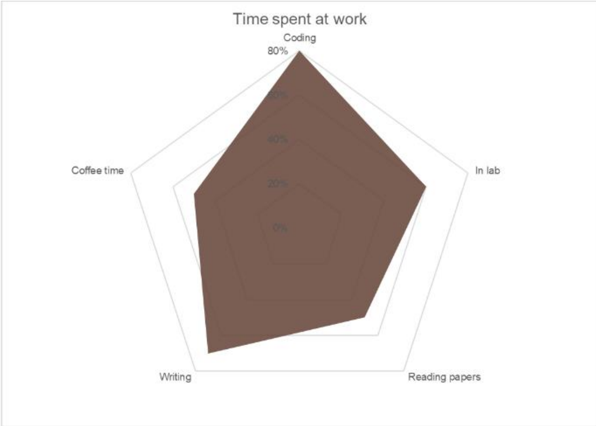

Geophysics Of Seismic And Gravitational Risks

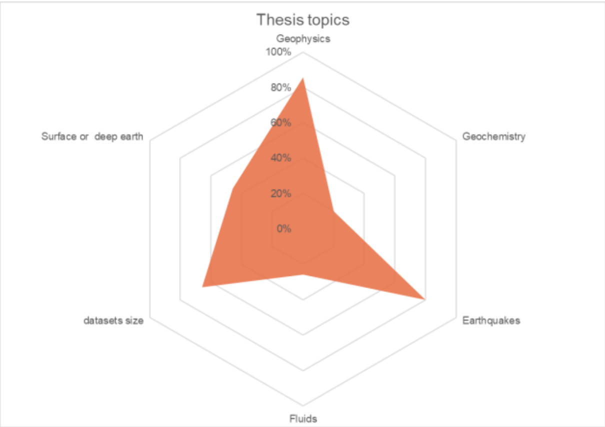

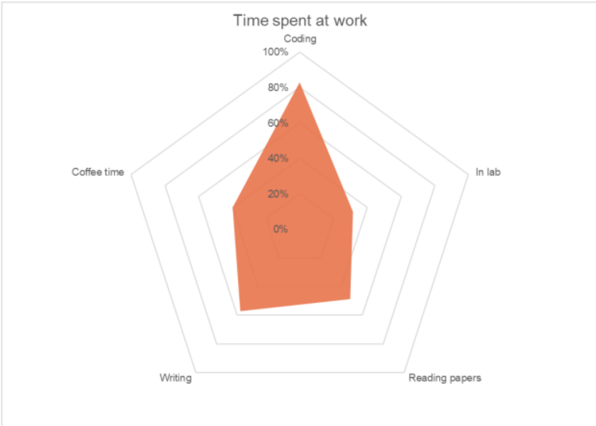

Geophysics Of Volcanoes & Geothermal Energy

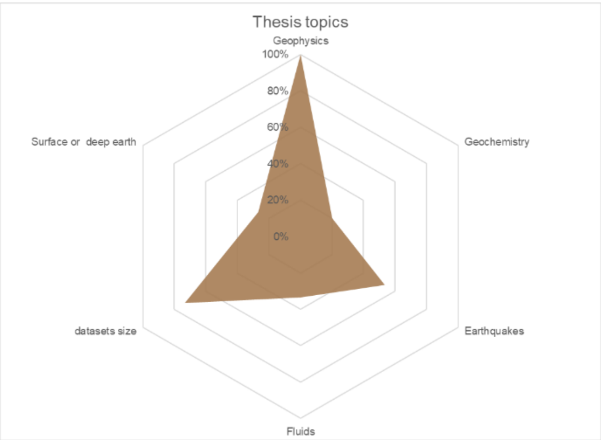

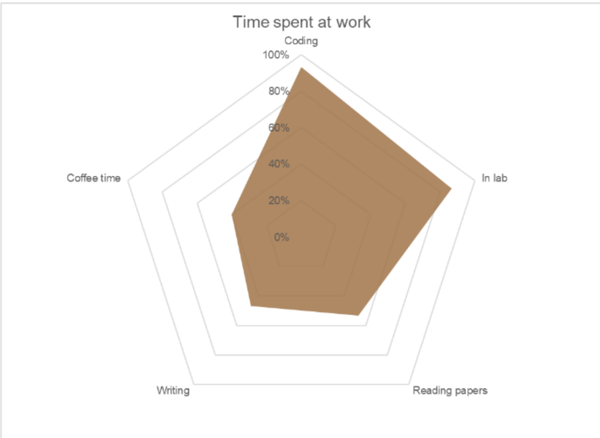

Mineralogy

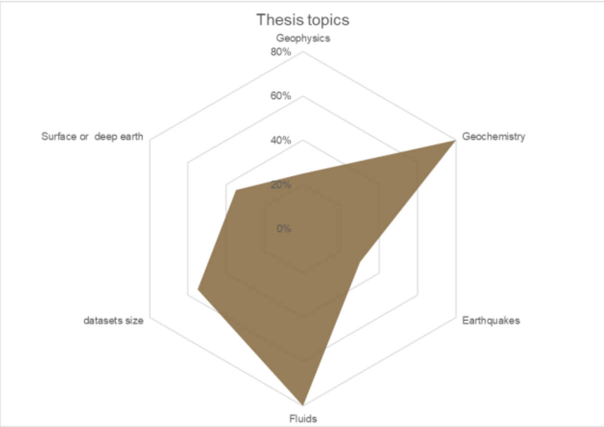

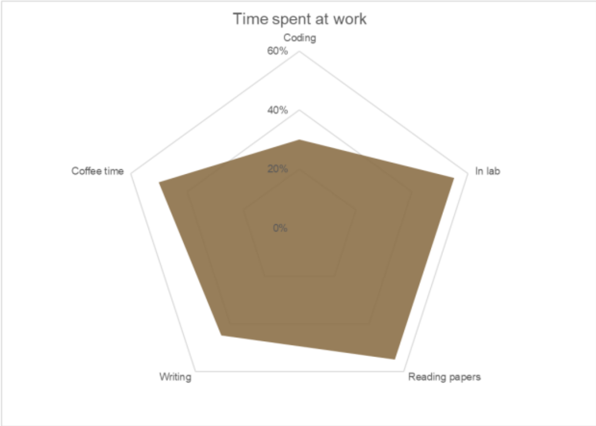

Seismic Cycle And Transient Deformations

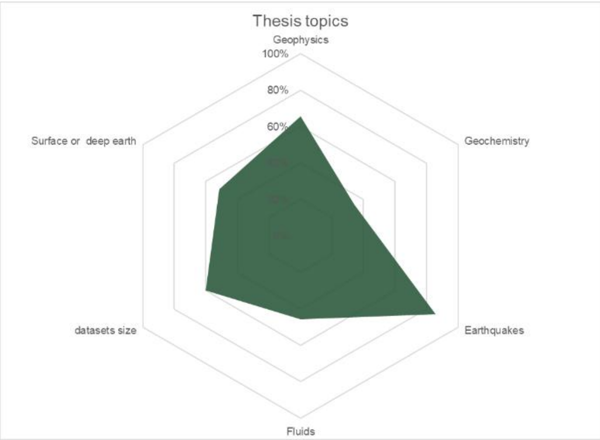

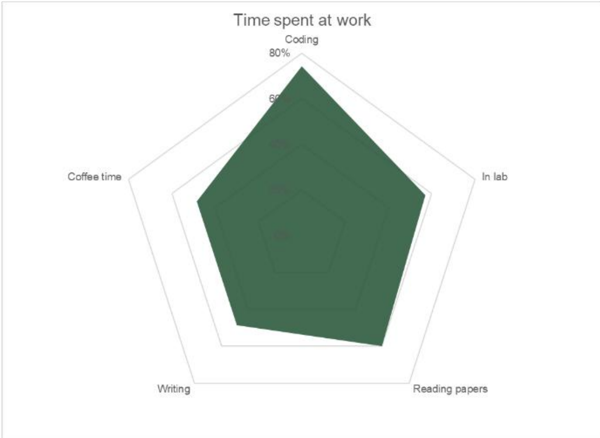

Tectonic, Relief And Basins

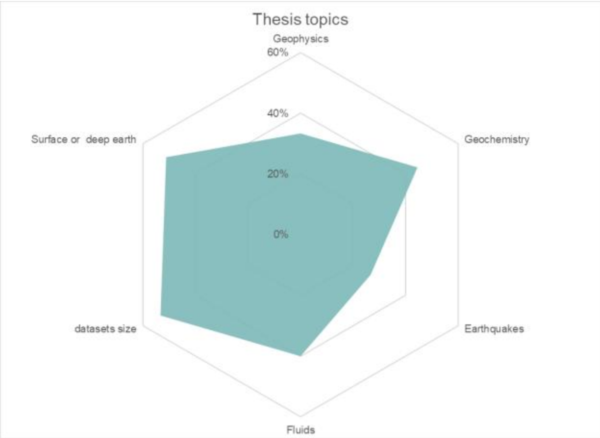

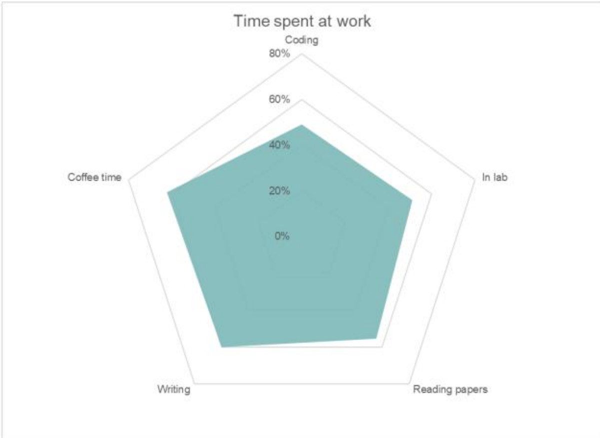

Waves And Structures

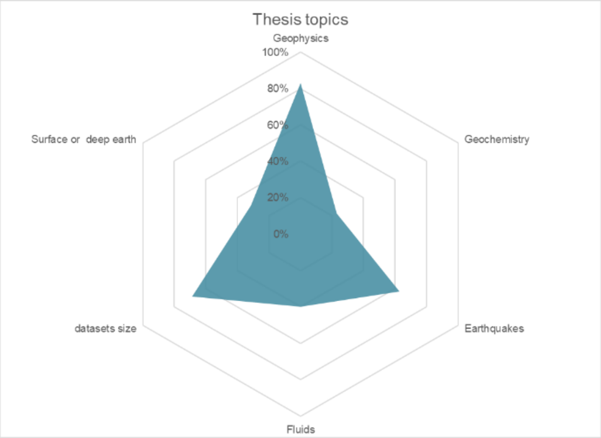

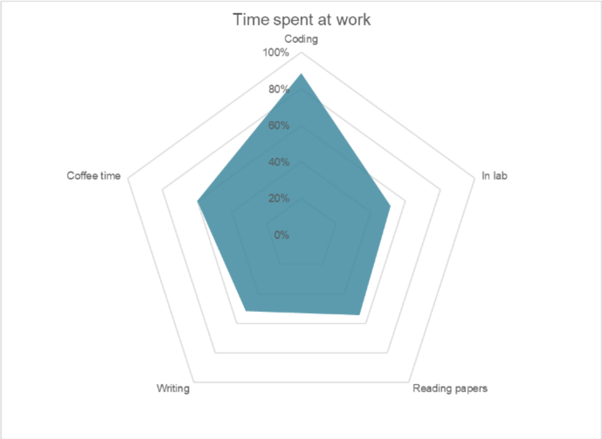

Active Tectonics And Seismicity

Alejandro Andrés-Escorihuela

Automatic detection and classification of seismic signals on an unstable rock slope in the Aiguilles Rouges massif (French Alps)

***Authors**: Alejandro Andrés-Escorihuela (ISTerre, France), Blandine Gardonio (ISTerre, France), Riccardo Vassallo (ISTerre, France), Clément Hibert (ITES, EOST, France), Joachim Rimpot (ITES, France), Laurent Metral (ISTerre, France)*

An unstable rock slope located on the western flank of the Chamonix Valley (French Alps), within the Aiguilles Rouges massif, is monitored to better understand slope processes and associated hazards. The site overlooks densely inhabited areas and critical infrastructure. A network of eight seismic sensors was deployed on and around it for over one year, complemented by extensometers.

Approximately 16000 seismic events were automatically detected from continuous recordings using a Short-Time Fourier Transform (STFT)-based detector combined with adaptive thresholding. Events were then classified using a self-supervised learning (SSL) framework adapted from Rimpot et al. (2025). Each event was converted into an image combining waveform and spectrogram information, from which feature embeddings were extracted. A two-step clustering approach, combining high-resolution K-means and hierarchical merging, was applied to group similar signals.

The classification reveals 375 clusters representing a wide diversity of sources, including anthropogenic activity, meteorological forcing, regional earthquakes, and slope-related processes such as rockfalls, rock granular flows, and microcracking. A distinct family of rockfall-related signals is identified and studied in detail. It is characterized by multi-peak waveforms and broadband frequency content, producing sharp, localized energy peaks in the spectrogram.

This automated workflow significantly reduces manual analysis effort and provides a scalable framework for long-term environmental seismic monitoring. The results demonstrate the potential of combining event-based detection and self-supervised learning to identify and characterize slope-related seismic activity in complex mountainous environments. However, some clusters remain difficult to clearly associate with a specific source, highlighting the inherent complexity of environmental seismic signals.

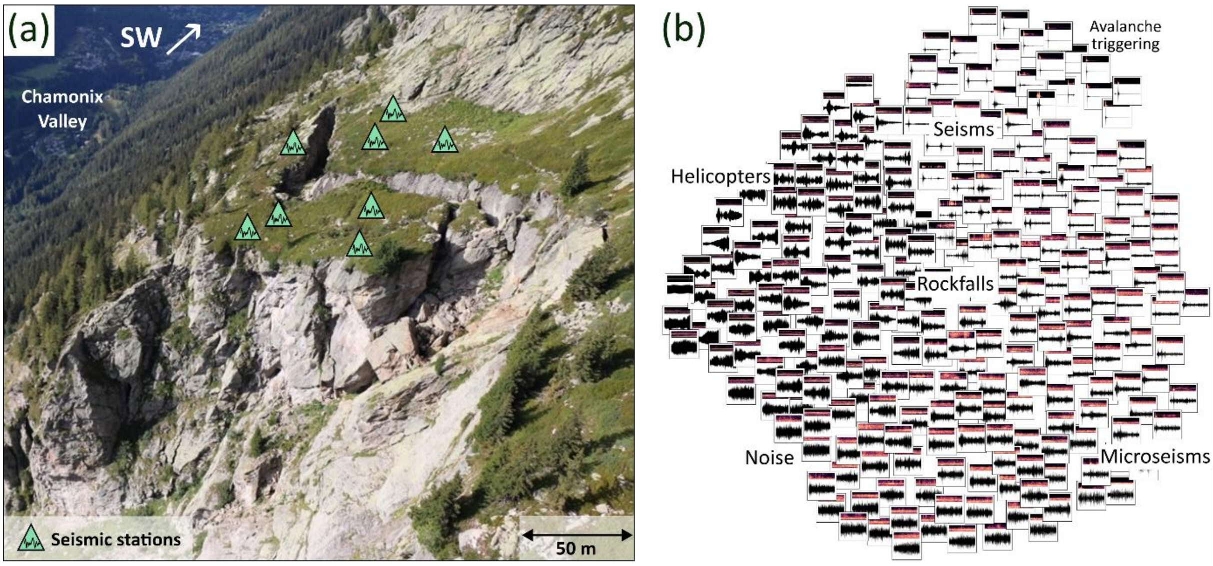

Figure: a) Drone image of the unstable rock slope showing the location of the seismic stations. b) Two-dimensional t-SNE projection of the signal embeddings, highlighting the different classes of seismic signals identified by the self-supervised learning (SSL) approach.

Eloise Granier

From Seismic Sequences to Swarms and Aftershocks: Properties of Western Alps Seismicity

***Authors**: Eloise Granier (ISTerre, France), Agnès Helmstetter (ISTerre, France), Maxime Godano (Géoazur, France), Christian Sue (ISTerre, France)*

Seismicity in the Western Alps occurs as isolated earthquakes, aftershock sequences following mainshocks, and earthquake swarms without a clear main event. While aftershocks are well documented as triggered events caused by stress redistribution, swarms display distinct behaviors including continuous activity, progressive hypocenter migration, and durations ranging from days to years. Their triggering mechanisms remain debated, with proposed explanations involving deep fluid transfer, slow slip events, or a combination of both.

This study analyzes seismic sequences containing more than 30 events from an Alpine catalog declustered using a 4D DBSCAN algorithm (latitude, longitude, depth, and time). Based on collective expert evaluation of temporal evolution, magnitude distribution, and spatial organization, sequences were classified into swarms (70%) and aftershock sequences (30%).

Using statistical analysis of more than 30 parameters combined with bootstrap resampling, we identified robust discriminators between the two sequence types. Aftershock sequences exhibit larger mainshock magnitudes (median 2.7 vs 2.2), clearer Bath's law signatures (ΔM = 0.75 vs 0.57), and faster temporal decay consistent with Omori's law ($p \approx 1$ vs $p \approx 0.5$). In contrast, swarms show larger spatial extent (1.6 vs 1.3 km), higher cluster-to-rupture ratios (12 vs 6), longer durations (816 vs 468 h), and higher pre-to-post mainshock event ratios (1.1 vs 0.4). The Gutenberg–Richter transition magnitude Mt is lower for swarms (2.5 vs 3.7), consistent with fluid-driven triggering models.

Focal mechanism analysis reveals a predominance of normal faulting in swarms relative to aftershock sequences (34.6% vs 24.7%), particularly within extensional domains of the Briançonnais and Piedmont arcs. Together, these results establish a statistical and physical framework for distinguishing swarms from aftershock sequences in the Western Alps.

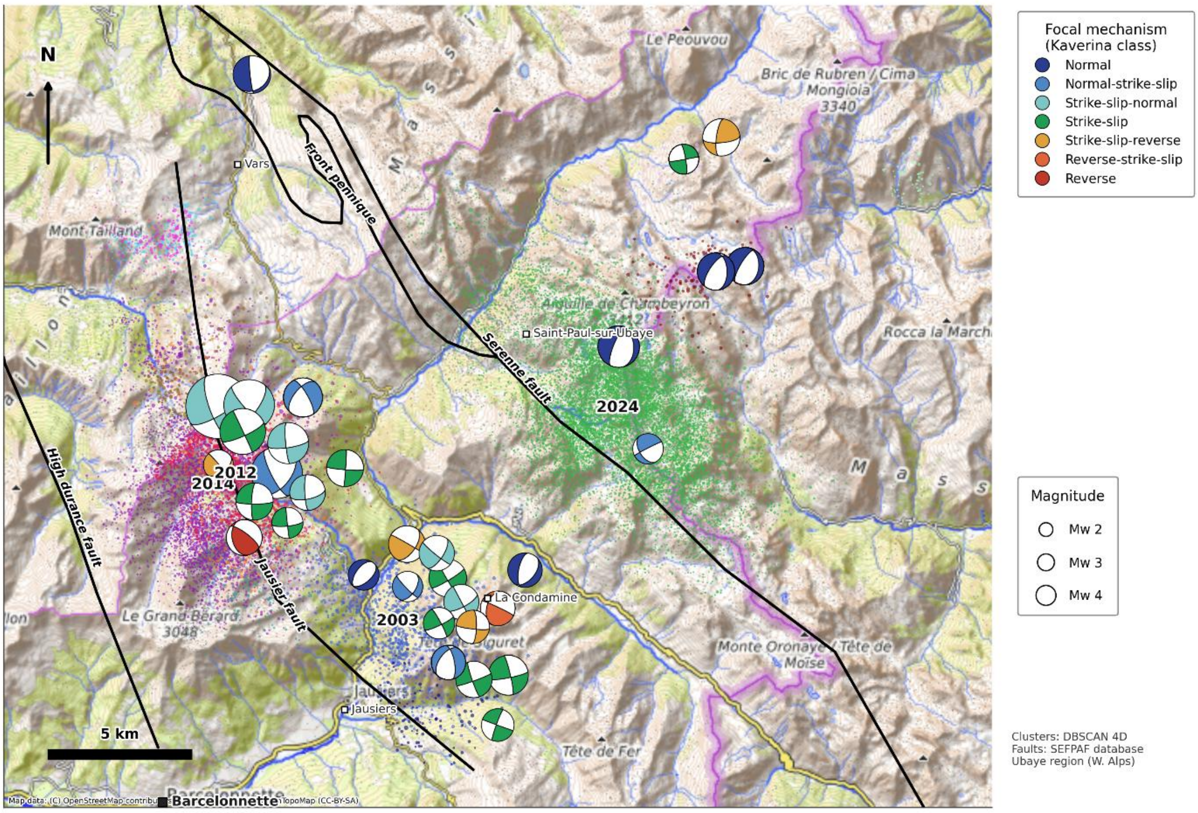

Figure: Example of seismic sequences identified in the Ubaye region (Western Alps). Focal mechanism solutions are represented as beach ball diagrams, classified following the Kaverina et al. (1996) scheme. Four seismic sequences are shown as illustrative examples of the clusters identified by the 4D DBSCAN algorithm applied to the Alpine catalog. The 2003 (Barcelonnette – La Condamine), 2012, and 2014 (Jausiers area) sequences were classified as swarms, characterized by diffuse spatial organization, absence of a clear mainshock, and mixed faulting regimes. The 2024 sequence (Saint-Paul-sur-Ubaye, Serenne fault) illustrates a more recent cluster. The dominance of strike-slip mechanisms in the Jausiers area and normal faulting near the Serenne fault is consistent with the extensional and transcurrent stress regime documented across the Western Alps. Major faults are drawn as thick black lines and are taken from the SEFPAF database (Mowbray et al., in prep.).

Victoria Mowbray

Assessing probabilistic seismic hazard including fault models in South-East France

Authors: *Victoria Mowbray (ISTerre, France), Céline Beauval (ISTerre, France), Christian Sue (ISTerre, France), Marguerite Mathey (ASNR, France), Anne Lemoine (BRGM, France), Stéphane Baize (ASNR, France)*

Attributing seismicity rates to specific faults is a challenging task in regions of low to moderate seismicity, such is the case of South-East France, given the diffuse spatial distribution of seismicity, limited temporal coverage of earthquake catalogs, and incomplete knowledge on fault geometry and activity. Consequently, fault-based models are not yet extensively explored in these cases, despite the rapid advance in geophysical data acquisition, notably in the Alpine chain and foreland.

In this study, we evaluate the impact of fault-based seismic source modelling on hazard estimates for South-East France. This model is based on idealized geometries and geodetic slip rates, given the uncomplete geological fault displacement evidences for the region. Slip rates are inferred from a dense GNSS network implementing simplistic across-fault velocity transects, assuming that a fraction of the observed offset displacement rate may be aseismic deformation. To account for off-fault seismicity, we combine the fault model with a smoothed seismicity model. Recurrence rates resulting from different combinations of these two models are analyzed for the region.

Uncertainties are explored to understand at which spectral period and return period the fault model starts contributing to the hazard. For the smoothed seismicity model uncertainties explored include the choice of declustering method, catalog completeness estimation and spatial smoothing parametrization. For the fault model, we account for uncertainties on fault trace and segmentation, slip rate ranges, the fraction of deformation to consider aseismic, as well as the recurrence model to implement and the minimum magnitude accounted for on the fault.

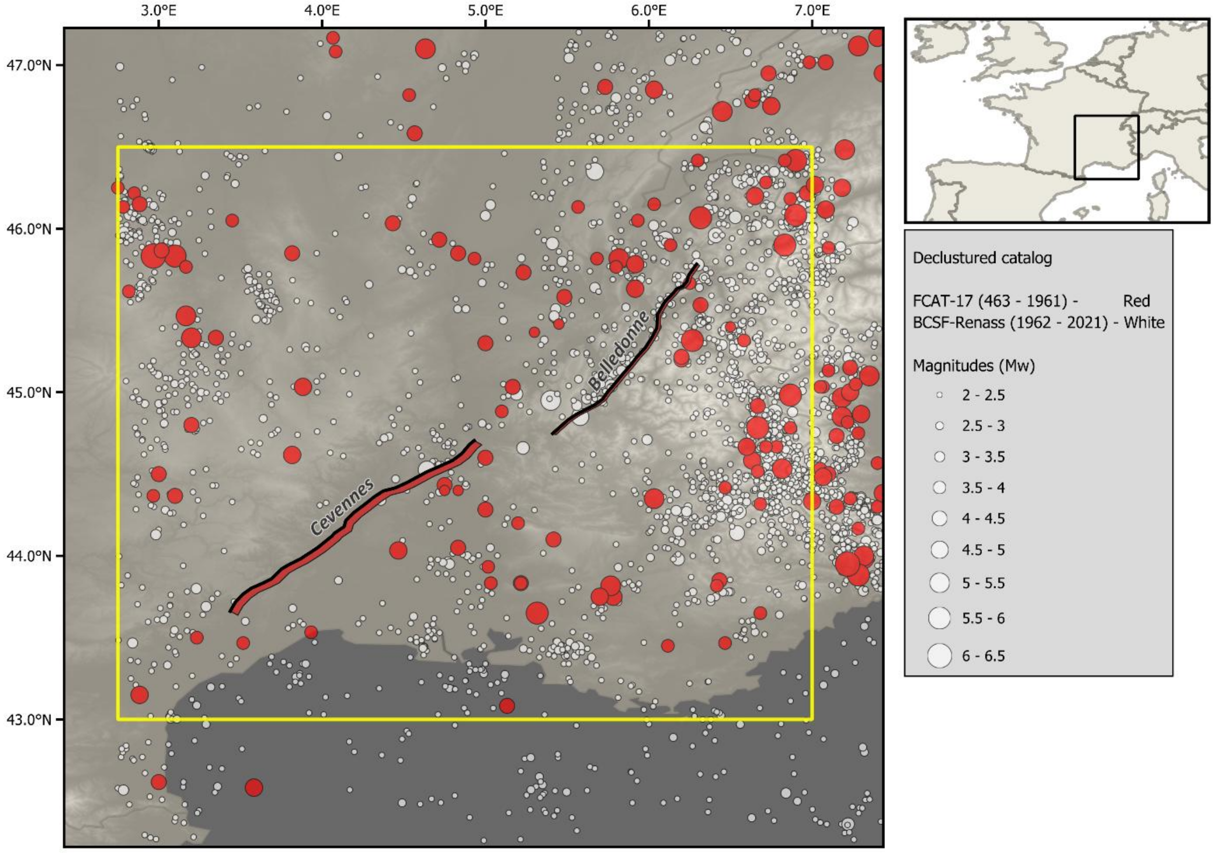

Figure: Historical and instrumental seismic catalogs for South East France, and fault traces and fault planes included in the fault model for seismic hazard assessment.

Charlotte Petrikowski

New geophysical insights into current deformation of the Jura Arc: Implications for groundwater resources

***Authors**: Charlotte Petrikowski (ISTerre, France), Andrea Walpersdorf (ISTerre, France), Julie Albaric (Chrono-Environnement, France), Christian Sue (ISTerre, France)*

The Jura is a low-strain active orogenic arc in the frontal part of the Alps, which has produced some of the strongest recent earthquakes in France (ML4.8 (2004) in Besançon, France; ML4.1 (2021) and ML4.4 (2023) in Mulhouse, Switzerland). To this day, the controlling processes remain under debate. We develop a multidisciplinary approach to study the linkage between crustal deformation, seismicity, tectonics and hydrogeological variations - thereby contributing to a better characterization of seismic hazard but also of water resources in the Jura region.

Here, I present the first results from a seismological study targeted to the northern Jura front, providing the first analysis of data from a local network of 33 stations processed through a machine-learning-based approach. The workflow of automated phase detection (PhaseNet and EQTransformer) and phase association (PyOcto and REAL) allows for the detection of previously unrecognized seismic events.

Over the period 2018-2021, this approach resulted in 1181 seismic event detections. All of the automated picks were manually reviewed and refined before classification, which revealed that roughly 70% of all automatic detections corresponded to quarry blasts or false detections. Once filtered from these detections, I characterized a total of 362 earthquakes with magnitudes ranging from ML−0.6 to ML2.8. Among them, 212 earthquakes are listed in the RENASS catalog but 150 were previously undetected. Further comparison with catalog data shows that the magnitude of completeness was locally improved from Mc1.2 (RENASS) to Mc0.6 (new study), ultimately allowing for an improved understanding of seismic activity and specifically microseismicity in this region.

In addition to the seismological analysis, this project will include a geodetic study based on an europe-wide network of roughly 90 permanent GNSS stations centered on the Jura, completed by the GPS-JURA permanent network (running since 2013) and a dense semi-permanent GNSS network (recording since 2000) in the South Jura. The integration of geodetic and seismological observations will provide new insights into the style, amplitude and spatial distribution of active deformation, with special focus on vertical movements, and will allow for an investigation of the relationship between crustal deformation and groundwater dynamics in the Jura.

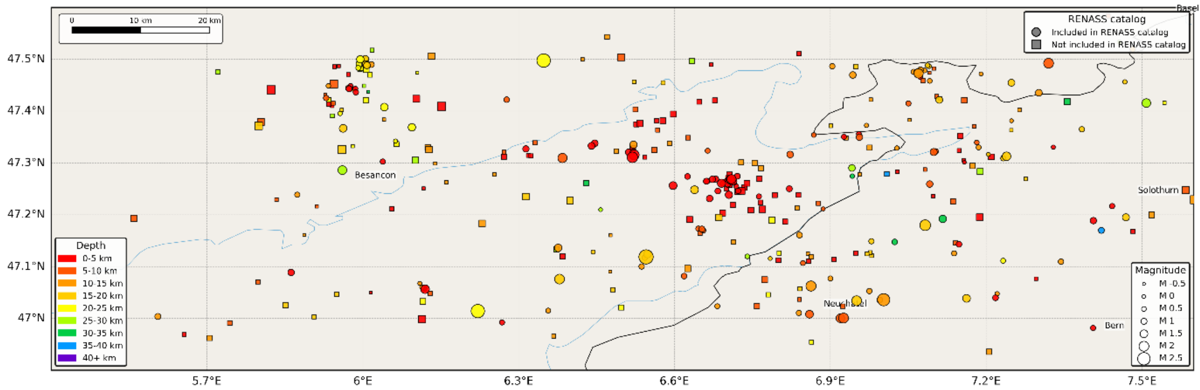

Figure: Earthquakes within the studied region in the Jura between 01/01/2018 - 29/11/2021. Earthquake detections are based on the RENASS catalog (https://renass.unistra.fr/fr/zones/), refined through manual pick adjustments (circle signatures) and complemented by additional detections using a machine-learning based approach (square signatures).

Juliette Raabe

Evaluation of tropospheric corrections for InSAR processing over the Western Alps.

Authors: *Juliette Raabe (ISTerre, France; Centre national d'études spatiales (CNES), France), Marie-Pierre Doin (ISTerre, France), Andrea Walpersdorf (ISTerre, France), Christian Sue (ISTerre, France)*

Using the InSAR-related NSBAS chain processing (Doin et. al 2011, Thollard et. al. 2021) and the 2016-2025 Sentinel-1 radar data, we aim at obtaining a velocity map over the European Alps with a target uncertainty of a mm/yr. Mountainous areas present inherent challenges for InSAR study such as geometric distortions, decorrelation due to vegetation or snow cover changes. To achieve millimeter-per-year precision, we must consider the atmospheric contribution (especially troposphere) since it has spatial and temporal variations that does not cancel when forming interferograms. Tropospheric variations are still a major factor limiting the accuracy of InSAR measurements: a change of 20% of relative humidity between two acquisitions is responsible for a 10 cm error in deformation interpretation (Zebker and Rosen, 1997). Moreover, if the differential troposphere delay between two considered dates goes beyond 5.6 cm, troposphere can be the source of unwrapping errors during processing.

Therefore, we explore the different possibilities available to mitigate the tropospheric contribution before unwrapping but also to remove its contribution from timeseries and avoid as much misinterpretation as possible in deformation analysis.

Tropospheric impact has been widely studied and several methods have been proposed to mitigate tropospheric noise. Among them, we focus on two main approaches: mitigation by trying to separate stochastic noise from signal (for example, exploiting empirical relationship between elevation and troposphere) and by the usage of external data. For the latter, two main sources of data are available. We can benefit from data from Global Atmosphere Models (GAM) (particularly the ERA5 and CERRA reanalyses of the ECMWF) or from Zenithal Troposphere Delays (ZTD) estimated during the GNSS processing.

In mountainous areas such as the Alps, assess the ability of the these three methods to correct tropospheric delays is crucial as their application is limited by the complexity of orogenic features and associated atmospheric flows.

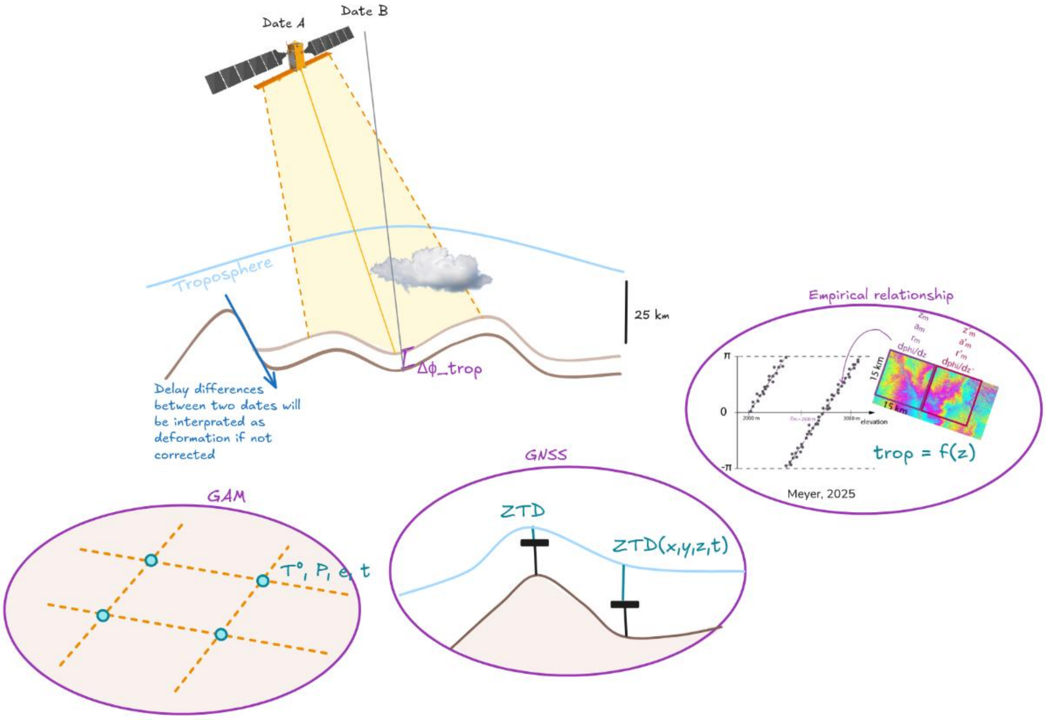

Figure: The 3 studied methods to compensate the tropospheric delay in interferograms' pairs

Aguilera Cortés Ricardo

Dendroseismological constraints on recent activity of the Magallanes-Fagnano Fault (Eastern Tierra del Fuego, Chile)

***Authors**: Ricardo Aguilera-Cortés (ISTerre, France), Laurent Astrade (EDYTEM, France), Joseph Martinod (ISTerre, France), Riccardo Vassallo (ISTerre, France), Christian Sue (ISTerre, France)*

We applied dendroseismological analysis to lenga beech trees (Nothofagus pumilio) growing on or near scarps of the Magallanes-Fagnano Fault in Tierra del Fuego, Chile, to evaluate whether tree-ring disturbances recorded the historical 1879 and 1949 major earthquakes. Two sectors located ~60 km apart were analyzed: western Lake Fagnano and Almirantazgo Gulf (Capo Toto). We combined anatomical observations from trunk sections with percent growth change (PGC) analysis from ring-width series, and we compare with reference trees that record the regional climatic signal.

The strongest dendroseismological evidence is provided by tree-ring anomalies observed in samples from western Lake Fagnano, where trees growing on or close to mapped fault scarps show eccentric growth, abrupt growth drops, and asymmetric ring development around the timing of the 1949 earthquake (Figure 1). These anomalies are result from tree tilting, growth compensation, and possible root or slope disturbance following coseismic deformation or strong shaking. PGC analysis supports this interpretation: the clearest 1949 signal is observed at Lake Fagnano sites located directly on an active scarp of the Magallanes-Fagnano Fault, where several trees record post-1949 growth increase. At Capo Toto, the 1949 signal is weak or absent in both anatomical observations and averaged PGC results.

For both sites, tree disturbances for 1879 remain unclear. Although at Capo Toto few trees show positive growth anomalies close to 1879, both sites lack of enough tree samples older than 1879 that may contribute a more conclusive result. Our results support the interpretation that the 1949 surface rupture propagated at least to western Lake Fagnano but probably did not continue farther west into the Almirantazgo Gulf. Conversely, the 1879 rupture may have involved a broader western segment of the fault. This study highlights the value of combining anatomical tree-ring evidence with PGC analysis to constrain historical ruptures in forested strike-slip fault zones.

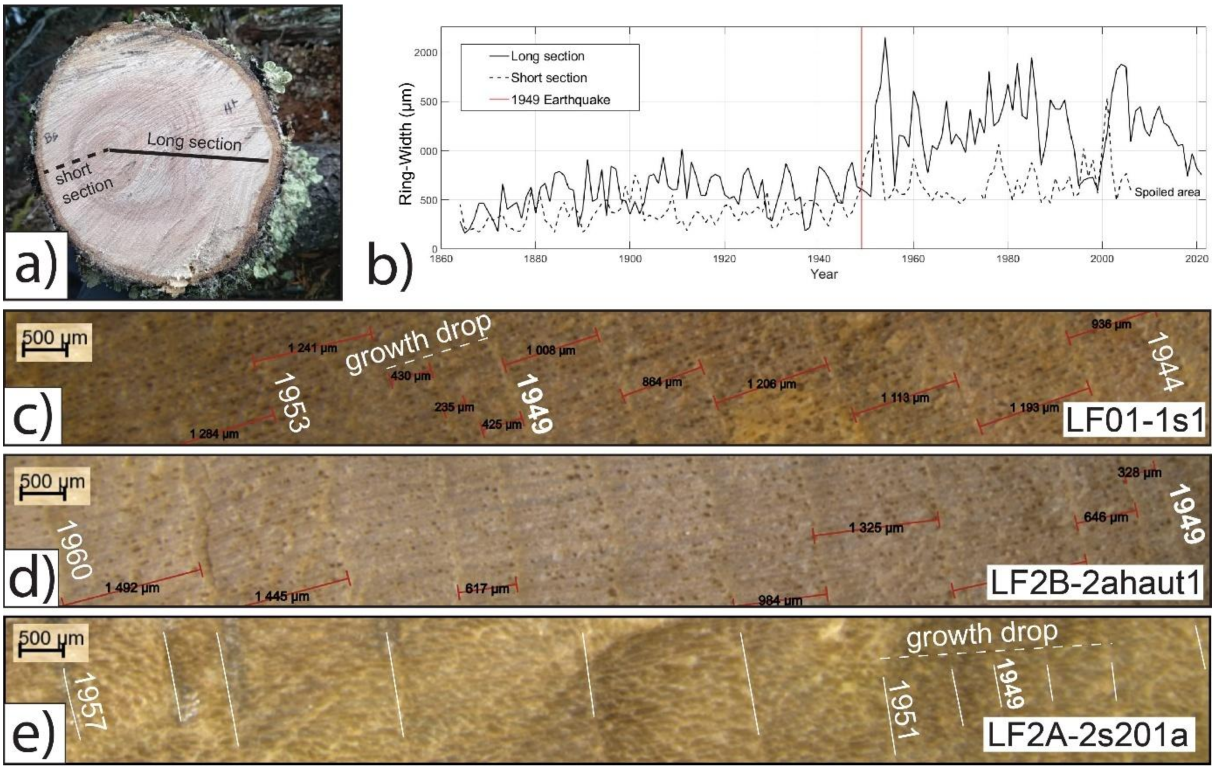

Figure: Tree growth anomalies locally observed in few samples. (a) Cut-section of the sample LF2A-2s201a showing the eccentric growth with the center displaced, indicating the long and short section measured. (b) Ring-width of long and short sections from the sample LF2A-2s201a. (c) Microscope photography of the sample LF01-1s1 evidencing a short abrupt growth suppression after 1949 (dotted white line). (d) Microscope photography of the sample LF2B-2ahaut1 showing a very short period of growth suppression of two rings after 1949. (e) Microscope photography of the sample LF2B-2s201a evidencing a short abrupt growth suppression of four rings around 1949 (dotted white line).

Amir Saker

Numerical Modeling of Piping Erosion via the Hole Erosion Test (HET)

***Authors**: Amir Sakera (ISTerre, France), François Nicot (ISTerre, France), Antoine Wautier (INRAE, France)*

Many hydraulic structures, such as dams or dikes, are made of porous geomaterials. Consequently, they are subjected to internal flows that may lead to the development of internal erosion, which affects structural stability and can potentially provoke failure. Internal erosion mechanisms are divided into four classes: backward erosion, contact erosion, suffusion, and piping erosion. The latter is arguably the most dangerous scenario, as it can lead to the complete failure of the structure within a few hours, leaving very limited possibilities to control the process once initiated. Experimentally, the Hole Erosion Test (HET) is used to assess the sensitivity of a material to piping erosion by quantifying both the critical shear stress and the erosion rate coefficient.

The main objective of this PhD project is to numerically model the Hole Erosion Test (HET) using a discrete element method (DEM) approach to understand the link between micromechanical properties and piping erosion dynamics. Through these numerical experiments, the macroscale mechanical properties of geomaterials and the erosion law will be derived as emerging properties of the micromechanical parameters. The DEM parameters (particle size distribution, contact laws, and local arrangement of particles) will first be calibrated based on experimental mechanical tests (e.g., triaxial tests), before running coupled fluid-grain simulations to predict laboratory HET results. These standard tests will serve as benchmarks to assess the predictability of the DEM model. Ultimately, this approach will relate the macroscopic erosion law to micromechanical parameters, which are themselves connected to the mechanical properties of the tested materials. Building this bridge between physico-mechanical and erosive properties is the main scientific challenge of this PhD project, paving the way for safer dams and dikes in the future.

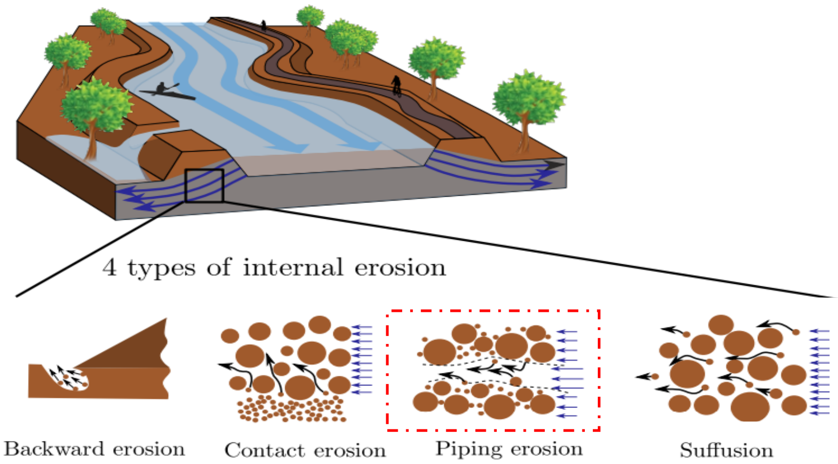

Figure: The 4 types of internal erosion (A. Wautier 2018)

Fault And Instability Mechanics

Anne-Sarah Amblard

Adding a granular transition in a visco-elasto-brittle model

***Authors**: Anne-sarah Amblard (ISTerre, France), Véronique Dansereau (ISTerre – IGE, France), Jérôme Weiss (ISTerre, France)*

Sea ice is a complex material that exhibits various mechanical behaviors depending on its level of fragmentation. In compact and largely intact regions, it behaves as a cohesive, damageable solid that is reasonably well represented by continuum visco-elasto-brittle models (Dansereau et al., 2016; Rampal et al., 2019; Ólason et al., 2022). In contrast, where it becomes highly fractured but dense - such as within large linear kinematic features - it behaves as a frictional, decohesive granular media, a regime that is challenging to describe within a purely continuum framework. Here we do not consider marginal ice zone (MIZ) where the ice is higly fractured and looser. To better capture the transition between the two regimes in such a framework, we enhance an existing visco-elasto-brittle model with additional physical ingredients : a damage-dependence of the Poisson's ratio, a damage-dependence of the cohesion, a friction criterion, and lateral healing. We present results of a simple biaxial compression test in which each of these ingredients is included or not, and demonstrate the strong interaction between their effect, highlighting the necessity of introducing them simultaneously to accurately reproduce the intermittency and localization of sea ice deformation.

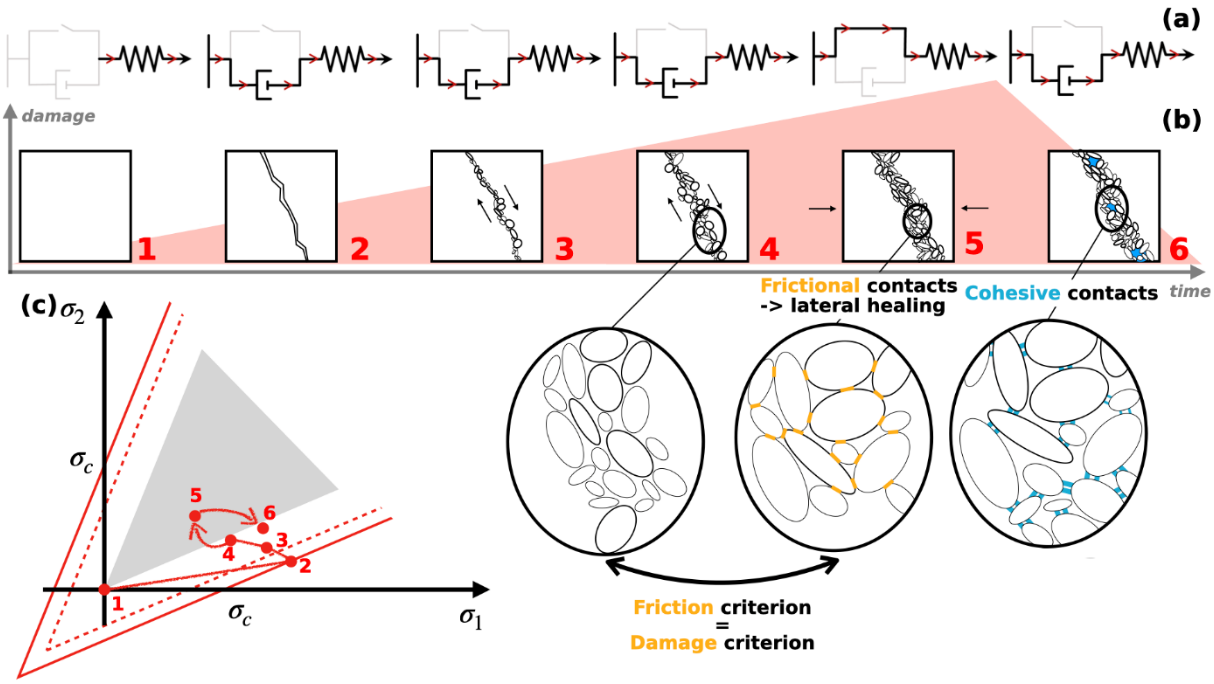

Figure: Illustration of the damage over a model grid cell from different points of view. (a) and (b), from left to right the element becomes damaged and eventually heals. (a) 1D scheme of an element which becomes damaged and heals. (b) Corresponding damage state of a 2D sea ice mesh, with representation of friction and cohesion. (c) Evolution of the stress state of the mesh in the principal stresses plane.

Laetitia Drumare

A phase-field modeling approach to sea-ice fracturing

Authors*: Laetitia Drumare (ISTerre, France & Njord Centre, Norway), Vidar Skogvoll (Njord Centre, Norway), François Renard (ISTerre, France & Njord Centre, Norway), Luiza Angheluta (Njord Centre, Norway), Véronique Dansereau (ISTerre, France & IGE, France)*

The thin ice that covers the polar oceans is a complex geomaterial that is constantly stressed and fractured by winds and ocean currents. In the central Arctic, this forcing produces deformations in the form of shear bands, within which individual ice plates detach, locally generating a granular medium. Capturing this transition from a continuous to a granular sea-ice cover has implications for the adequate representation of the mechanical and dynamical behavior of sea-ice in regional and large-scale models used for operational and climate prediction purposes. Our work investigates the feasibility of a phase-field approach to capture this granularization processes and focuses on fracture propagation in the material. The model combines a double-well free-energy formulation with an overdamped displacement response. The governing equations are solved using a spectral method in Fourier space. The implementation accounts for body forces, representative of the main forcings on sea-ice, and remains computationally tractable despite the highly nonlinear character of the double-well energy formulation. We first validate the framework against a benchmark problem: the opening of an inclusion embedded into an elastic matrix under tensile loading. Then, additional simple shear configurations are investigated: an inclusion solicited under plane shear and a cylindrical Couette experiment, for which the analytical solution of the displacement field is known. The resulting fracture patterns and displacement fields demonstrate that our phase-field framework captures key features of tensile and shear fracture propagation, including the linear scaling between crack speed and applied load predicted by the Griffith's theory.

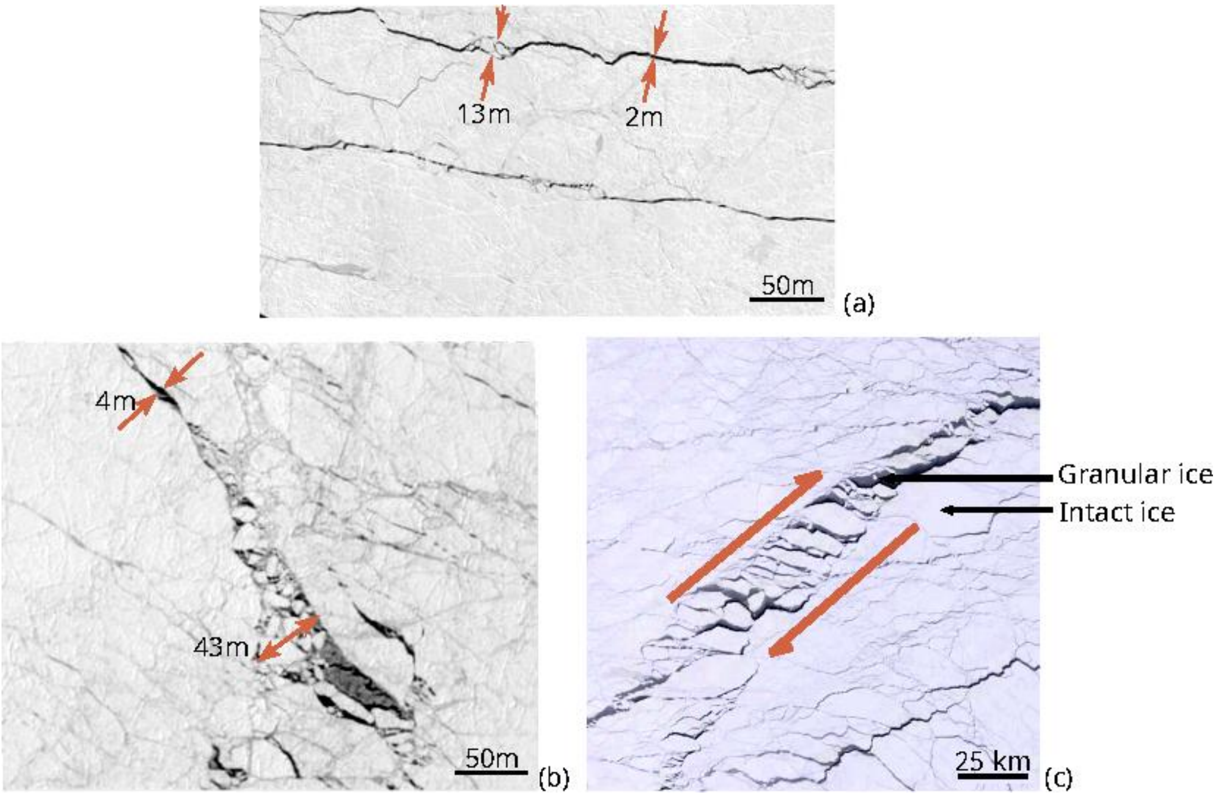

Figure: Satellite images of shear fractures in sea-ice at different scales and different deformation stages. (a) Early stage deformation, showing a single dominant fracture prior to gouge formation; (b) resulting granular state of ice within a shear band at small scale. USGS EarthExplorer images courtesy of the U.S Geological Survey. (c) Resulting granular state of ice within a mature shear band at larger scale. Image generated using NASA Worldview (NASA ESDIS).

Vincent Guigonnet

On the Mechanical Behavior of Permafrost: Experimental Insights and a Multiscale Mesodirectional Modeling Approach

***Authors**: Vincent Guigonnet (ISTerre, France), François Nicot (ISTerre, France), Jérôme Aubry (ISTerre, France)*

Permafrost mechanical behavior depends on the interplay between ice content, temperature, and strain rate (Arenson, 2002). With ongoing climate warming driving widespread permafrost degradation, there is a growing need for constitutive models capable of informing slope stability and infrastructure risk assessment in mountain regions. This study proposes an extension of the H-model (Nicot and Darve, 2011) (originally developed for granular soils) to frozen ground, building on the bonded contact law introduced for snow (Miot et al., 2025). The work is complemented by experimental testing on laboratory frozen soil analogues (Yamamoto and Springman, 2014).

The H-model is a mesodirectional model in which the granular microstructure is represented as a collection of hexagonal grain assemblies (H-cells), enabling a physically grounded scale transition from grain-scale mechanics to a continuum constitutive relation. Contact laws at the grain scale account for elastic stiffness, Glen-type viscous creep in ice bonds, frictional sliding, and temperature-dependent bond failure (Petrovic, 2003; Fish and Zaretsky, 1997). Stresses are then obtained via the Love-Weber formula and averaged statistically over all H-cell orientations.

A key feature of the model is its ability to account for temperature variations that directly modify ice content through a soil freezing curve which in turn updates the bond geometry and the mechanical response. Strain rate dependence emerges naturally from Glen's law: slow loading allows viscoplastic relaxation producing ductile behavior, while fast loading leads to brittle-like failure and higher peak stress.

Initial biaxial simulations correctly capture the qualitative influence of ice content (Calvetti and Wang, 2022), strain rate, and temperature on peak strength prior to full calibration. Next steps include parameter calibration and extension to rock slope stability problems.

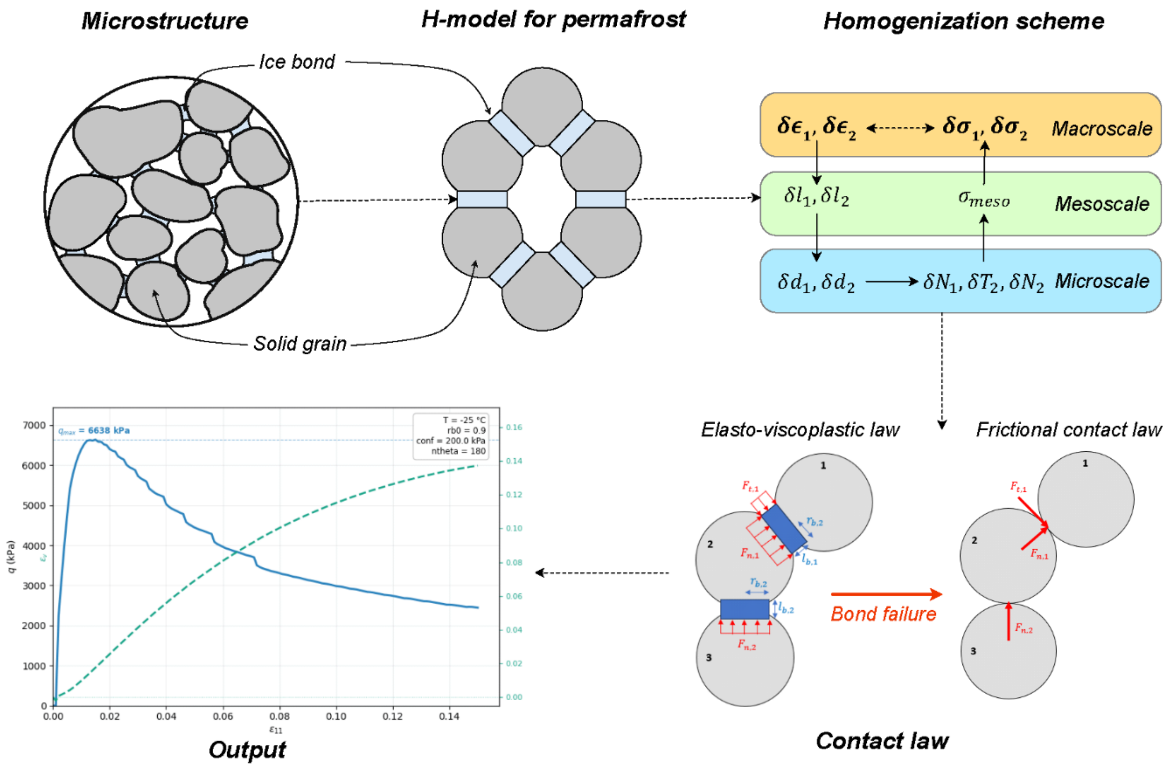

Figure: Multiscale framework of the H-model extended to permafrost. The H-cell represents the permafrost microstructure (solid grains bonded by ice bridges) following the bonded granular configuration of Pouragha et al. (2023). The homogenization scheme of Nicot and Darve (2011) bridges three scales, from macroscopic strains down to grain-scale contact forces and back up to macroscopic stresses. Contact laws follow Miot et al. (2025). Bottom left is a biaxial test simulation output for a given configuration.

Romain Iaquinta

3D Fractal Analysis of Co-seismic Damage in the Nojima Fault Using X-Ray Tomography and SHPB Experiments

***Authors**: Romain Iaquinta (ISTerre, France), Mai-Linh Doan (ISTerre, France), Frederic Victor Donzé (ISTerre, France)*

Active fault cores commonly exhibit intense damage whose origins remain debated. This study investigates the co-seismic contribution to this damage by analyzing the Nojima fault, which ruptured during the 1995 Kobe earthquake (Mw 6.9). The Hirabayashi borehole, drilled about one year after the event, provides a rare opportunity to characterize fault zone damage shortly after a major earthquake.

As part of the French ANR AlterAction project, we collected drill core samples along the borehole and analyzed them using X-ray computed µ-tomography (µCT) at ~50 µm resolution. Our methodology focuses on 3D fractal analysis of the spatial distribution of void voxels (empty space) versus solid voxels (rock matrix) in the tomographic volumes. The fractal dimension D ranges from 2 (highly clustered voids) to 3 (homogeneously distributed voids). This metric directly reflects the transition from localized fracture networks to volumetric pulverization, and correlates with fracture-induced porosity.

Open fracture density increases toward the core but drops significantly in its immediate vicinity, likely due to rapid post-seismic cementation. Fractal analysis reveals D values near 2 for clustered damage zones, increasing toward 3 where damage becomes volumetric. Some samples exhibit intense micro-fracturing with minimal macroscopic deformation, resembling "pulverized rock" observed around other active faults. This microfracturing without significant strain suggests high strain-rate loading during the earthquake.

To validate the dynamic origin of this damage, we performed Split Hopkinson Pressure Bar (SHPB) experiments on intact borehole samples. We established a linear relationship between strain rate and absorbed energy. Combined with µCT scan analysis, this relationship distinguishes two fracture propagation modes: diffuse pulverization (similar to near-fault observations) and poorly connected fracture networks. Fractal dimensions from experimental samples confirm these contrasting morphologies and their correlation with generated porosity.

Our results demonstrate that intense damage observed in the Nojima fault core likely originated from co-seismic processes, characterized by specific fractal patterns linked to high strain rates.

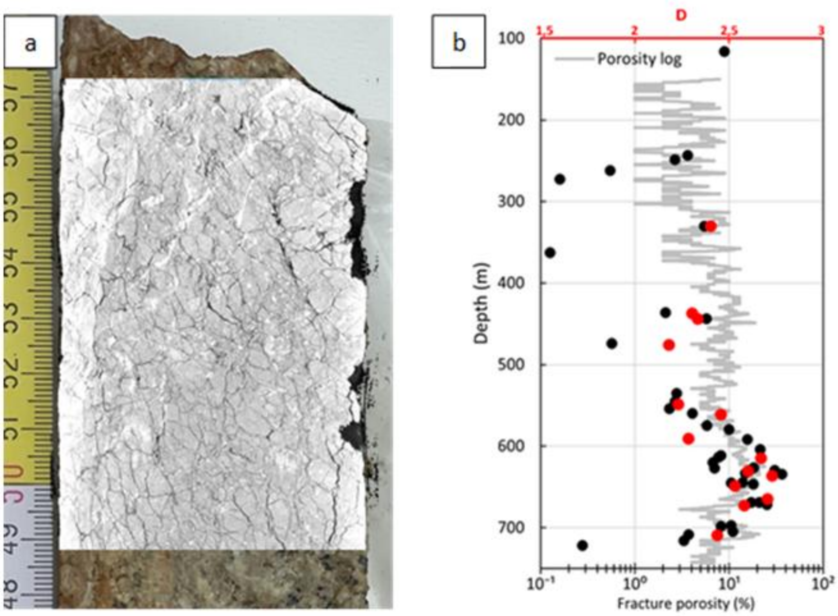

Figure: (a) μ X-ray tomography of a core sample at 668m depth, close to the fault core ; (b) Porosity (black circles) and D (red circles) profiles along the Hirabayashi borehole

Pei Pei

Post-seismic evolution of the hydraulic properties and its effect on slip tendency at the Tohoku plate boundary fault zone

***Authors**: Pei Pei (ISTerre, France), Mai-Linh Doan (ISTerre, France), Expedition 405 Science Party*

The Mw 9.1 earthquake that occurred near the trench at the northeast coast of Japan in 2011 triggered a tsunami. The earthquake produced more than 50 m of slip near the trench axis, highlighting the important role of shallow fault weakening within subduction zones. In such environments, the coupling between fluid flow, permeability evolution, and pressure diffusion strongly modifies pore-fluid pressure and effective stress, thereby influencing fault stability, shallow rupture propagation, and earthquake generation. Despite its importance, the post-seismic evolution of in-situ fluid systems within plate boundary fault zones (PBFZs) remains poorly understood.

Here we integrate hydraulic and geophysical observations from International Ocean Discovery Program Expeditions 343/343T (2012, JFAST) and 405 (2024, JTRACK) at Site C0019 across the Japan Trench plate boundary fault zone to investigate the post-seismic evolution of fluid circulation and stress state over 13.5 years following the earthquake. The JFAST and JTRACK boreholes provide a valuable opportunity to directly compare in-situ hydraulic conditions within the same fault zone at two different stages of the seismic cycle. Our analysis reveals the development of a ~3m permeable band within the PBFZ that traps upward-migrating fluids and progressively increases pore-fluid pressure over time. Compared with shortly after the earthquake in 2012, the 2024 borehole data indicate enhanced fluid accumulation and a more localized fluid-flow structure within the shallow fault zone.

This progressive fluid pressurization reduces effective normal stress while shear stress loading remains relatively insignificant during the post-seismic period, thereby increasing the slip tendency of the shallow fault. Our results suggest that post-seismic hydraulic sealing and fluid-pressure buildup can maintain a mechanically weak state in the shallow megathrust long after a giant earthquake. These observations provide new constraints on the evolution of hydrogeological properties within subduction-zone PBFZs and demonstrate how post-seismic fluid processes may control the mechanical recovery, instability, and future shallow slip behavior of megathrust faults.

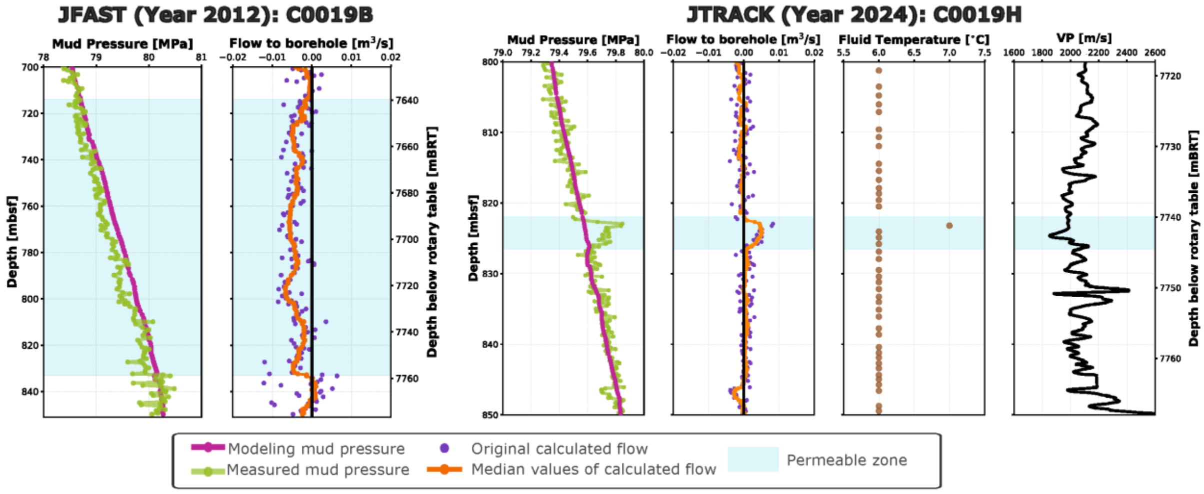

Figure: Fiigure: Comparing fluid flow profiles from Expedition 343 (A,B) and Expedition 405 (C,D,E). Expedition 343 results: (A) Measured (green line) and modeled (purple line) mud pressures; (B). Resulting flow in/ out of the borehole (blue line). Expedition 405 results: (C) Measured and modeled mud pressures; (D). Resulting flow in/ out of the borehole; (E) Measured fluid temperature during drilling. Comparing (B) with (D), a fluid pressure increasing zone (highlight by yellow area) is determined, this zone corresponds to a clear temperature anomaly in (E) (see more details in the main text). To better compare these two datasets, both meters below seafloor (mbsf) and meters below drill ship's rotary table (mBRT) are used.

Romain Rousseau

Estimation of Frost-Induced Stress Using Time-Lapse Ultrasonic Testing and their Effect on the Dynamics of an Alpine Rock Pillar

***Authors**: Romain Rousseau (ISTerre, France), Juliane Starke (ISTerre, France), Pierre Bottelin (ISTerre, France), Ludovic Moreau (ISTerre, France), Laurent Baillet (ISTerre, France), and Eric Larose (ISTerre, France)*

Rock fracturing plays a key role in the formation of mountain landscapes and natural hazards. Freezing is one of the main triggers of erosion and fracturing in the Alps. However, questions remain about the impact of freezing on the resonance frequency of rock pillars and the quantification of mechanical stress generated by ice in natural cliffs.

To better understand the effect of frost at the centimeter and meter scale, long-term recordings were made using repeatable ultrasonic signals to measure both sound velocity and waveform changes. These observations are combined with the measurement of the pillar's fundamental resonance frequency. The investigated Tête Noire rock pillar consists of micaschist and is instably hanging above the city of Trient in the western Swiss Alps.

The results show that during freezing, the fundamental resonance frequency increases by 50 %, the P-wave velocity increases by 17 %, and for later arrivals (coda wave) velocity increases by 4 %. After the freezing period, a irreversible drop in P-wave and coda wave velocities is visible, but not in the fundamental resonance frequency which is coming back to its initial value. This decrease in velocity is accompanied by a decorrelation of the ultrasonic waveforms. Reproducing the observed P wave velocity changes on 0.5m thick layer on a finite element COMSOL simulations of the pillar, we determine that the changes in velocity in the rock do not explain the fundamental resonance frequency changes. We therefore propose that the increase in fundamental resonance frequency results from ice filling the rear crack, and we estimate an order of magnitude of about 1.7 m for the ice height, compared with the initial crack size of 10 m.

To estimate the freezing stress, from the measured velocity changes, we determined the acousto-elastic constant of the Tête Noire micaschist on a representative laboratory sample using uniaxial compression experiments. Those results reveal that the generated freezing induced stress are in the subcritical regime with an order of magnitude of a few tens MPa and are, hence able to damage slightly the rock, irreversibly. The drop in correlation coefficient and in the waves velocity support this conclusion.

This work was funded by the European Research Council (ERC) under grant No. 101142154 - Crack The Rock project.

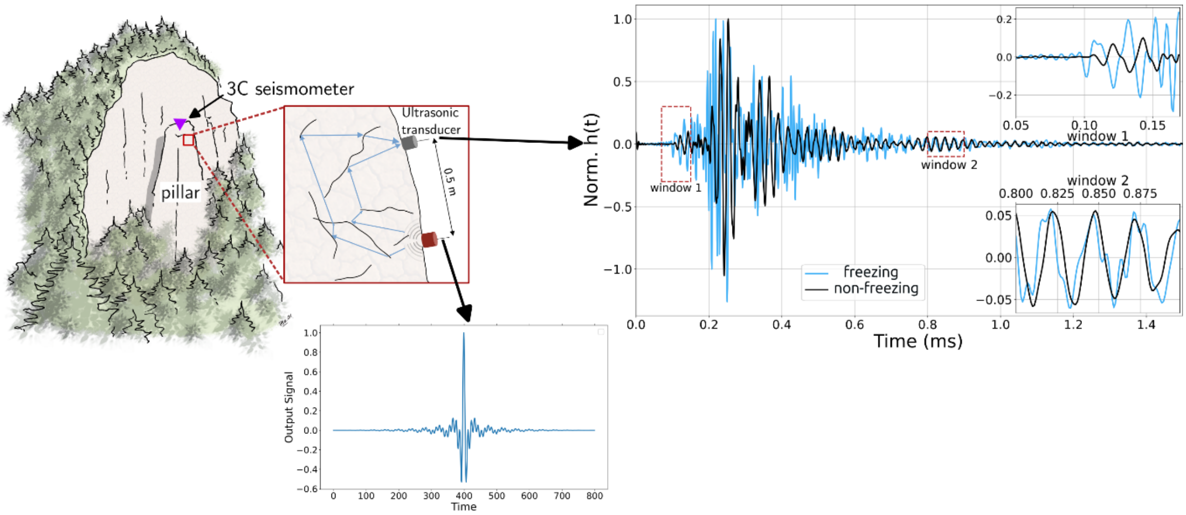

Figure: Experimental set up

Juliane Starke

Acoustic Fingerprints - Tracing Irreversible Damage in Natural Cliffs

***Authors**: Juliane Starke (ISTerre, France), Romain Rousseau (ISTerre, France), Alex Rolland (ISTerre, France), Laurent Baillet (ISTerre, France), Eric Larose (ISTerre, France)*

Progressive damage and failure in rock masses is governed by multi-scale processes ranging from micro-crack growth to meter-scale fracture opening. We present an active acoustic monitoring approach that captures these evolving processes through time-lapse waveform fingerprinting, providing a quantitative measure of the temporal evolution of rock mass stiffness and scattering properties. We deployed acoustic sensors on three highly fractured rock cliffs (two limestone sites in southern France and one gneiss site in western Switzerland) and conducted repeated active acoustic measurements every few minutes over periods of several weeks to more than one year. Each source-receiver path yields a unique acoustic response whose complexity increases with fracture density and scattering. By tracking phase shifts and waveform distortions, we 'draw' time-lapse waveform fingerprints that are highly sensitive to small changes in crack density, fracture aperture, and contact stiffness. The waveform fingerprints reveal strong repeatability under similar meteorological conditions, with coincident patterns observed on days sharing comparable temperature and moisture regimes. Distinct fingerprints emerge under different rock cracking and damage states reflecting reversible thermo-hydro-mechanical effects. Some rocks are indeed more reactive to external forcings than others. At longer timescales, partial but incomplete recovery of the fingerprints is observed. In the one-year data set, major fingerprint features reappear under similar climatic conditions, but with persistent residual changes, indicating the accumulation of irreversible damage within the rock mass.

Future work could apply diffuse acoustic wave spectroscopy and acoustic correlation-based imaging to spatially locate damage and quantify fracture growth, enabling the transition from qualitative fingerprints to quantitative maps of rock degradation.

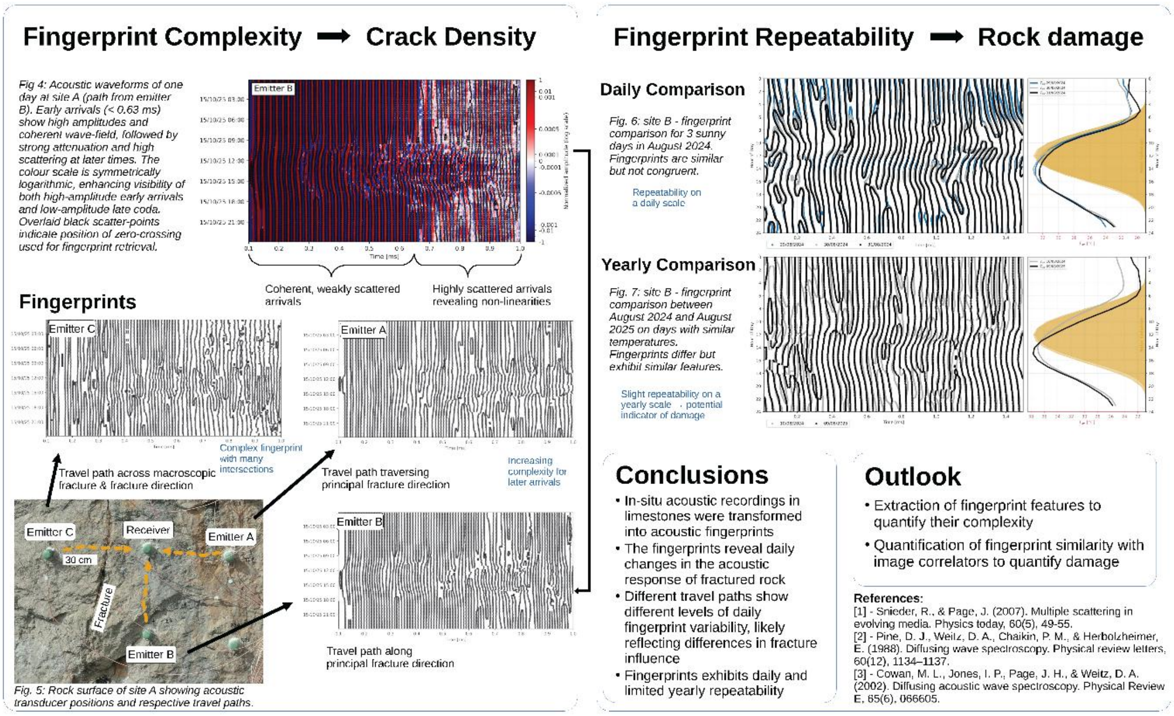

Fingerprint Complexity ➡ Crack Density
Fig 4: Acoustic waveforms of one day at site A (path from emitter B). Early arrivals (< 0.63 ms) show high amplitudes and coherent wave-field, followed by strong attenuation and high scattering at later times. The colour scale is symmetrically logarithmic, enhancing visibility of both high-amplitude early arrivals and low-amplitude late coda. Overlaid black scatter-points indicate position of zero-crossing used for fingerprint retrieval.
Emitter B
Time [ms]
Coherent, weakly scattered arrivals
Highly scattered arrivals revealing non-linearities
Fingerprints
Emitter C
Emitter A
Complex fingerprint with many intersections
Travel path across macroscopic fracture & fracture direction
Travel path traversing principal fracture direction
Increasing complexity for later arrivals
Emitter C
Receiver
Emitter A
30 cm
Fracture
Emitter B
Emitter B
Travel path along principal fracture direction
Fig. 5: Rock surface of site A showing acoustic transducer positions and respective travel paths.
Fingerprint Repeatability ➡ Rock damage
Daily Comparison
Fig. 6: site B - fingerprint comparison for 3 sunny days in August 2024. Fingerprints are similar but not congruent.
Repeatability on a daily scale
Yearly Comparison
Fig. 7: site B - fingerprint comparison between August 2024 and August 2025 on days with similar temperatures. Fingerprints differ but exhibit similar features.
Slight repeatability on a yearly scale → potential indicator of damage
Conclusions
• In-situ acoustic recordings in limestones were transformed into acoustic fingerprints
• The fingerprints reveal daily changes in the acoustic response of fractured rock
• Different travel paths show different levels of daily fingerprint variability, likely reflecting differences in fracture influence
• Fingerprints exhibits daily and limited yearly repeatability
Outlook
• Extraction of fingerprint features to quantify their complexity
• Quantification of fingerprint similarity with image correlators to quantify damage
References:
[1] - Snieder, R., & Page, J. (2007). Multiple scattering in evolving media. Physics today, 60(5), 49-55.
[2] - Pine, D. J., Weitz, D. A., Chaikin, P. M., & Herbolzheimer, E. (1988). Diffusing wave spectroscopy. Physical review letters, 60(12), 1134–1137.
[3] - Cowan, M. L., Jones, I. P., Page, J. H., & Weitz, D. A. (2002). Diffusing acoustic wave spectroscopy. Physical Review E, 65(6), 066605.

Ptashanna Thiraux

Exploring and simulating earthquakes interactions

***Authors**: Ptashanna Thiraux (ISTerre, France), Jérôme Weiss (ISTerre, France), David Marsan (ISTerre, France)*

Exploring and simulating earthquakes interactions Earthquakes and faults are often considered as a paradigm of crackling noise, i.e. slowly driven complex systems that respond through intermittent events [1] characterized by scale-free statistics such as a power law distribution of seismic moments (the Gutenberg-Richter law), space/time correlations expressed e.g. by a slow decaying rate of aftershocks (the Omori's law) associated to scale free (sub)diffusion. Understanding the physical origin of these scaling laws is also obviously of primary importance in terms of natural hazards forecasting. Slider-blocks model, incorporating (only) simple static friction and elastic interactions, have been proposed for a long time to simulate fault mechanics and earthquakes[2]. The seminal 1D models were later extended to 2D using cellular automata with a simplified (short-range) version of elastic stress redistribution[3]. If these models are able to simulate intermittent events, power-law distributed in slip sizes, they do not incorporate a timescale, so are unable to simulate aftershocks and the associated space and time clustering. More recently, deterministic rheologies (e.g. viscous-elastic [4] or rate-and-state [5]) of the blocks were introduced to simulate these complex space/time properties. A goal of this project will be to introduce timescales at a more fundamental level by allowing the thermal activation of the slip of individual blocks, in order to explore the coupled effects of thermal activation and elastic stress redistribution on earthquakes self-organization. This is also a means to introduce temperature effects on earthquake triggering. In addition, the effect of the nature of the elastic redistribution kernel (short-range vs (more realistic) long-range) will be explored as well. In the meantime, the PhD will also analyze experimental data coming from different (existing) laboratory fault models[6,7], and compare them to real seismic catalogs and model results. In the end, more complex modelling setups, e.g. introducing temperature gradients to simulate subduction zones, will be developed and analyzed.

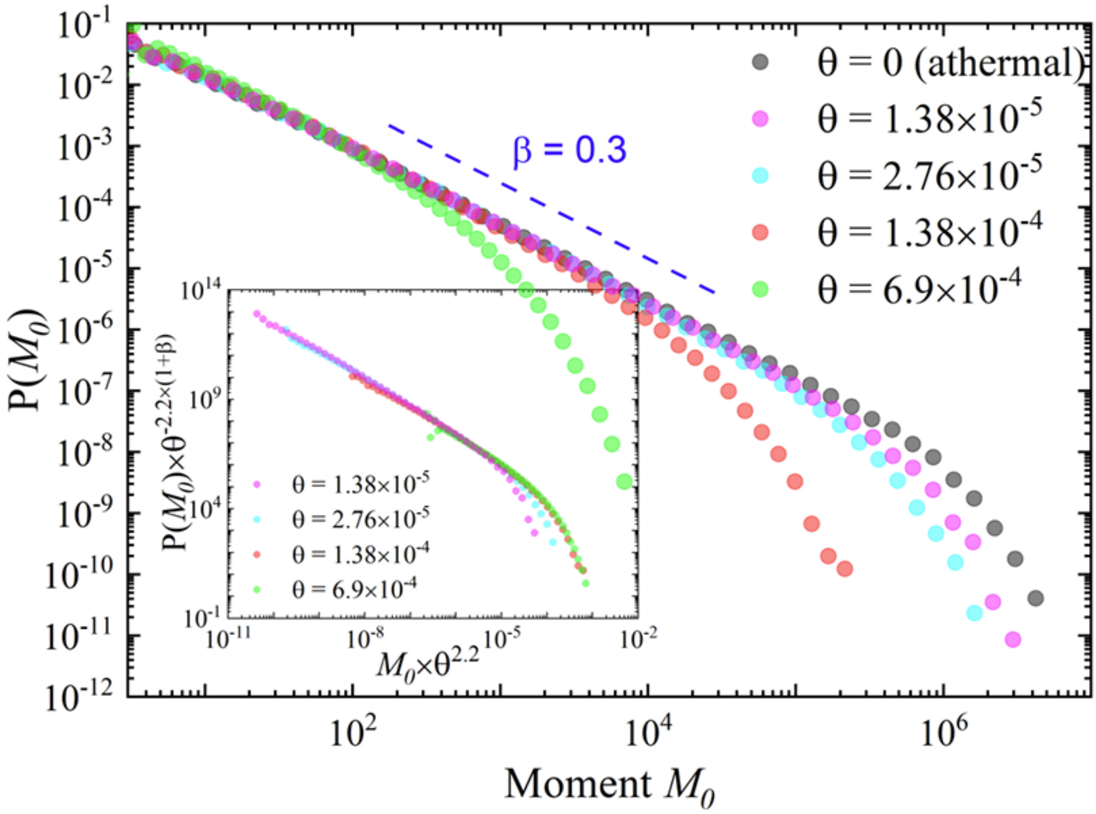

Figure: Effect of temperature on the distribution of seismic moments. Distribution of the seismic moments M0, calculated for different catalogs obtained from the athermal model (grey symbols) or the model with thermal activation for different temperatures θ, but the same dissipation d = 4 × 10−5 in all cases. The blue dashed line represents a power law distribution with an exponent β=0.3. The inset represents the rescaled distributions P(M0) ∼ M−(1+β) 0 g M0 M∗ 0, assuming a cut-off M∗ 0 scaling with temperature θ as M∗ 0 ∼ θ−2.20, see text for details.

Juan Carlos Verano Espitia

Statistical physics of creep rupture of heterogeneous materials

***Authors**: Juan Carlos Verano-Espitia (Aalto Yliopisto Department of Applied Physics, Finland & ISTerre, France), Jérôme Weiss (ISTerre, France), Mikko Alava (Aalto Yliopisto Department of Applied Physics, Finland), Tero Mäkine (Aalto Yliopisto Department of Applied Physics, Finland)*

In this work, the creep behavior of heterogeneous materials, i.e., those subjected to a constant load, is studied using experimental, theoretical, and numerical approaches. Understanding how materials deform, damage, and approach failure is relevant in fields such as materials science, geophysics, and engineering. Nevertheless, in classical mechanics and engineering literature, the so-called "creep" failure is described mostly empirically. Such empirical laws are common to most brittle materials, soft materials, ductile metals, and granular media. Therefore, the universality of this phenomenon across a wide range of materials remains an open question, still lacking a full theoretical understanding. Therefore, in this project (i) we tracked the progressive damage during creep of heterogeneous brittle materials, using various monitoring tools such as acoustic emission, and (ii) we introduced statistical physics theory and numerical approaches (fiber bundle models, progressive damage model, kinetic Monte Carlo algorithm) to interpret this damage evolution. The final goal was to predict failure in the early stages of creep experiments, leveraging all acquired knowledge, using a Bayesian inference framework. This research has potential applications in material diagnostics and failure prediction, which are highly relevant to civil engineering and risk analysis, as well as to geophysical phenomena such as landslides and rockfalls.

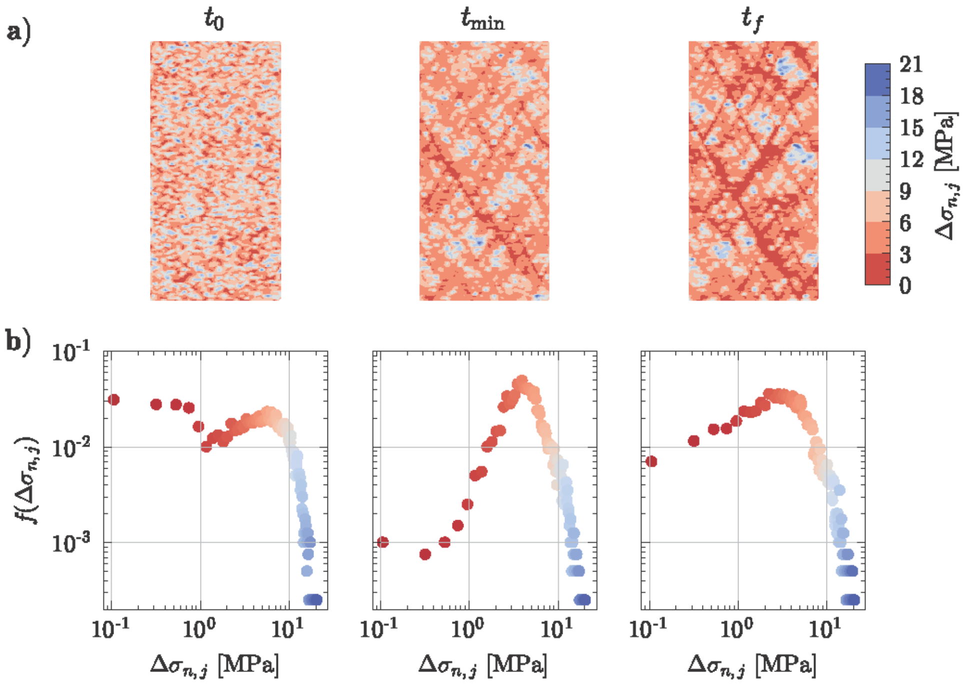

Figure: a) Example of the evolution of the stress gap field $\Delta\sigma_{n,j}$, and b) its respective stress gap distribution $f(\Delta\sigma_{n,j})$ at different stages: onset of the creep behaviour t_0, end of primary creep t_{min} and the rupture time t_f.

Imme Wienk

Seismic Velocity Variations as Indicators of Hydromechanical Processes in the Séchilienne Landslide (France)

***Authors**: Imme Wienk (ISTerre, France), Antoine Guillemot (Géolithe, France), Olivier Béjean-Maillard (Chrono-Environnement, France), Mathilde Radiguet (ISTerre, France), Eric Larose (ISTerre, France)*

The Séchilienne landslide in the French Alps is a large, deep-seated landslide whose dynamics are strongly influenced by hydro-geological conditions. Between 2011 and 2016, the landslide underwent an active phase marked by an initial increase and a subsequent decrease of displacement rates. Since then, the landslide has remained largely stable. The site has been instrumented with a seismic network since 2012 (French National Landslide Observatory (OMIV)), providing the opportunity to link relative seismic velocity changes (dV/V) to hydro-geological observations and landslide deformation. We observe clear seasonal cycles in seismic velocities in the shallow, fractured part of the landslide. Velocities decrease during periods of elevated groundwater levels and increase during dry conditions, indicating a reversible response to water table fluctuations. Superimposed on this seasonal behavior, dV/V shows a long-term trend during the active phase of the landslide. At shallow depths, there is an anticorrelation between dV/V and displacement rates. During the stable period, dV/V shows no prominent long-term trend. These results indicate sensitivity of dV/V to landslide kinematics. The results show that seismic interferometry captures short-term hydrologically driven variations and longer-term changes connected to landslide kinematics. The approach provides valuable insight into hydromechanical processes governing landslide evolution and highlights the potential of continuous seismic monitoring for slope stability assessment.

We acknowledge help from the ISTerre-SIG team for operating the seismic network. We acknowledge the support of the European Research Council (ERC) under the grant agreement no. 101142154 (Crack The Rock).

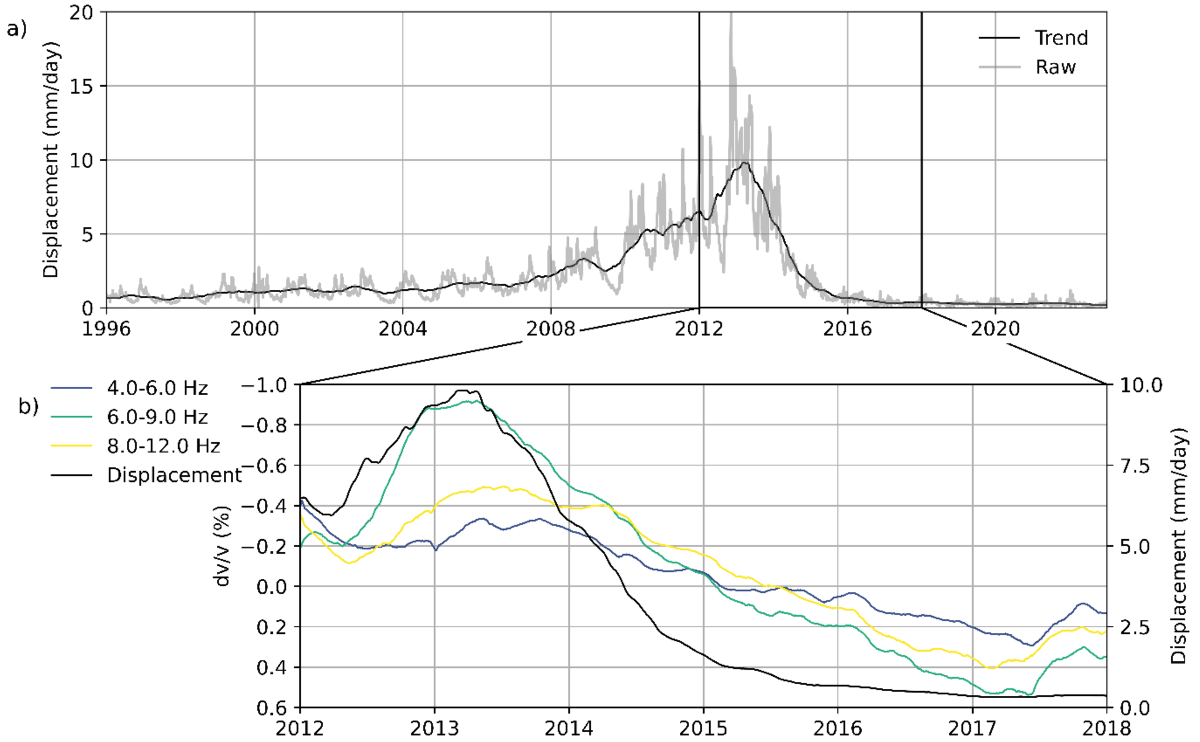

Figure: a) Displacement rates measured by extensometer located on the landslide. b) Trend of displacement rates compared to the trend in dv/v for the three frequency bands sensitive to the fractured part of the landslide during the active period.

Yan Yao

Beyond the Water-Rich Paradigm: Experimental Evidence for H_2 Generation and Abiotic Hydrocarbon Formation in Vapor-Dominated Serpentinizing Systems

Authors: *Yan Yao (ISTerre, France), Frederic Victor Donze (ISTerre, France), Laurent Truche (ISTerre, France)*

Hydrogen (H_2) generation during serpentinization is commonly investigated in water-rich laboratory systems. However, in many natural ultramafic settings, water availability can be limited, and the system may evolve from liquid-water-dominated to water-vapor-only conditions as reactions proceed. This raises a key question: as a system shifts toward nearly dry conditions, can serpentinization and H_2 production continue, and what carbon-bearing gases form (if any)? We conducted controlled hydrothermal experiments at 200℃ with three objectives: (1) assess water availability and phase state as first-order controls on serpentinization and H_2 generation; (2) clarify the role of CO_2 and test whether a "H_2 promotion window" exists; and (3) constrain the conditions for abiotic hydrocarbon formation in serpentinized systems.

Our results show that H_2 is produced under both liquid- and vapor-phase conditions. The phase state strongly affects kinetics: H_2 generation persists after the system becomes water-vapor-only, but the production rate decreases by about a factor of 10 compared with liquid-dominated conditions. This provides direct experimental evidence that vapor-phase serpentinization can sustain H_2 generation, offering a process-based explanation for the spatial heterogeneity of H_2 production in natural systems where fluid supply varies.

Contrary to the expectation that CO_2 uniformly inhibits H_2 production, we find its effects are variable depending on conditions and reaction stage. In water-rich experiments where serpentinization had already progressed for one month, CO_2 injection increased the H_2 generation rate, pointing to a probable "promotion window". In water-limited experiments, CO_2 had little effect on the H_2 generation rate but consistently shortened the production time window of H_2, resulting in earlier plateaus and lower cumulative yields.

Natural hydrogen seeps worldwide are often accompanied by CH_4 whose compositional variability remains poorly understood. By systematically simulating abiotic hydrocarbon generation under controlled temperature and water-availability conditions, we find that CH_4 production exceeding background levels is only observed at 250℃ with no detectable signal at lower temperatures. These results provide an experimental baseline for interpreting co-emitted gases at hydrogen seeps and assessing natural hydrogen resource potential.

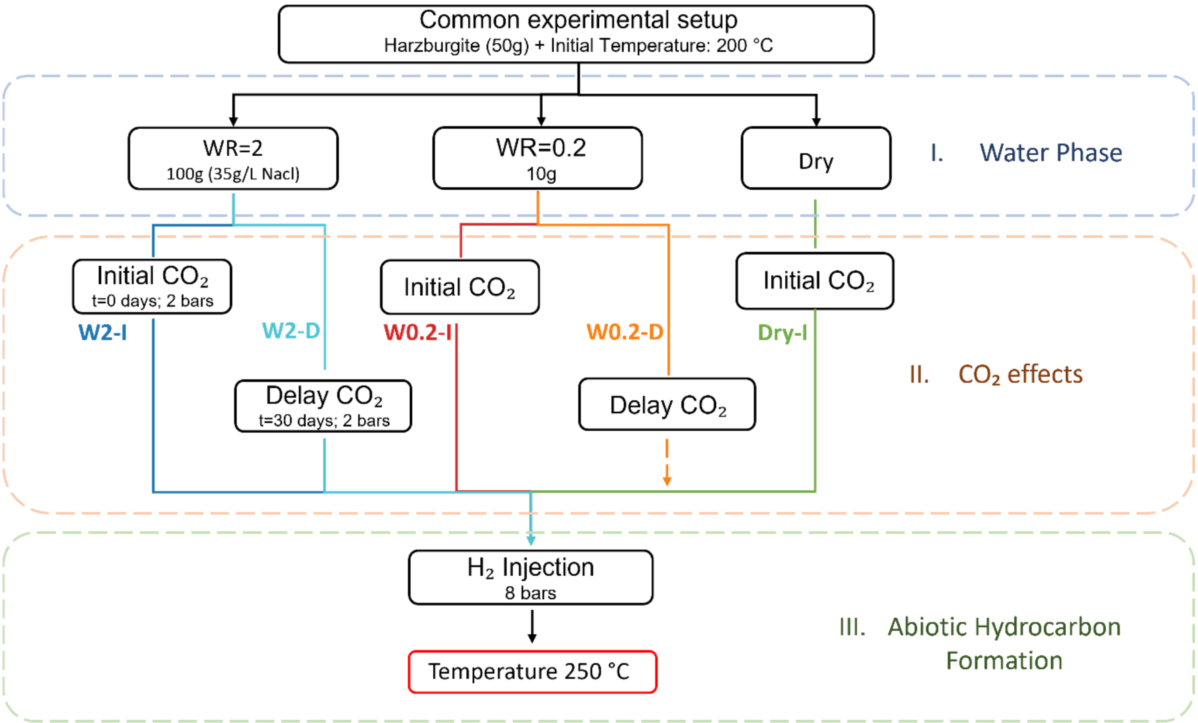

Figure: The flow chart of autoclave experiment designs

Love Zetterberg

Creep vs relaxation in brittle disordered solids

***Authors**: Love Zetterberg (ISTerre, France), Jérôme Weiss (ISTerre, France), David Amitrano (ISTerre, France)*

When studying materials that are subjected to loading over long periods of time, two phenomena, creep and stress relaxation, emerge as a sort of mirror image of one another. Creep is defined as the slow deformation of a material under constant load, while relaxation is defined as a material held at constant strain and displaying a slow decrease of the internal stress. In the case of brittle heterogenous materials, these two phenomena can be linked to thermally activated microfracturing. Primary creep is most commonly modelled as a power law decrease of the strain rate with time. Similarly, relaxation is often observed as a logarithmic decrease of the stress with time, corresponding to a stress-rate decaying as 1/t. In both cases these descriptions remain phenomenological and do not explain the underlying process.

Modelling the material as a collection of subvolumes, each capable of deforming and damaging once a local "yield" stress is reached athermally, or by thermal activation, one can create more physically grounded models for creep and relaxation of disordered brittle materials. A 1st order approach, analytically tractable, is to describe primary creep from a statistical exhaustion model, assuming thermal activation of individual subvolume damage, but ignoring elastic stress redistribution. However, this idealized approach neglects spatially and temporally localized effects which have been shown to increase the strain rate and decrease the time to failure through internal stress redistribution.

In order to better understand the relationship between primary creep and relaxation in brittle materials, and aiming to clarify the relationship between these two phenomena, we analyze tests performed on concrete samples, and in particular acoustic emissions. This is compared to what is expected from a simple exhaustion model in order to reveal the combined role of quenched disorder, thermal activation and elastic stress redistributions on these processes.

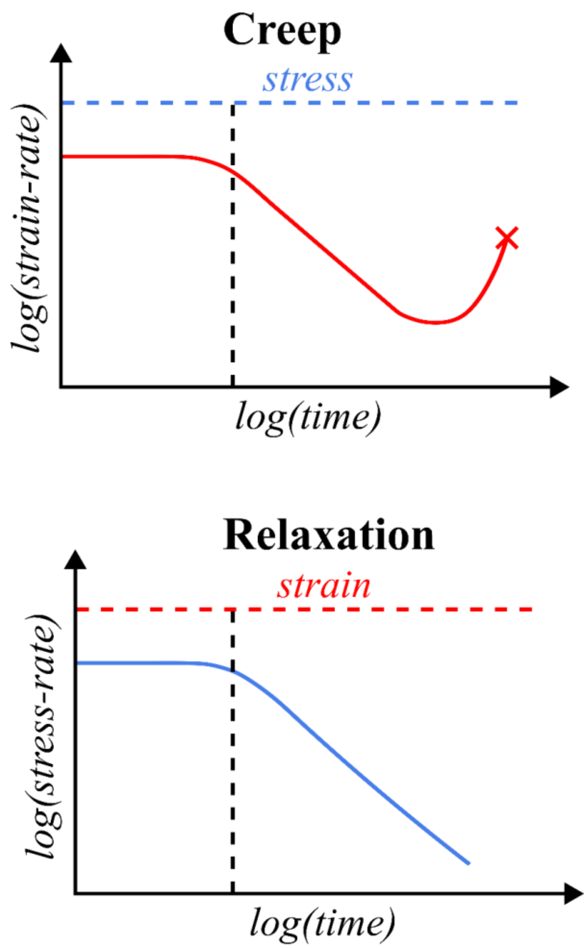

Figure: Creep and relaxation curves respectively. The strain and stress-rates are constant up to some characteristic time, after which they decrease proportionally to log(time). In the case of creep, a mimimum strain-rate might be reached, followed by an acceleration and complete system failure.

Geochemistry

Duong Binh Au

Investigating the Nucleation of Calcium Carbonate in Cement Pores

***Authors**: Duong Binh Au (ISTerre, France), Alejandro Fernandez-Martinez (ISTerre, France), Alexander E.S. Van Driessche (IACT, Spain)*

Cement is the world's most widely used construction material and is primarily composed of clinker, which is produced by calcining limestone at high temperatures, a process that releases substantial amounts of CO_2. Cement production alone accounts for approximately 8% of global anthropogenic CO_2 emissions, equivalent to roughly 1.6 billion metric tons in 2022. In this context, the methods of carbon capture and storage into the cementitious materials are gaining the increasing attention worldwide, among them, carbon-dioxide mineralization allows for permanent CO2 storage in the form of thermodynamically stable carbonation products.

From a scientific perspective, carbonation mechanisms involve the diffusion of CO_2 into the (pore) solution, dissolution of cement phases (mainly CaO, SiO2, and Al2O3), and subsequent precipitation of novel phase assemblages, primarily calcium carbonate ($CaCO_3$) in various polymorphic forms, aside with the amorphous calcium carbonate (ACC), which is well-known as the least thermodynamically stable material in the nature environment. The persistence of ACC during cement carbonation underscoring a key knowledge gap in understanding the kinetics of $CaCO_3$ precipitation and the mechanisms governing its polymorphic transformation in cement pore solutions. By combining the Classical Nucleation Theory (CNT) and the time-resolved UV-Vis spectrophotometry, this project aims to provide a comprehensive investigation of CaCO3 nucleation pathway in the model system with the cement pore condition. A deeper fundamental understanding of $CaCO_3$ precipitation in complex environments will provide critical insights into the cement carbonation mechanism, enabling improved control over the process for sustainable cement technologies.

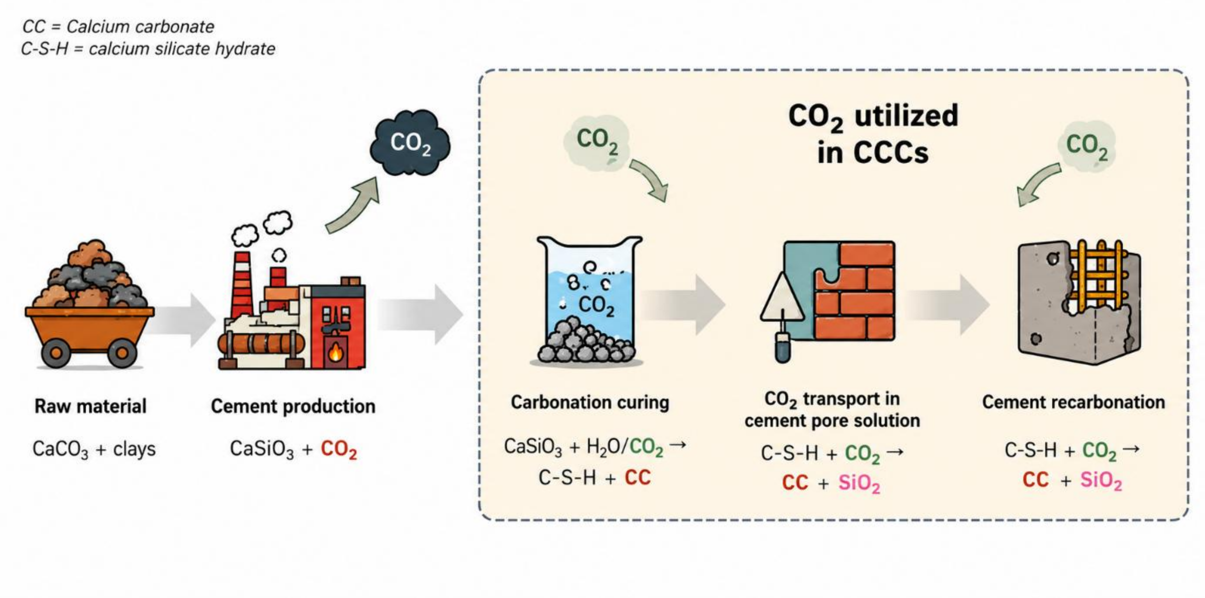

Figure: The image illustrates CO_2 emissions from cement production and how captured CO_2 is reused during carbonation curing and re-carbonation. In these steps, CO_2 reacts with cement phases to form stable calcium carbonate, enabling partial CO_2 capture and storage within cement-based materials.

Sara Capriotti

Reconstructing Iron Age Ceramic Production Technology at the Church of the Holy Sepulchre (Jerusalem): A Multi-Analytical Approach

***Authors**: Sara Capriotti (Department of Earth Sciences, Italy), Laura Medeghini (Department of Earth Sciences, Italy), Alejandro Fernandez-Martinez (ISTerre, France)*

Pottery has long been one of the most extensively studied artefacts within archaeological contexts, providing key information on both the cultural and technological aspects of ancient societies, as well as their interaction and exchange systems. This study focuses on Iron Age ceramic fragments recovered from the archaeological site of the Church of the Holy Sepulchre in Jerusalem, one of the most important Christian sacred sites, traditionally identified as the place of Christ's death and resurrection (Stasolla, 2022). A total of 54 ceramic sherds, uncovered during excavations conducted by Sapienza University of Rome, were analysed. The assemblage derives from fill layers associated with the Basilica foundations, where the original stratigraphic context has been lost. The aim of this study is to reconstruct the technological framework and provenance of the raw materials in order to investigate ceramic production profiles. A multi-analytical approach was applied, combining Optical Microscopy (OM), Fourier Transform Infrared Spectroscopy (FTIR), and X-ray-based techniques, including X-ray Powder Diffraction (XRPD), X-ray Absorption Fine Structure spectroscopy (XAFS), and Pair Distribution Function (PDF) analysis. These methods allowed the characterization of the mineralogical and petrographic composition of the ceramic bodies, the identification of firing temperatures, and the definition of petrographic fabrics.

Preliminary results suggest relatively consistent production processes. Based on the clay mineral fraction, two main compositional groups were identified. The first is characterized by carbonatic components, mainly dolomite and/or microfossils, while the second is dominated by fine quartz inclusions. On this basis, three main petrographic fabrics were defined: Dolomite-rich Fabric, Microfossil-rich Fabric, and Quartz-rich Fabric (Fig.). In addition, four samples were classified as loners due to their distinct compositional signatures. The mineralogical assemblages are consistent with the geological setting of the Jerusalem region, dominated by Upper Cretaceous to Paleogene carbonate sequences, including limestones, dolostones, chalks, and marls (Schulze et al. 2005).

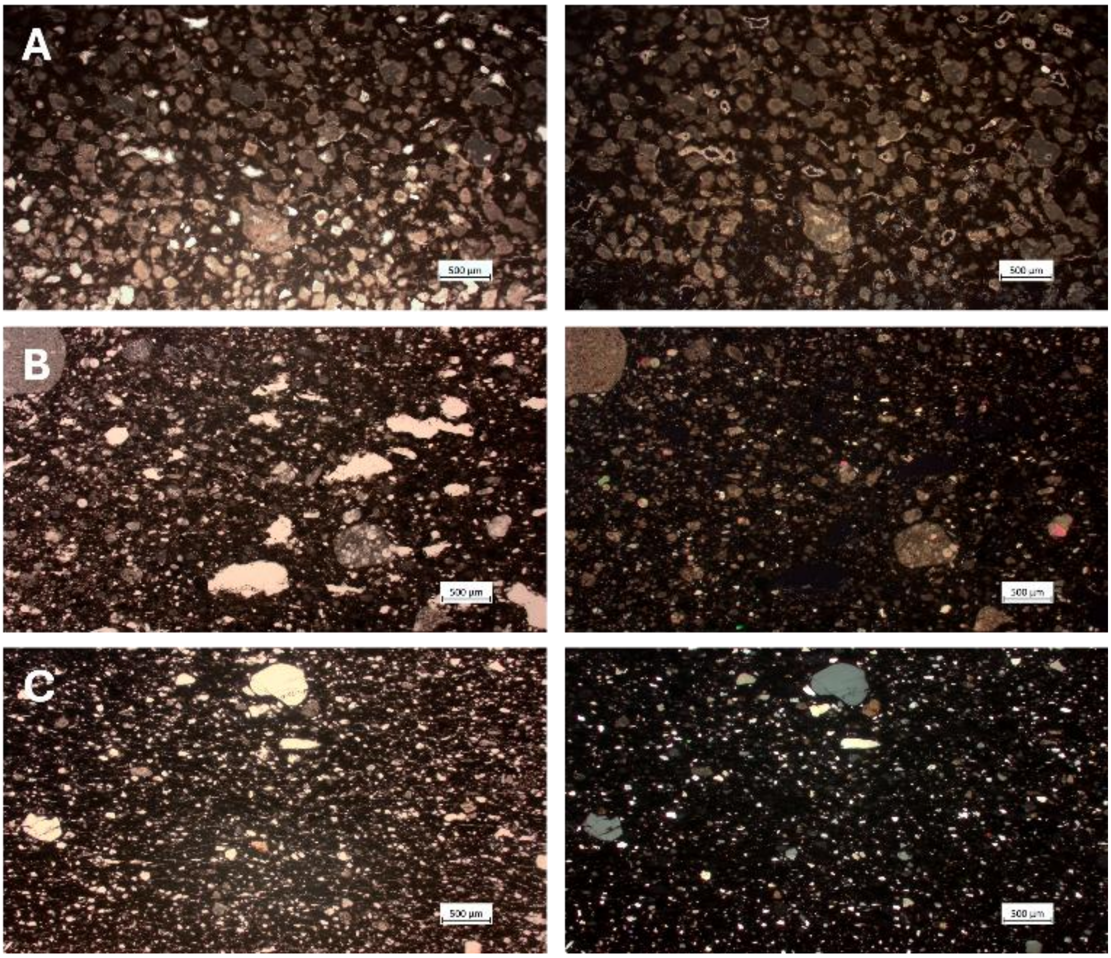

Figure: Optical microscopy (OM) images of the three identified fabric groups in plane-polarized light (PPL) and cross-polarized light (XPL). Scale bar = 500 µm. (A) Dolomite-rich fabric; (B) Microfossil-rich fabric; (C) Quartz-rich fabric.

Yiran Jin

Mineralogical evolution of a cementitious grouting under unsaturated conditions for deep geological repositories

***Authors**: Yiran Jin (ISTerre, France), Alejandro Fernandez-Martinez (ISTerre, France), Damien Daval (ISTerre, France)*

The long-term durability and transformation of the cementitious material MREA (Annular Space Filling Material), developed by ANDRA for sealing disposal cells of high-level radioactive waste in Callovo-Oxfordian clay formations, are investigated under unsaturated and CO_2-rich conditions representative of deep geological storage environments. The study aims to improve understanding of the mineralogical and geochemical evolution of MREA and to evaluate the influence of relative humidity, CO_2 concentration, and temperature on its stability and reactivity. Particular attention is given to conditions simulating hydrogen generation, initial thermal effects, and variations in partial CO_2 pressure, which may significantly affect the long-term performance of sealing materials.

Controlled laboratory carbonation experiments are combined with advanced multi-scale characterization techniques. Bulk analyses are performed using FTIR, TGA, and XRD, while micro- and nanoscale investigations employ SEM-EDX, micro-Raman spectroscopy, FIB-TEM, and NanoSIMS. In addition, $^{13}C/^{12}C$ isotopic analyses are conducted for carbonate quantification, supported by thermodynamic and kinetic modeling to better understand reaction pathways and phase transformations occurring within the material.

This interdisciplinary approach provides valuable insights into cement–mineral interactions under conditions close to those encountered in deep geological repositories. The results contribute to the assessment of the long-term safety, durability, and reliability of engineered barrier materials used in radioactive waste disposal systems.

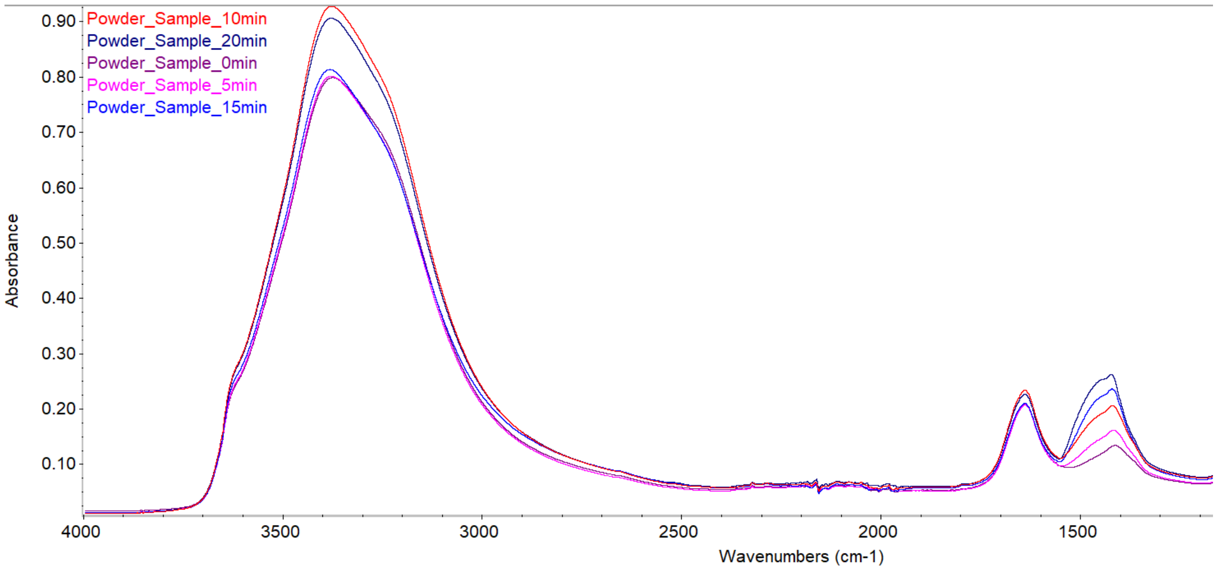

Figure: This figure illustrates the carbonation process of a powder sample exposed to air in an open container over time. The five curves correspond to FTIR spectra collected at 5-minute intervals between 0 and 20 minutes after air exposure. A progressive increase in the absorption peak area near 1400 cm $^{-1}$, from approximately 4 to 21, is observed, indicating the gradual carbonation of the sample with time.

Fabien Letort

Application of µXRF mapping, XANES and HERFD-XAS spectroscopies to determine the distribution and speciation of cadmium in hydroponically grown cacao under micronutrients (Fe, Mn, and Zn) deficiencies

Authors: *F. Letort (ISTerre, France & ESRF, The European Synchrotron, France), G. Sgabiero Montanha (ESRF, The European Synchrotron, France), O. Filimonova (ESRF, The European Synchrotron, France), L. Amidani (ESRF, The European Synchrotron, France), H. Castillo-Michel (ESRF, The European Synchrotron, France) and G. Sarret (ISTerre, France)*

Cadmium (Cd) is a non-essential metal classified as class 1 carcinogen (WHO/IARC, 2025), which can induce detrimental effects for humans. For the general population (excluding smokers), dietary intake is the primary route of Cd exposure. In France, 47.6% of the general adult population exceeded the critical cadmium concentration for bone effects (Oleko A et al., 2021) proposed by ANSES (ANSES, 2019). Understanding Cd speciation in crops is essential to unravel its transport and accumulation pathways, particularly to develop effective mitigation strategies aimed at reducing Cd levels in edible parts. At the European Synchrotron Radiation Facility (ESRF), micro-X-Ray Fluorescence (µXRF) mapping was performed on stem cross-sections to investigate Cd distribution. Under all micronutrient deficiency (Fe, Mn, and Zn) Cd was mainly detected in mucilage cavities, where water and nutrients are stored, as well as in a few cell walls. In addition, X-Ray Absorption Near Edge Structure (XANES) and High Energy Resolution Fluorescence Detected X-Ray absorption spectroscopy (HERFD-XAS) were applied to better understand the speciation of Cd in the different organs of cacao (leaves, stem, roots). Results indicate that Cd is predominantly bound to oxygen ligands. Furthermore, several Cd reference compounds were analysed by XANES and HERFD-XAS in order to develop an open-access database for future Cd speciation studies in crops. Compared with conventional XANES, HERFD-XAS provides enhanced spectral resolution, with sharper and more intense features, as well as additional spectral details. These results offer promising perspectives for identifying Cd speciation in complex environmental samples.

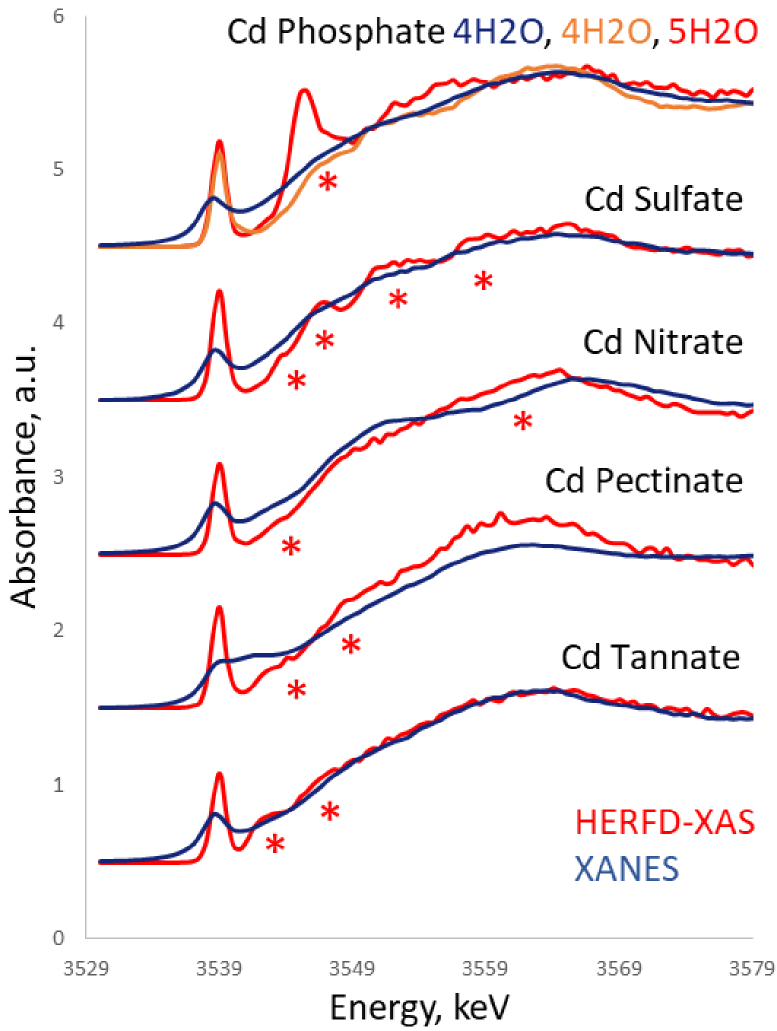

Figure: Comparison of cadmium reference compounds analysed by XANES, in blue, at the ID21 beamline and by HERFD-XAS, in orange and red, at the BM20 beamline, of the ESRF. The new features are showed with the red stars.

Malaury Luzet

Microbial contribution to calcite microtopography and reactivity: Insights from incubations in lake waters

***Authors**: Malaury Luzet (ISTerre, France), Karim Benzerara (IMPMC, France), Delphine Tisserand (ISTerre, France), Didier Jézéquel (IPGP et CARRTEL, France,, Luca Stigliano (University of Oxford, Department of Earth science, United Kingdom), Philippe Ackerer (ITES, France), Damien Daval (ISTerre, France)*

While microorganisms are known to contribute to mineral alteration in natural environments, their relative contribution to chemical weathering remains as debated as the microtopographic features they may generate on mineral surfaces. In this study, we aim to quantify the contribution of lake water microbial communities to calcite dissolution and assess their influence on calcite surface microtopography.

To reach this goal, polished calcite coupons were incubated in waters from four French lakes with different calcite saturation states. Experiments were conducted at two different ecological scales. At the microcosm scale, dissolution experiments were performed under controlled conditions (temperature, light, pCO2) in 0.2 µm-filtered lake water (microorganism-free) or unfiltered lake water. At the macrocosm scale, calcites chips were incubated in Lake Chavoley (Ain, France), either directly exposed to lake water or enclosed in filtration devices preventing contact with microorganisms.

We employed several microscopic techniques, in particular vertical scanning interferometry, to achieve high-resolution surface characterization. Dissolution rates were calculated from these topography images, and microtopography was characterized using quantitative parameters (e.g., surface roughness) and statistical approaches (power spectral density, semi-variograms)

Together, the results collected so far suggest that relationships between microtopography and dissolution conditions (fluid saturation state and microbial presence), previously demonstrated in controlled conditions and with a single-strain biofilm(Stigliano et al., 2023 ; Stigliano, et al., 2025) , may also operate in natural settings.

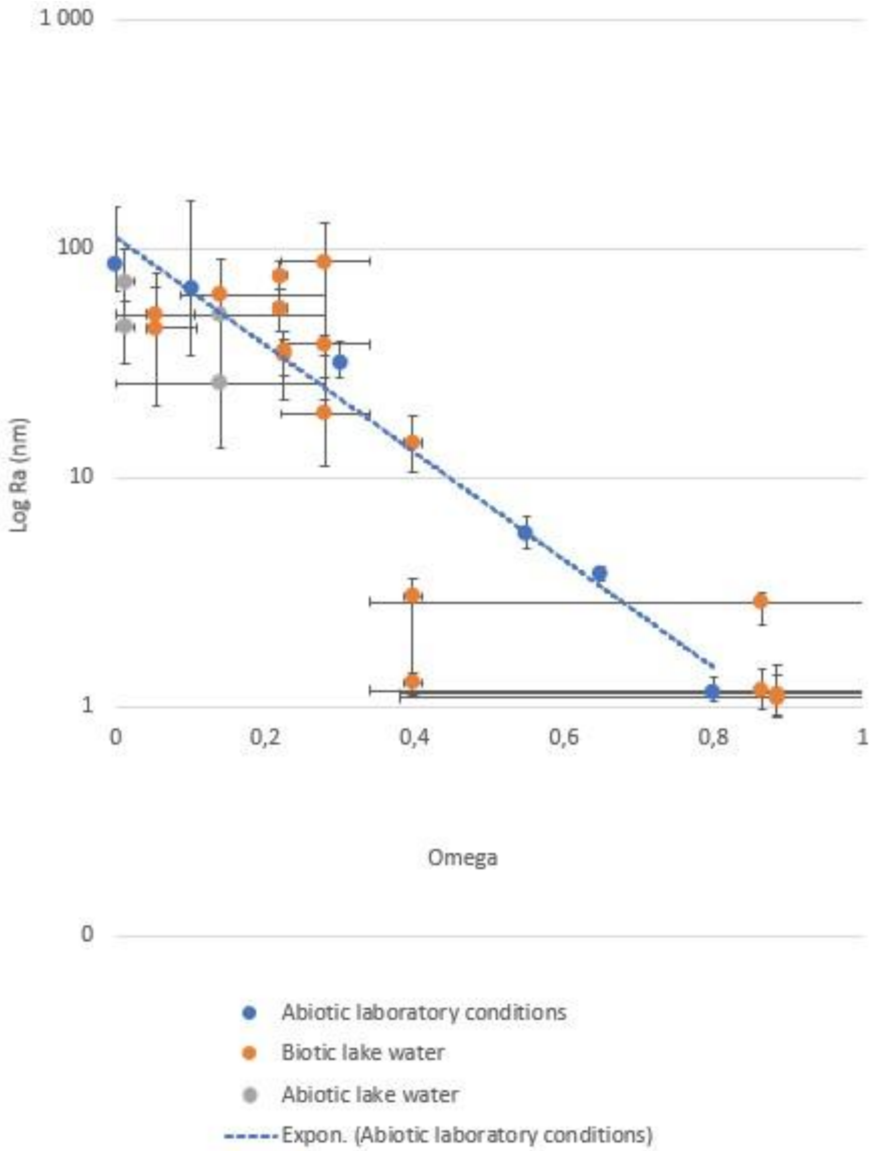

Figure: Surface roughness as a function of the fluid saturation regarding calcite (omega), measured after dissolution in controlled laboratory conditions (fluid containing NaCl, NaHOC3 and different concentrations of CaCl2) or in lake water containing microorganisms or not.

Arpad Pusztai

Shedding new light on basaltic glass weathering by combining reactor and soil column experiments

Authors: *Arpad Pusztai (ISTerre, France), Bastien Wild (ISTerre, France), Damien Daval (ISTerre, France)*

The weathering of calcium and magnesium silicates plays a significant role in the long-term carbon cycle, by initiating the formation of carbonate rock and providing important nutrients for surface ecosystems. Basaltic glass, one of the most reactive and abundant silicate phases, has been extensively studied in laboratories for its dissolution rates and kinetics under varying pH, temperature, and solution compositions. However, laboratory measurements made on freshly ground powders and surface area conversions relying mainly on BET surface area are not necessarily suitable for scaling with dissolution rates. Additionally, only considering surface alteration layers and potential biotic enhancements fails to explain weathering rates measured in natural settings.

To address this gap, this study examined the dissolution of basaltic glass using monoliths with controlled initial surface properties. An approach based on surface sensitive techniques, including vertical scanning interferometry (VSI) and atomic force microscopy (AFM), enabled accurate scaling of the weathering rates to geometric surface area. In-depth investigations of the resulting surfaces unraveled signatures of weathering processes associated with various dissolution conditions. In parallel, similar samples were introduced in soil columns cored from Réunion Island to shed light on factors controlling basaltic glass dissolution in more complex environment. Where overall surface retreats as well as specific retreats related to observed microorganisms were studied.

In addition, we are studying the surface alteration layers developing in both of these experiments to understand a potential reason for observed long term low weathering rates.

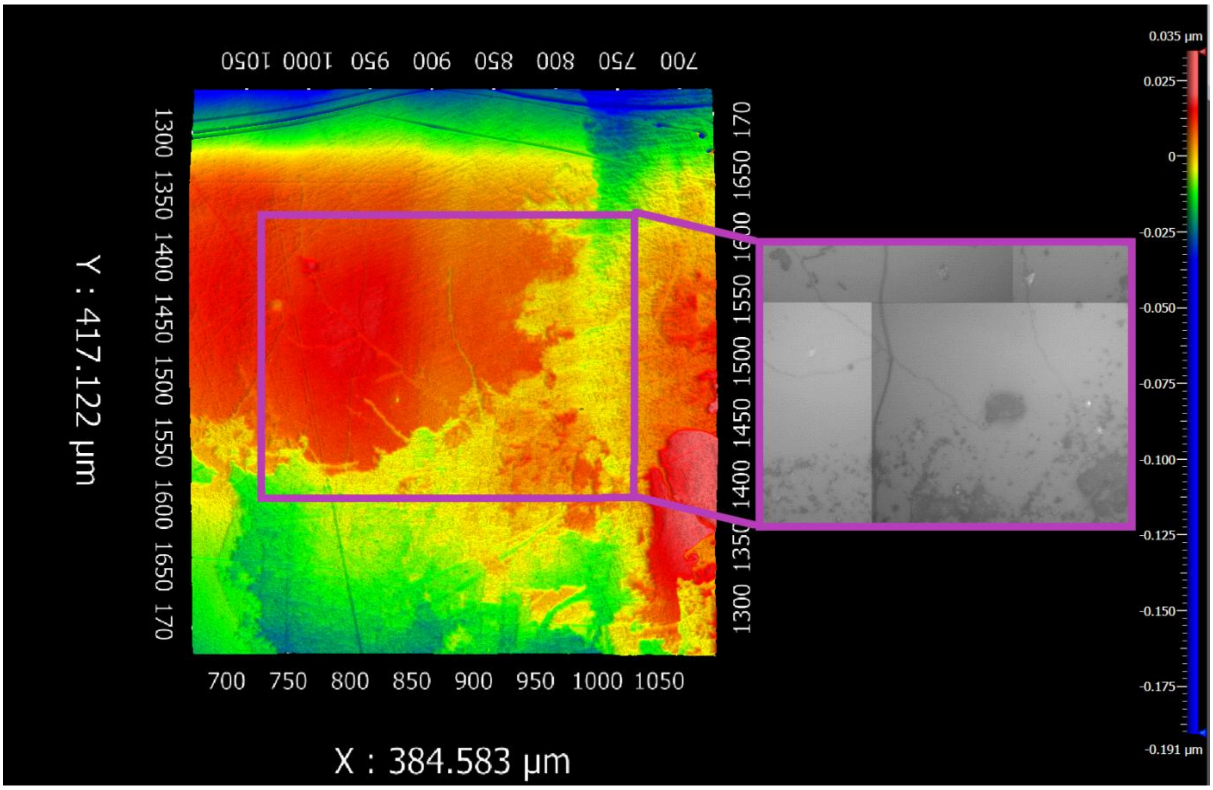

Figure: Side by side topographical (left) and optical image (right) of a fungal colonised basaltic glass surface and resulting direct weahtering enhancement.

Mario Vasquez-Gonzalez

Understanding Mineral Nucleation under Confinement

Authors: *Mario Vasquez-Gonzalez (ILL, ISTerre, France), Alex Fernandez-Martinez (ISTerre, France), Diane Rebiscoul (CEA, ICSM, France), Gabriel Cuello (ILL, France).*

Mineral nucleation pathways have been extensively studied in bulk solutions, where disorder precursors such as ion pairs eventually lead to precipitation through liquid-liquid separation and dehydration in the well-known prenucleation cluster (PNCs) pathway. However, the evolution of these systems under Single-Digit Nanoconfinement (SDN) remains poorly understood.

In mesoporous silica MCM-41 confinement alters electrostatic screening and hydration structure, thereby modifying the stability and mobility of cations, anions, ion pairs. As a consequence, the SDN regime can promote ions adsorption and pore clogging.

Understanding how electrolyte interactions under SDN lead to precipitation is critical for developing reliable technologies such as those related to fluid transport in geological media (e.g., nanopores in clay minerals), or separation membranes such for water desalination, which often encounter problems related to mineral precipitation and scaling.

Here, we employed a methodology for ion sorption in MCM-41 followed by characterizations such as ATR-FTIR, and Pair Distribution Function (PDF) derived from high-resolution XRD measurements at ID22 (ESRF). Our aim is to extract essential information of the interactions governing the confinement, and, thus, how nucleation proceeds under these specific conditions.

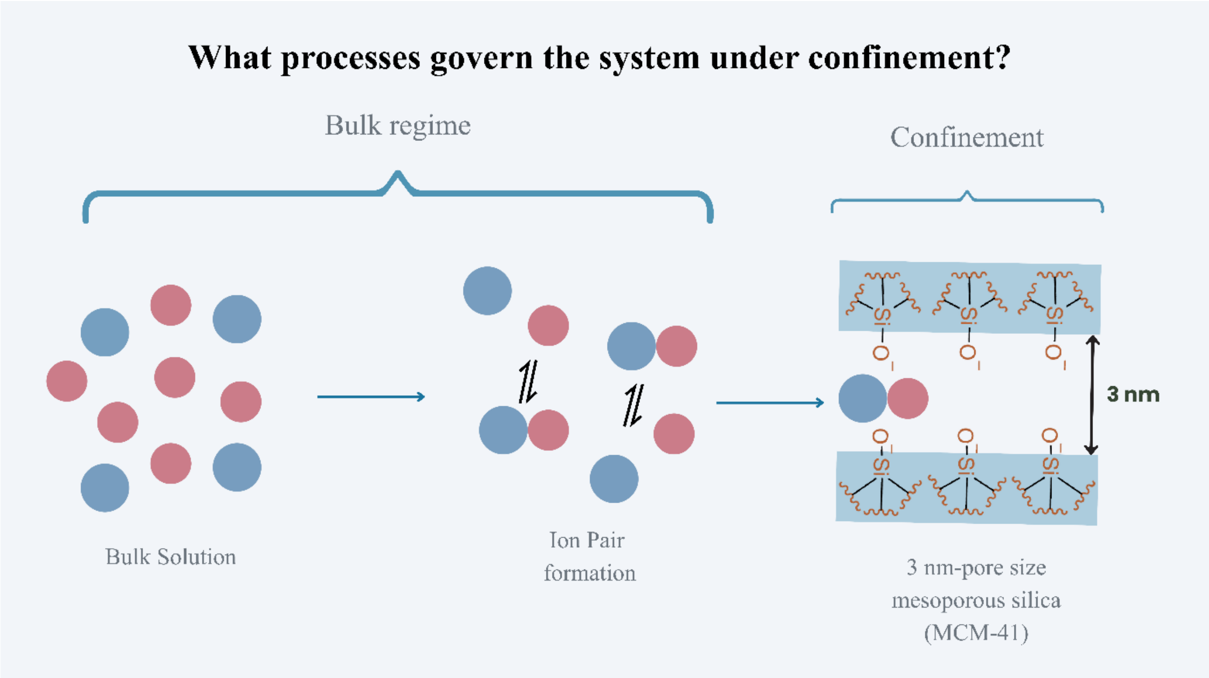

Figure: From ion pairs in bulk solution to nucleation under confinement.

Geodynamo

Lucie Canet

The effect of iron on the local structure and density of silicate melts under extreme conditions.

***Authors**: Lucie Canet (ESRF and ISTerre, France), Angelika D. Rosa (ESRF, France), Renaud Deguen (ISTerre, France), Silvia Boccato (IMPMC, France), Lélia Libon (Carnegie, USA), Clemens Prescher (Freiburg University, Germany), Christoph Otzen (Freiburg University, Germany), Mohamed Mezouar (ESRF, France), Guillaume Morard (IMPMC, France).*

Seismic observations of ultra-low velocity zones (ULVZs) at the core-mantle boundary (~2900 km depth) suggest the presence of a silicate dense melt layer at the base of the mantle. Such a layer is commonly interpreted as a remnant basal magma ocean, preserved after metal-silicate differentiation and partial crystallization of the early Earth's mantle. The existence of a stable melt layer at these extreme conditions has important implications for the chemical stratification of the lowermost mantle, the evolution of mantle convection, and the long-term storage of incompatible elements and volatiles. Geodynamic models and geochemical proxies support the potential for melt retention at the core-mantle boundary, yet the stability of silicate melts remains debated due to their typically lower density relative to surrounding crystalline phases. Resolving this requires quantitative constraints on melt density and structure under lower-mantle pressures.

Experimental data addressing the effect of iron on silicate melt properties at relevant pressures, however, remain sparse because of the challenges associated with probing weakly scattering amorphous materials at extreme conditions. To address this, we conducted in situ synchrotron X-ray diffraction experiments on Fe-bearing silicate glasses of composition (Mg1-xFex)SiO3 (x = 0, 0.1, 0.2, 0.4) up to 135 GPa at the ESRF ID27 beamline. High-energy X-rays (55 keV) combined with an optimized multichannel collimator system allowed data acquisition over an extended Q range, enabling detailed pair distribution function analyses. Mass density estimates indicate a pronounced effect of Fe content above ~20 GPa, while the atomic density remains nearly constant, consistent with Fe substituting for Mg in the silicate structure. Combined, these studies advance our understanding of the physical and chemical behavior of silicate melts at core-mantle boundary conditions, addressing fundamental questions about melt stability, density, and the role of iron.

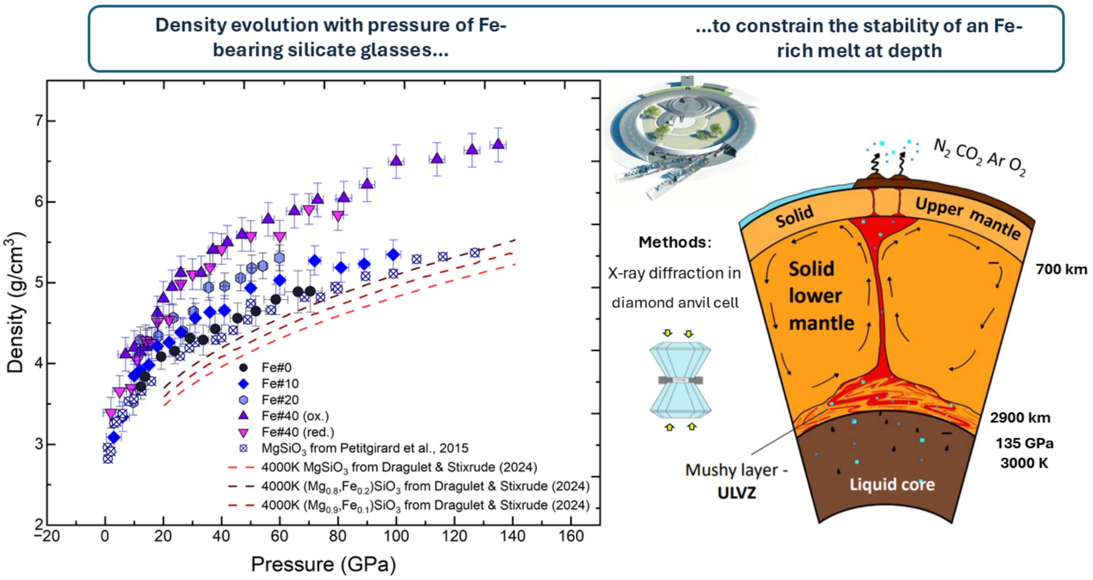

Figure: Left - Density evolution with pressure of several Fe-bearing glasses experimentally measured at 300 K, compared to AIMD simulations by Dragulet and Stixrude (2024) at 4000 K (dashed lines) and previous experimental data from Petitgirard et al. (2015). Middle - Sketch of synchrotron ESRF and diamond anvil cell, which correspond to the method used in this study. Right - Drawing of present-day Earth's interior highlighting a deep mushy layer at the core-mantle boundary.

Thea Lepage

Response of a Fluid Core to Variations of an External Magnetic Field

***Authors**: Thea Lepage (ISTerre, France), Dominique Jault (ISTerre, France), Nicolas Gillet (ISTerre, France)*

The electric conductivity of the Earth's lowermost mantle remains a terrestrial property under ongoing investigation. The magnetic field originating from the core has to penetrate the mantle before reaching the surface. Due to its non-zero conductivity, the mantle acts as a filter on this field. In order to study this quantity, different methods are in use. One of them is electromagnetic tomography, where the external and internal magnetic field are inputs for the inversion of mantle conductivity profiles. The difficulty lies in the depth, where the uncertainties become more significant. In particular, evidence from other methods such as seismology or mineralogy hint towards higher conductivity in a shallow area on top of the core-mantle boundary, possibly related the large-scale structures such as large low velocity provinces and ultra low velocity zones.

In this work we want to investigate on the method's assumption of a solid core. The response of a solid differs significantly from that of a fluid, and this simplification might affect the accuracy of mantle conductivity studies from above. Core configurations with different rotation rates and dynamo magnetic fields are used to compare their solid and fluid response, respectively. To illustrate the complexities that can arise, the figure below shows how decreasing the rotation rate (and thus increasing the magnetic Ekman number) affects the fluid response. In the upper panel the fluid response (lines) coincides remarkably well with its solid counterpart (background). The next panels, however, deviate increasingly both in length scale and in complexity. One objective is to see at what point the solid assumption breaks and understand the physics behind. On the other hand, we would like to comment on the reliability of the conclusions on a conducting layer at the bottom of the mantle and its lateral variations.

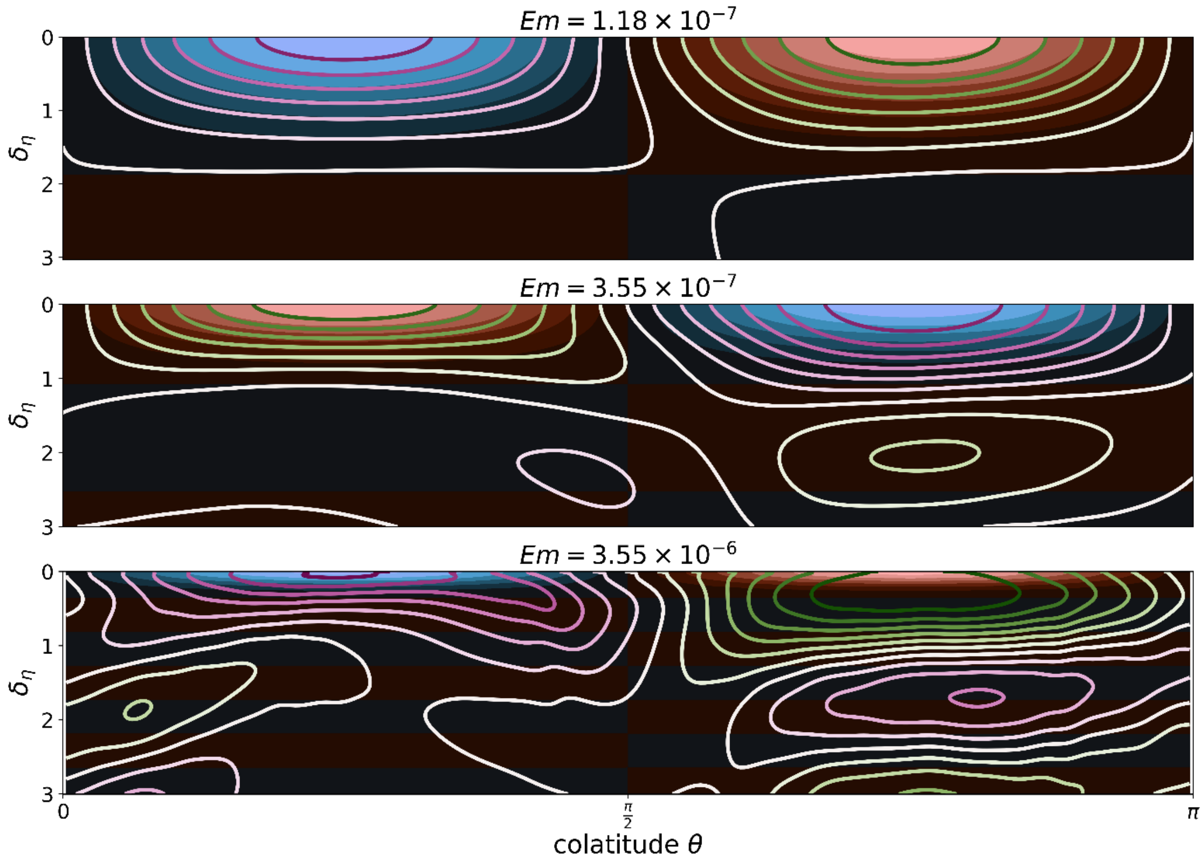

Figure: The spheroidal magnetic field inside a cross section of the boundary layer for three skin depths and different magnetic Ekman numbers. The simulated fluid response is drawn as lines on top of the analytical solid response. The scaling of the contours is the same for fluid and solid.

Preshtibye Raggoo

Inner Core Rotation, Waves in Earth's Core, and Length-of-Day Variations: Characterizing Torsional Alfvén Wave Reflection Using High-Resolution Simulations

***Authors**: P. Raggoo (CNES, France & ISTerre, France), N. Gillet (ISTerre, France), D. Jault (ISTerre, France)*

Recent seismic observations indicate that the differential rotation of Earth's solid inner core experienced a multidecadal transition from prograde to retrograde around 2008 [2]. Such variations fundamentally involve fluid motions within the liquid core, which are magnetically and gravitationally coupled to both the inner core and the solid mantle [1]. High-resolution geomagnetic data from satellite missions (CHAMP, Swarm, and Macau MSS) have captured rapid, interannual core surface flows. Yet, closing the global angular momentum budget to reconcile observed geodetic Length-of-Day (LOD) variations remains a persistent puzzle. While 7-year non-axisymmetric hydromagnetic waves propagate near the equator [3], global angular momentum transfer is dominated by axisymmetric torsional Alfvén waves (TAWs) oscillating throughout the fluid volume [4]. The efficiency of this coupling depends heavily on how TAWs reflect off or dissipate within a thin, conducting layer at the base of the mantle. As a critical step toward resolving this coupling mechanism, my current work focuses on testing and comparing both axisymmetric and non-axisymmetric wave signatures using the 3-D numerical code XSHELLS [5]. To ensure that our simulations are robust enough to transition into complex geometries, we benchmark our hydrodynamic profiles against the established axisymmetric framework of torsional wave absorption at the equator developed by Schaeffer and Jault (2016) [6]. Specifically, we model a localized geostrophic TAW pulse interacting with a thin conducting mantle boundary layer ($\Delta = 0.025$). Operating at extreme regimes (E = 10−10, S = 104) requires a highly refined grid (N R = 5000) to resolve the microscopic boundary layer structures. We map the wave reflection coefficient (|R|2) across a wide spectrum of the mantle conductance parameter Q (10−3 ≤Q ≤102). The models successfully capture the transition from an insulating regime to perfect transmission at the resonance threshold (Q ≈1). Crucially, we identify severe numerical instabilities triggered by sharp magnetic gradients at the fluid-solid interface and outline the grid optimizations necessary to maintain stability. This framework establishes the foundational boundary parameters necessary to later ingest space-based magnetic observations into a complete dynamical model.

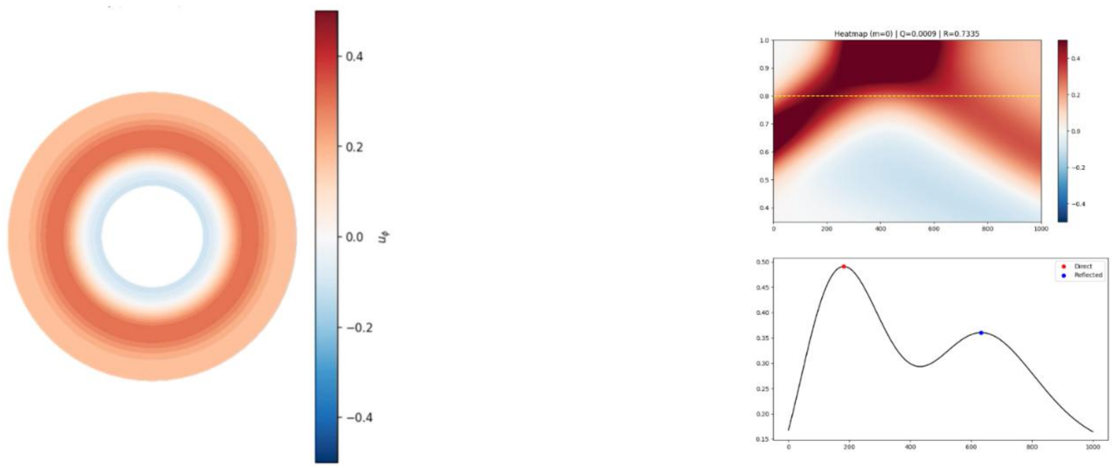

(a) Equatorial snapshot of u_ϕ.

(b) Space-time peak tracking.

Figure: XSHELLS benchmarking diagnostics for a simulated torsional Alfvén wave (TAW) pulse. (a) Equatorial cross-section of the azimuthal velocity field (uϕ), displaying the axially invariant geostrophic rings characteristic of axisymmetric core waves. (b) A radius-time heatmap evaluation under a weakly conducting mantle regime (Q = 0.0009). Peak identification isolates the incoming direct wave front from the boundary-reflected wave packet to quantify the global reflection coefficient (R).

Amélie Schulze

Two Phase Compaction-Convection Model for Inner Core Flows

Authors: *Amélie Schulze (ISTerre, France), Renaud Deguen (ISTerre, France), David Cébron (ISTerre, France), Stéphane Labrosse (LGL-TPE, France)*

Partially molten layers are common in geophysics, from solidifying magma oceans to icy satellite shells or the lowermost lunar mantle. Their thickness can reach hundreds of kilometres, making microscale simulations of solid–liquid interactions impractical.

Building on mesoscopic volume-averaging approaches, we develop a unified non-linear fluid dynamics model describing percolation, compaction, convection, and phase change in two-phase flows. Phase transitions are treated by relating melt fraction to the phase diagram, enabling efficient calculations. We also examine how different formulations of the viscous stress tensor affect convective vigor, an open question in the literature. Finally, we introduce a smooth, self-consistent treatment of the transition between partially molten and fully solid or fully liquid regions, allowing robust modelling of evolving planetary interiors. Future work will explore whether the seismic anisotropy of the Earth's Inner Core could originate from compaction-driven convective flows.

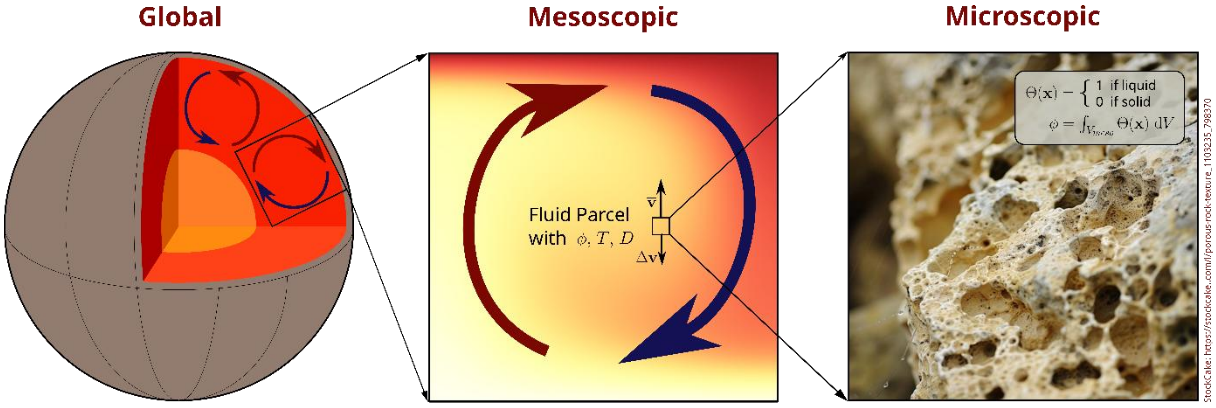

Partial melting in a convecting solid layer of a planetary body

= pressure changes and volatile elements locally alter melting temperature of the rock

Fluid parcels in the simulation still contain a **large** number of pores

Solid viscously deforming crystal matrix with **liquid**-filled pores

Geophysics Of Seismic And Gravitational Risks

Houssam AL JAMAL

Comprehensive seismic damage predictions at building scale in Beirut for a large earthquake on the Mount Lebanon thrust fault

Authors: *Houssam AL JAMAL (ISTerre, France & American University of Beirut, Department of Civil and Environmental Engineering, Lebanon), Cécile CORNOU (ISTerre, France), Mayssa DABAGHI (American University of Beirut, Department of Civil and Environmental Engineering, Lebanon), Mathieu CAUSSE (ISTerre, France)*

Ground motion simulation is essential for seismic risk assessment in regions with limited strong-motion records. Lebanon lies along the Dead Sea Transform fault system, which has generated major historical earthquakes despite recent low to moderate seismicity. One of the largest events, the AD 551 offshore Lebanon earthquake (Ms 7.3), linked to the Mount Lebanon Thrust fault (MLT), devastated Beirut. Given Beirut's dense population, the recent introduction of seismic design regulations, and the lack of recorded strong-motion data from MLT, simulating ground motions from the MLT is critical. In this thesis, I first identified plausible earthquake scenarios for the AD 551 earthquake on the MLT by integrating historical and geological evidence and matching observed coastal uplift data with simulated static deformations from candidate MLT scenarios. Next, I developed an improved hybrid ground motion simulation method that combines deterministic low-frequency (LF) simulations with stochastic high-frequency (HF) modeling. The LF component simulation uses kinematic rupture models and a recently developed one-dimensional velocity model for Lebanon, while the HF component applies a near-fault site-based stochastic model conditioned on LF ground-motion characteristics. The developed approach will be used to simulate ground motions across a grid of sites in Beirut and generate pseudo-spectral acceleration spectra for the selected rupture scenarios. The figure below shows pseudo-spectral acceleration of simulated broadband ground motions from one of the identified plausible ruptures at one station in Beirut. Future work will use the simulated ground motions for comprehensive city-scale structural damage assessment in Beirut, which can provide valuable insights into the seismic risk in the city.

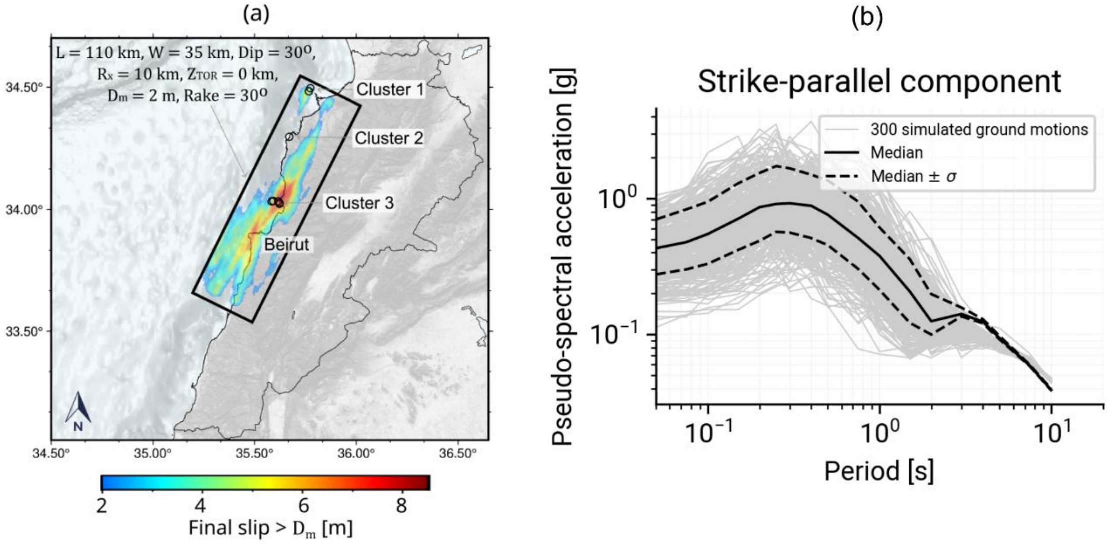

Figure: Broadband ground-motion simulation in Beirut for an AD 551–like earthquake scenario on the Mount Lebanon Thrust fault. (a) Map of the selected most plausible earthquake scenario, including its source characteristics and the slip distribution of its corresponding best kinematic rupture model. (b) Pseudo-spectral acceleration of 300 simulated broadband ground motions at a station in Beirut, generated using the same kinematic rupture model shown in (a) but different realizations of the site-based stochastic model parameters.

Pauline Georges

Evaluation of apparent anelastic attenuation in Europe and Ground Motion Models

Authors: *Pauline Georges (ISTerre, France), Sreeram Reddy Kotha (ISTerre, France) and Emmanuel Chaljub (ISTerre, France)*

Waves travelling through the Earth are attenuated by the intrinsic caracteristics of the medium and the asperities of the model called scattering. Estimating the attenuation is necessary in hazard assessment, estimating magnitudes and imagery of the Earth. Despite many studies, attenuation is complicated to model because attenuation is dependant to the path so extracting it from a seismic network is difficult. Moreover the interdependance of magnitude estimation and attenuation complexifies the problem.

Generally, attenuation is constrained as a decrease with distance, but many studies show 3D variation. That is why a response spectra ground-motion model (GMM) has been constructed for shallow crustal earthquake in Europe taking into account a large amount of data and small magnitudes, and a better estimation of the regionalised attenuation with a grid regionalisation and a better estimation in the model. To analyse directly the response of the ground, the model is adapted in Fourier amplitude. The model is a partially non ergodic GMM presenting a regionalised attenuation for Europe. However, the model is data-driven and if many earthquakes are recorded in Greece, Italy or the Alps who have high seismicity, other countries or regions as Parisian basin in France or the north of Europe who have lower seismicity can lack of records. Then the model cannot be adapted to those regions and hazard assessments are limited. To solve this problem, a better understand of the attenuation phenomenon is required. Focusing on France where data are largely available, regionalised attenuation model from GMM is compared to attenuation tomography. Then this attenuation is correlate to geophysical and geological parameters to estimate a proxy. In a further time, this work could be improve the modelisation of the GMM and directly the hazard assessment.

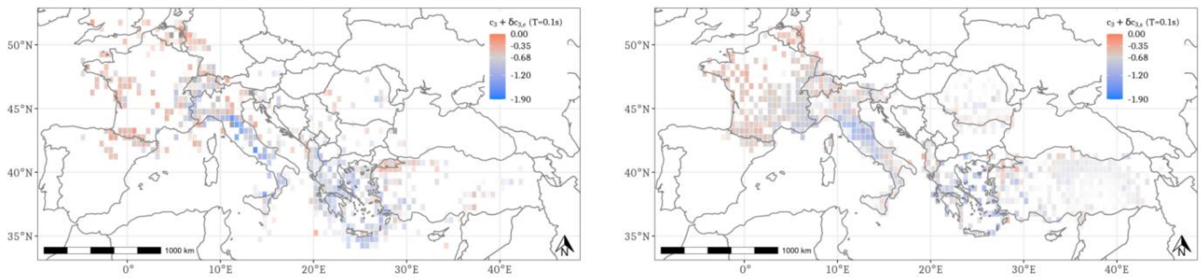

Figure: Spatial distribution of apparent anelastic attenuation variability across Europe for T = 0.1 s. Left: source-based attenuation (colored for cells containing earthquakes); right: site-based attenuation (colored for cells containing stations). Blue colors indicate regions with lower ground motion due to higher attenuation relative to the median prediction; red colors indicate regions with higher ground motion due to lower attenuation relative to the median prediction.

Aude Gounelle

Understanding multi-physics multi-scales phenomena governing seismic ground motion predictions -- Application to the Le Teil earthquake

***Authors**: Aude Gounelle (BRGM, France & ISTerre, France), Florent De Martin (BRGM, France), Emmanuel Chaljub (ISTerre, France)*

On November 11, 2019, a magnitude Mw = 4.9 earthquake shook Le Teil town (Ardeche), occurring on a fault not identified as active during the construction of the active fault base (BDFA Jomard et al., 2017). Le Teil region is marked by a major sedimentary basin, filling the Messinian canyon of the Rhone River. This generates major site effects. However, the influence of geology on seismic wave behaviour is not solely linked to site effects generated by recent sedimentary deposits: bedrock, often considered a homogeneous layer, can also present a complex structure, incorporating lithological interfaces with strong impedance contrasts, a potential source of reflections and refractions.

Numerical modelling enables us to study the impact of the above-mentioned structures on wave paths, and thus to better understand the effects of geology, which can locally modify the hazard. However, models are based on uncertain data: poorly documented lithostratigraphy's structure, relationship between geological structures and seismic velocity structures, etc. Therefore, to improve hazard knowledge, it is necessary to identify all these sources of uncertainty, and to study them to understand their impact on the seismic signal and thus be in a position not only to quantify the uncertainty linked to the hazard, but also to guide future research to reduce it. To this aim we have done a global sensitivity analysis using Sobol Indices (Sobol 2001), testing both sources and velocity model parameters, and highlighting the impact of surface structures velocities, up to 50% of the variability in some part of the model.

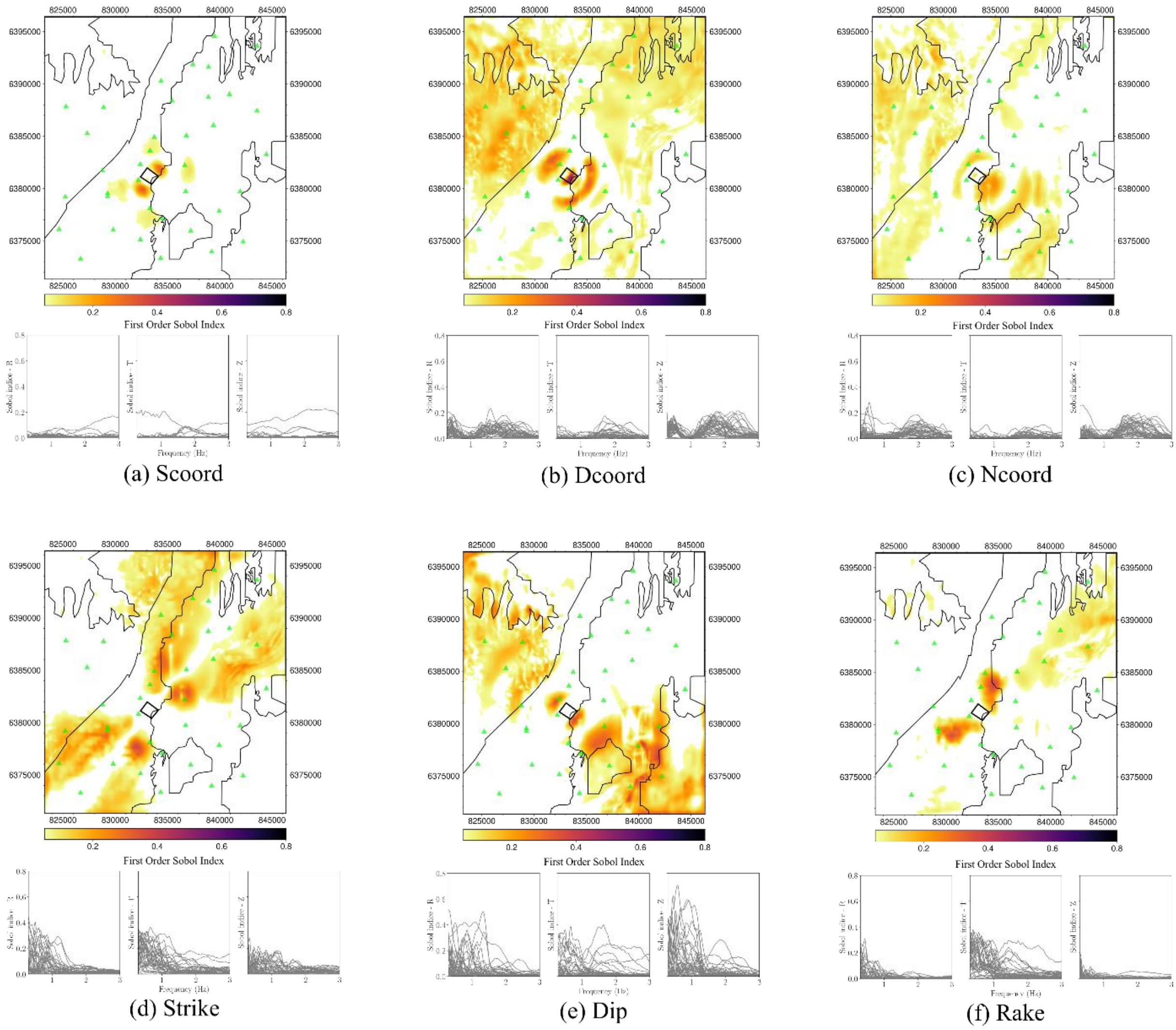

Figure: Sobol indices computed on both PGV map and receptor FFTs for source mechanism (d-f) and location (a-c) parameters. The black rectangle on the map indicate the source uncertainty area, the green triangle the receptor locations. On the Sobol indices over FFTs plot, each curve is a different receptor.

Laureen Maury

Large Scale Slope Deformation in Upper Mustang (Nepal) : Factors and Impacts

***Authors**: Laureen Maury (ISTerre, France), Kristen Cook (ISTerre, France), Basanta Raj Adhikari (Tribhuvan Univeristy, Nepal), Pascal Lacroix (ISTerre, France)*

Climate change is expected to have a significant impact on geomorphological activity, especially in high mountain ranges. Models predict increased ground movement due to (1) an increase in water infiltration from melting snow, (2) reduced soil and rock cohesion caused by permafrost degradation, and (3) post-glacial slope decompression. This project focuses on slow-moving landslides (~1 m/y), which allow detailed monitoring of their physical properties. We focus on Upper Mustang, a high-altitude (>3,000 m), dry sedimentary valley located between the Himalayas and the Tibetan Plateau. Its landscapes are highly sensitive to climate variations and marked by large-scale slope deformations, making it ideal for studying landslide evolution. Although these landslides have been recognized for a long time, their characteristics (location, extent, speed) have never been systematically studied, largely due to the valley's remote location and high altitude. Our approach combines two remote sensing methods: optical image correlation and InSAR (Interferometric Synthetic Aperture Radar). By analyzing high-resolution Pleiades images (2013–2025) and Sentinel-1 InSAR data (2014-2025), we mapped ground deformation over a decade, creating an exhaustive landslide inventory. Time-series of displacement were generated using PlanetScope images (2016–2025) for landslides moving at cm/y to m/y, and Sentinel-1 data for slower deformations (mm/y to cm/y). A field mission helped to characterize the landscapes of major landslide areas (Muktinath, Dhe, Yara-Ghara). The results highlight the complementary nature of InSAR and optical image correlation for mapping and monitoring slope deformation in Upper Mustang, which has so far enabled the detection of ~200 landslides covering 90 km^2 (9.6% of the study area), predominantly in upper valleys, suggesting permafrost influence. Their temporal evolution varies which could indicate different triggering and controlling factors (climate, human activity, geology). This study demonstrates the critical role of slow-moving landslides as indicators for understanding broader landslide mechanisms, including both slow and rapid events.

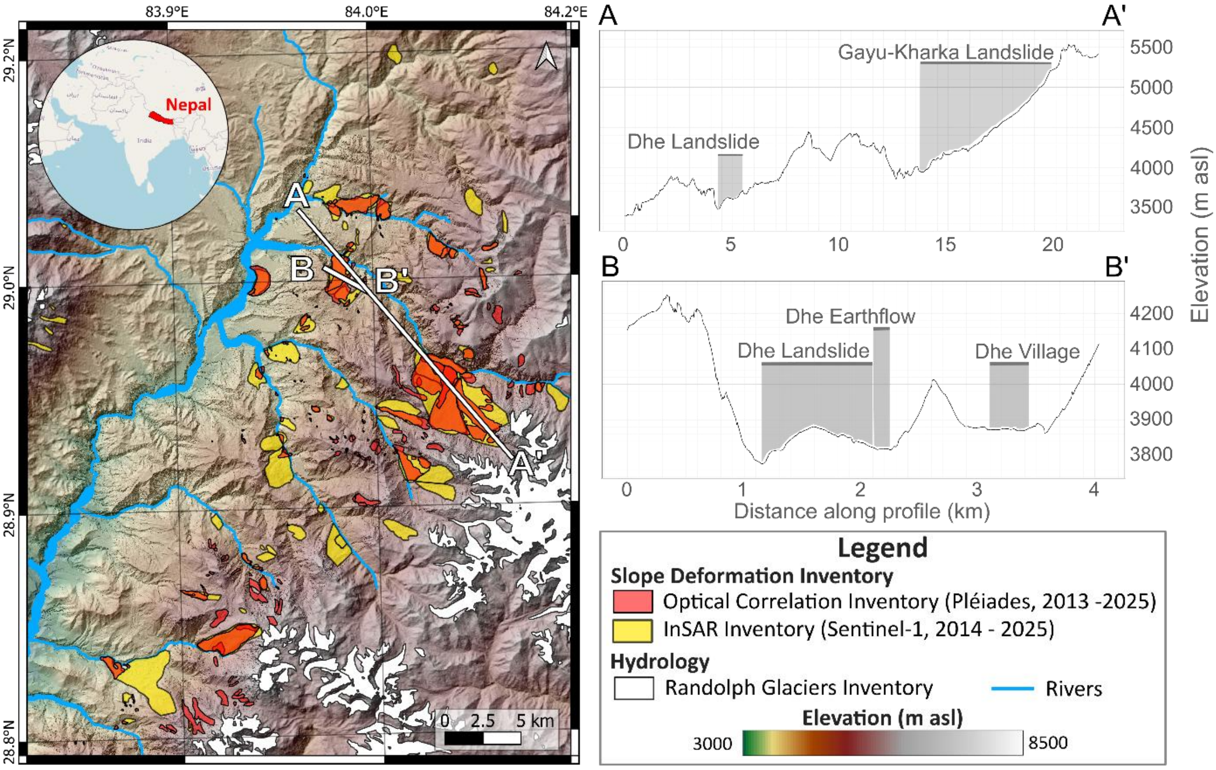

Figure: Inventory of active slope deformations between 2013 and 2025 in Upper Mustang (Nepal) produced using optical image correlation of Pléiades Images (red) and InSAR processing of Sentinel-1 data (yellow). Elevation profile of two major areas of interest, the Dhe tributary valley (A-A'), showing the deformations at Dhe and Gayu Kharka, and a focus on the Dhe area (B-B'), illustrating the diversity of deformations, with a slow-moving zone (~1 m/y), a rapid earthflow (several meters per year), and the Dhe village built above a highly weathered area, prone to mass movement.

Georges Sabback

High-Resolution Multi-Scale Multi-Dimensional Seismic Numerical Twin Based on Massively Parallel High-Performance Computing and Artificial Intelligence - Application to Microzonation of Alpine Valleys

Authors*: Georges Sabback (BRGM, France & ISTerre France), Cécile Cornou (UGA, France), Florent De Martin (BRGM, France)*

The Grenoble basin (French Alps) is a deep alpine sedimentary valley where seismic site effects are strongly controlled by complex 3D wave propagation within kilometer-scale deposits and surrounding high-relief massifs. Reliable seismic microzonation in such settings requires physics-based modelling that goes beyond 1D assumptions and accounts for basin geometry and heterogeneities.

This study combines high-resolution numerical simulations and data-driven analysis within a Seismic Numerical Twin framework using the spectral-element code EFISPEC3D (up to 2 Hz). A variance-based global sensitivity analysis (Sobol indices) is performed on 512 3D simulations with vertically incident plane-wave excitation in two horizontal polarisations. Key uncertain parameters include P- and S-wave velocity gradients and sediment attenuation (Q factors), constrained by 1D dispersion inversions and combined velocity models (ESG2006 and Ito et al., 2021). So far, results for PGD show that sediment velocity structure and attenuation dominate ground-motion variability.

In parallel, a clustering framework is developed for microzonation by integrating 1D and 3D response spectra, observed H/V ratios, and Eurocode 8 (EC8) parametric spectra. Features from 15 input accelerograms are analysed using k-means and learned embeddings to derive compact representations of site response. Clusters are consistent with sediment thickness, basin-edge effects, and resonance frequencies inferred from H/V data.

Overall, the sensitivity analysis identifies key physical controls on seismic response, while clustering translates heterogeneous datasets into coherent microzonation patterns. The combined approach provides a robust basis for uncertainty-aware seismic hazard characterisation in complex alpine valleys.

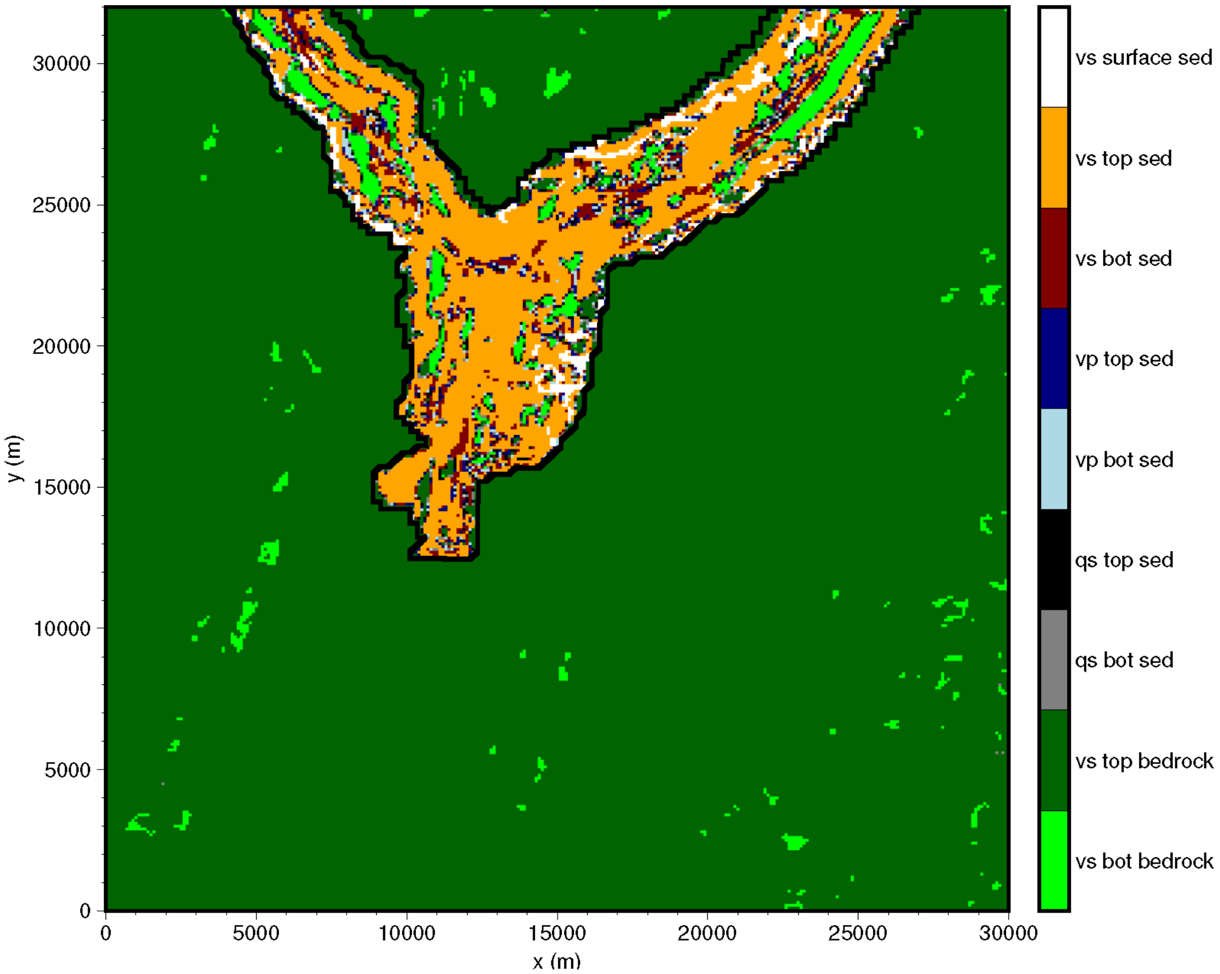

Figure: Dominant parameter controlling peak ground displacement (PGD) in the 3D simulations for the East–West (X) component, defined as the parameter with the highest first-order Sobol sensitivity index among the nine tested uncertain inputs. Colour code indicates the corresponding parameter for each location.

Valentin Schindelholz

Soil-compaction rates from PS-InSAR as a future proxy for resonance periods inferred in various sedimentary valleys

***Authors**: Valentin Schindelholz (ISTerre, France), Emeline Maufroy (ISTerre, France)Cécile Cornou (ISTerre, France)*

Alluvial valleys are made of sedimentary deposits that accumulate over long periods of time, building up a rather soft soil layer in comparison with the more rigid underlying bedrock. The resulting impedance contrast leads to the so-called sedimentary site effect that tends to increase both in amplitude and duration the earthquake ground motion. To assess the sedimentary site effect, different parameters are commonly used, such as the fundamental-resonance frequency of the sedimentary column (f0) or the depth of the bedrock (Hbed). To retrieve those parameters, it is possible to carry out expensive and time-consuming in situ measurements. To complement them, we propose a new proxy to estimate the fundamental-resonance period (T0, the inverse of f0) based solely on freely available vertical ground displacements from Persistant Scatterers Interferometric Synthetic Aperture Radar (PS-InSAR) at the European scale (EGMS).

Outside of active tectonic deformations and of anthropogenic disruptions such as fluid pumping or mining, the compaction of Quaternary sediments caused by their own weight results in land surface subsidence. When the thickness of the sediment column increases, the compaction rate is larger, leading to a faster subsidence rate. Thicker soft sediment deposits are also characterized by larger T0. By measuring accurately the soil surface displacement, it is possible to find an estimate of T0. The PS-InSAR technique allows us to obtain millimetric precision of vertical-displacement rates averaged over multiple years, with a decametric spatial resolution in urban areas.

Using available T0 and Hbed data in various sedimentary valleys, we derive models allowing us to retrieve the spatial variation of T0 (or Hbed), with a high spatial resolution. We observe that the obtained models are different between each valley, and that their parameters are related to the age and nature of the deposits. This soil-compaction proxy could be used for microzonation and site characterization studies.

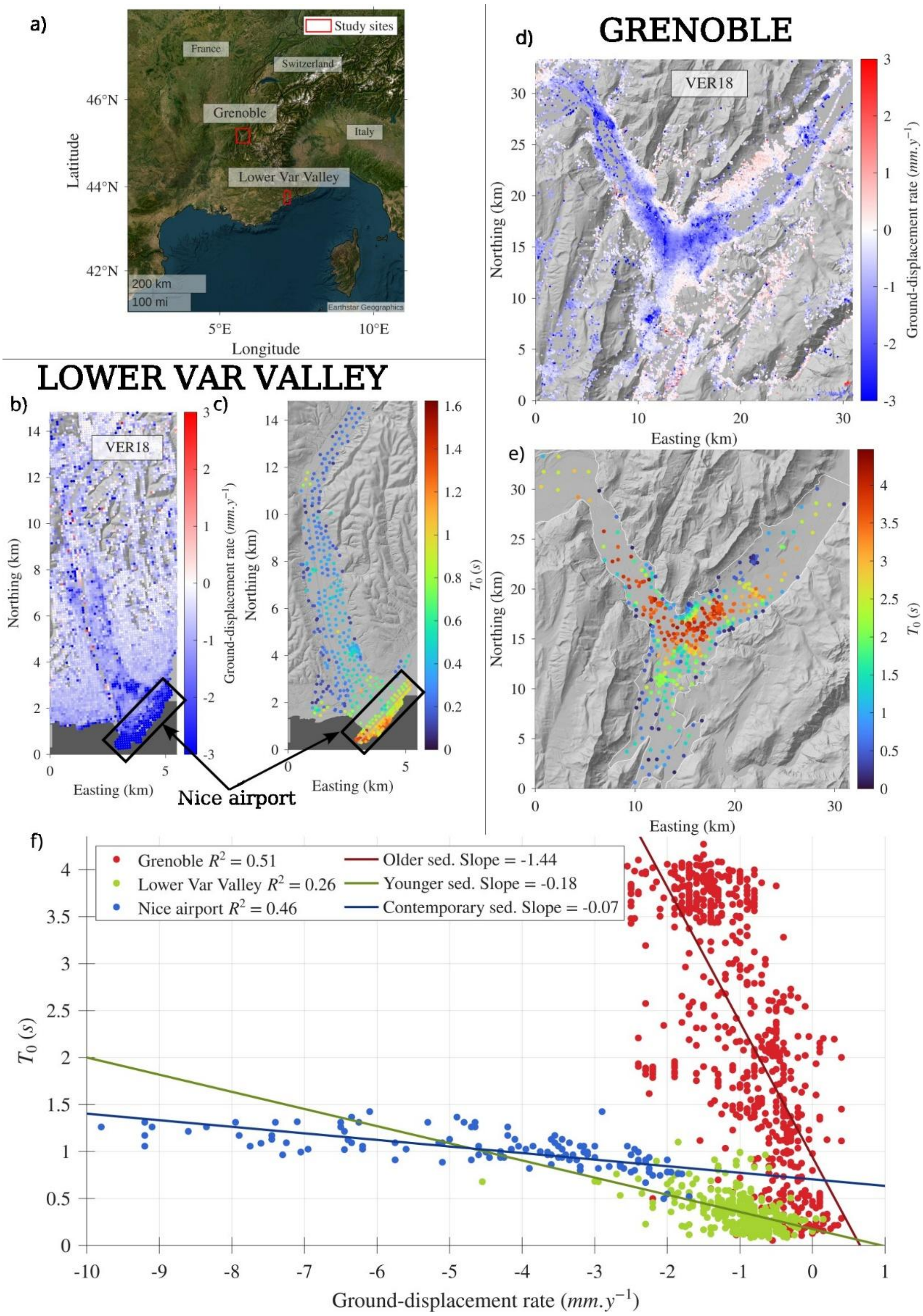

Figure: a) Location of the two valleys used in this work. b) and c) Maps of the subsidence rates and resonance periods, respectively, in the Lower Var valley, Nice. The sub-area of the Nice airport is delimited by the black square. d) and e) Maps of the subsidence rates and resonance periods, respectively, in the Grenoble valley. f) Scatter plot and linear *regression of the resonance period vs the ground-displacement rates for the Grenoble valley (red), the Lower Var valley (green), and the Nice airport (blue).*

Hongyi Su

A bayesian framework for near-fault ground motion reconstruction from in-situ observation: case study of the 2019 Le Teil earthquake

***Authors**: Hongyi Su (ISTerre, France), Mathieu Causse (ISTerre, France), Cécile Cornou (ISTerre, France), Sébastien Hok (ASNR, France), Céline Gélis (ASNR, France)*

Near-fault ground motion (NFGM) plays a critical role in seismic hazard assessment, particularly in regions located close to surface-rupturing faults. However, global strong-motion networks remain sparse, and data are often unavailable in the immediate vicinity of ruptured faults. This limitation is exacerbated by the occurrence of earthquakes on faults which activity was not recognized, which prevents effective pre-event deployment of strong-motion instruments. A notable example is the 2019 Mw 4.9 Le Teil earthquake in southeastern France, which ruptured La Rouvière fault. Despite the absence of strong-motion instruments in the epicentral area, many in-situ observations, such as broken rocks, displaced grave slabs, and building damage in Le Teil were systematically documented shortly in the aftermath of the event.

We present a Bayesian framework for simulating NFGMs using kinematic source modelling constrained by in-situ observations. The primary aim of this work is to quantify how such in-situ observations can provide constraints on ground motion and source parameters. First, we generate prior NFGMs from a suite of kinematic rupture models on outcropping rocks. We conduct sensitivity analyses on key rupture parameters, including corner frequency, rise time, and nucleation position, and assess their impact on the resulting NFGMs. Some kinematic source parameters are already constrained by observations, such as a low-frequency slip model inverted from InSAR data and rupture duration constrained by far-field seismological observations. These prior NFGMs are then used to simulate the displacement of grave slabs and building-damage grades (with taking site effect into account), following the methods of Causse et al. (2021) and Iskandar et al. (2023). A likelihood function is constructed by comparing the simulations with the observations. By combining the prior NFGMs with the likelihood, we obtain posterior distributions of NFGMs. Evaluating which prior NFGMs yield predictions most consistent with the observations allows us to identify the most plausible kinematic rupture parameters. This approach demonstrates that kinematic rupture source parameters can be constrained even in the absence of strong-motion records and provides an alternative means of estimating these parameters when conventional strong-motion data are unavailable.

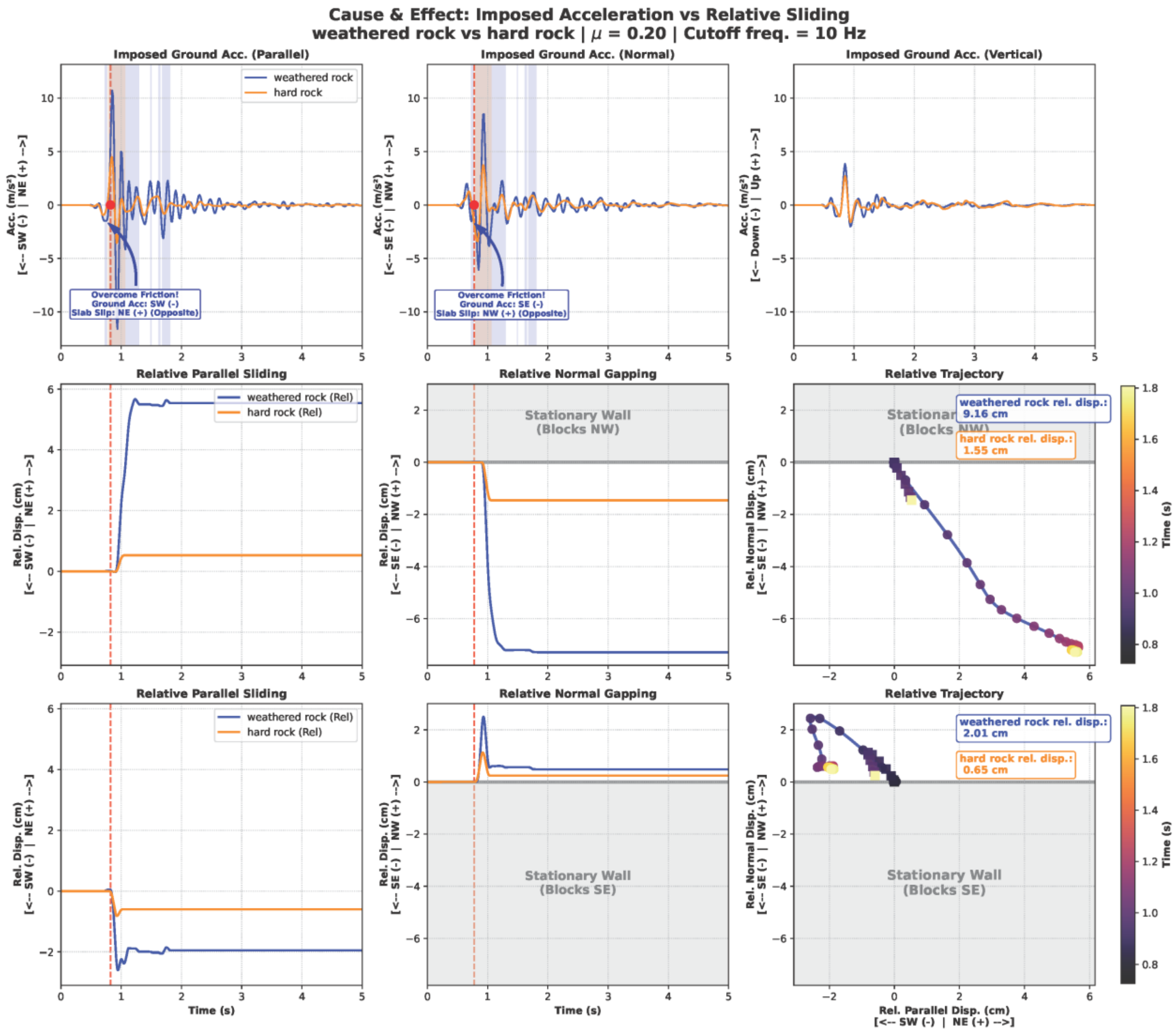

Figure: An example of an imposed seismogram and two sets of slab displacements on weathered or hard rocks. Depending on the slab's position relative to the headstone, it can move either NW or SE. The seismogram and corresponding slab motion are rotated into directions parallel and normal to the headstone. The relative displacement trajectories are shown, with the colorbar indicating time. For the imposed horizontal acceleration time series, the shaded areas mark periods when inertial forces exceed friction, i.e., when the slab begins to move.

Geophysics Of Volcanoes & Geothermal Energy

Pierre Bouygues

Characterization of activity at Semeru volcano using high resolution radar and optical imagery

Authors: *Pierre Bouygues (ISTerre, France), Fabien Albino (ISTerre, France), Virginie Pinel (ISTerre, France)*

At Semeru volcano, dome growth, lava emplacement, and pyroclastic density currents commonly occur over short timescales within sustained eruptive activity, producing rapid and large-amplitude changes in topography and surface deformation. At such andesitic systems, these processes are often concentrated in steep summit areas where direct observations remain limited for ground-based measurements. However, quantifying surface mass redistribution and subsurface deformation processes remains challenging due to the rapid and localized nature of these changes. Here we show that the combined analysis of multi-temporal topography and high-resolution ground deformation provides quantitative constraints on these processes at the scale of the volcanic edifice. Between 2015 and July 2021, the edifice experienced progressive accumulation of material, with a net volume bounded between 24.008 ± 0.114 Mm^3 and 24.219 ± 0.114 Mm^3. This construction phase was followed by a major reorganization following the December 2021 eruption, associated with dome collapse and the emplacement of large pyroclastic density currents, resulting in a net volume loss bounded between -30.946 ± 0.034 Mm^3 and -30.995 ± 0.034 Mm^3. X-band Interferometric Synthetic Aperture Radar (InSAR) time series reveal localized deformation affecting recent pyroclastic deposits on the southeastern flank, with displacement rates of 2 to 4 cm yr^{-1} consistent with long-term gravitational adjustment, while no clear evidence of sustained post-eruptive magmatic inflation or deflation is detected. These results demonstrate that jointly analyzing topographic changes and ground deformation improves the interpretation of satellite observations in rapidly evolving volcanic environments.

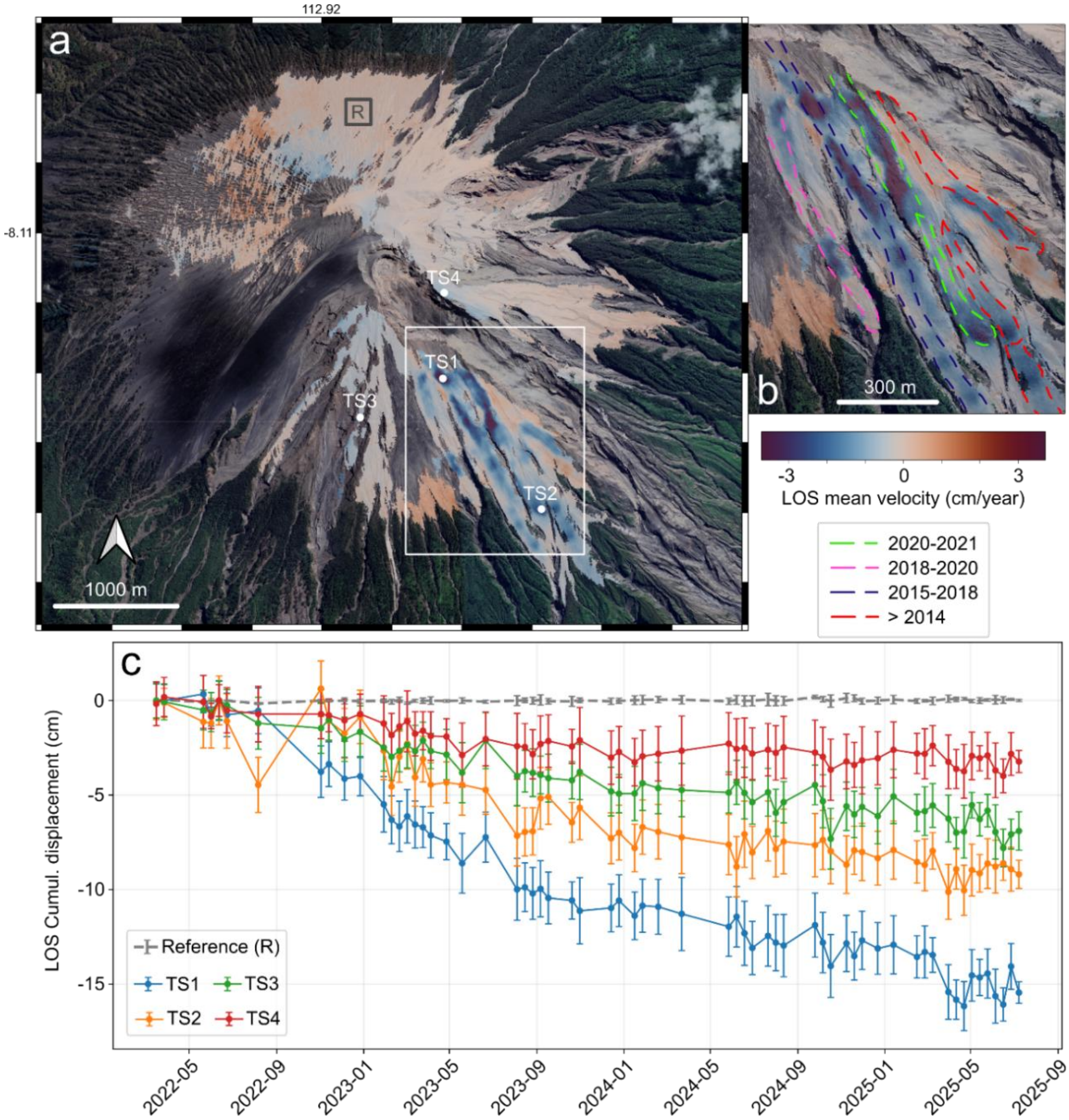

Figure: Spatial and temporal evolution of ground deformation at Semeru derived from TerraSAR-X InSAR observations between March 2022 and July 2025. (a) Mean line-of-sight (LOS) velocity map draped over an optical satellite image of the volcano with negative velocity values indicate motion away from the satellite. Four representative pixels (TS1–TS4) are selected on the southeastern flank to illustrate the temporal evolution of deformation, while the grey marker (R) indicates the reference area assumed to be stable. (b) Zoom of the southeastern flank showing the spatial organization of the deformation signal within the main deposition channel. Colored dashed outlines delineate deposits emplaced during successive eruptive periods based on DEM differencing results: deposits formed after 2014 (red), 2015–2018 (blue), 2018–2020 (pink), and 2020–2021 (green). (c) LOS cumulative displacement time series extracted at the locations shown in panel (a). The reference area (R) remains stable around zero displacement, while TS1–TS3 display progressive negative LOS displacement. Error bars represent the temporal variability of the displacement evaluated from RMS values derived from the SBAS inversion.

Katherine Andrea Vargas Alva

Magmatic Inflation and Fault Reactivation at Sabancaya Volcano (Peru) Revealed by InSAR and Numerical Modeling

Authors: *K. Vargas (ISTerre, France & Geophysical Institute of Peru, Peru), V. Pinel (ISTerre, France), J. Villegas (Geophysical Institute of Peru, Peru), H. Tavera (Geophysical Institute of Peru, Peru)*

Sabancaya volcano, located in southern Peru, began its current eruptive phase in 2016 and remains active. Previous InSAR and GNSS observations revealed a persistent inflation source located about 6 km north of the volcanic edifice. However, the observed deformation pattern is spatially heterogeneous, suggesting strong structural control.

In this study, we investigate the relationship between magmatic inflation and fault reactivation using InSAR time series analysis and Coulomb stress modeling. The InSAR time series were generated using the NSBAS approach from Sentinel-1 ascending data covering the period October 2014 to May 2025.

The results reveal cumulative inflation reaching ~40 cm between 2014 and 2025, superimposed on deformation associated with nearby faults. The Mojopampa fault mainly exhibits long-term creeping behavior, while the Pungo–Hornillo fault shows episodic normal faulting with several reactivation events between 2016 and 2021.

Preliminary Coulomb stress modeling highlights the important role of topography in stress transfer. When topography is included, inflation-induced stress changes promote slip conditions on shallow portions of the Pungo–Hornillo fault. In contrast, the Mojopampa fault appears less sensitive to magmatic inflation.

These results emphasize the structural control on deformation at Sabancaya and demonstrate the importance of integrating geodetic observations with mechanical modeling to better understand volcano-tectonic interactions in active volcanic systems.

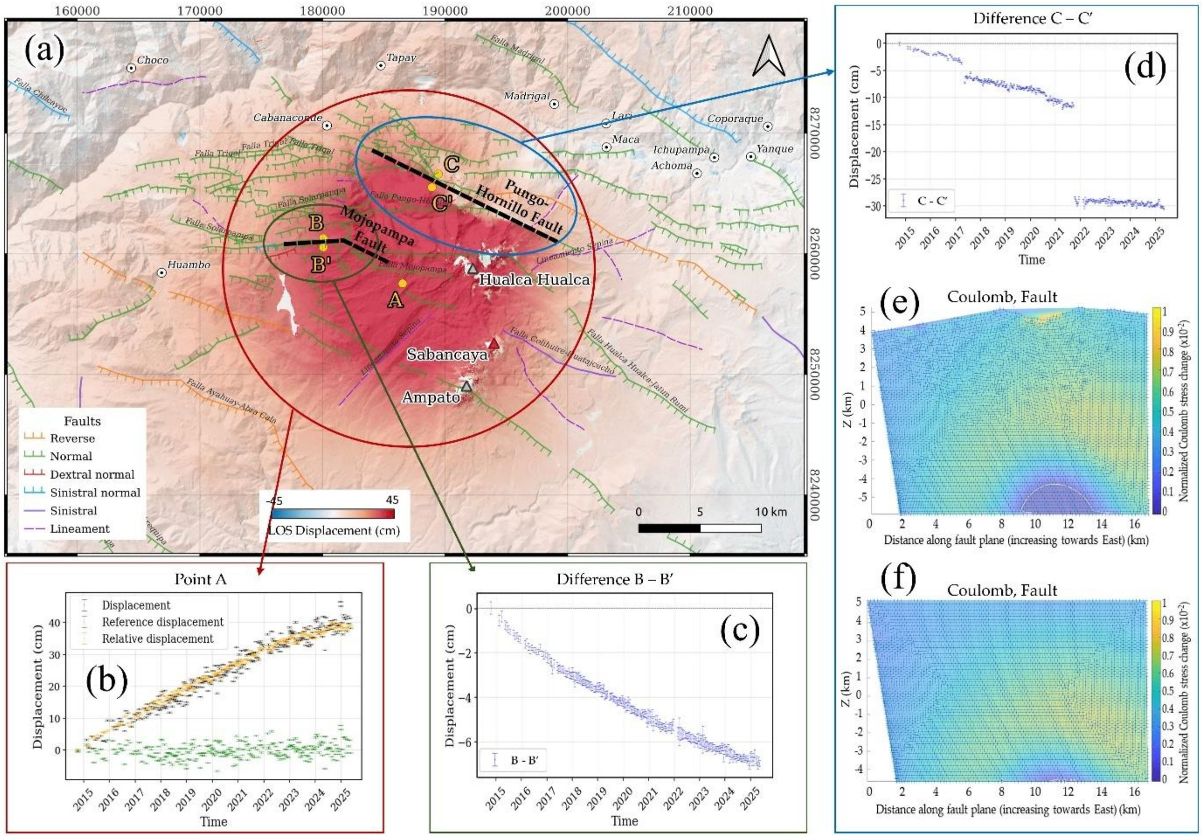

Figure: Deformation detected around Sabancaya volcano. In the map and time series, positive values indicate motion toward the satellite. (a) LOS deformation in ascending orbit. (b) Time series at point A showing inflation. (c) Displacement difference between points B and B' across the Mojopampa Fault. (d) Displacement difference between points C and C' across the Pungo–Hornillo Fault. (e) Coulomb stress model for the Pungo–Hornillo fault considering topography, and (f) the same model without topography.

Louise Lizé

Crustal fracture classification and parameter estimation from InSAR displacement fields with interpretable descriptors

***Authors**: Louise Lizé (LISTIC, France), Christophe Lin-Kwong-Chon (LISTIC, France), Valérie Cayol (Laboratoire Magmas et Volcans, France)*

Satellite-based remote sensing enables large scale and precise monitoring of natural hazards. In particular, InSAR measures surface displacements that can be analyzed by inverse modelling to provide information on the processes driving deformation. Because inverse modelling is computationally costly, we investigate a machine learning approach to identify deformation source types from displacement fields, distinguishing magmatic intrusions from tectonic faults, while also exploring the estimation of physical parameters.

Inspired by the classification framework of Cayol et al. (2014), which uses ratios of surface displacement extrema to support mechanism diagnosis and parameter estimation, we introduce a machine learning based approach for more robust mechanism classification and parameter estimation. We compute interpretable descriptors from displacement fields, including global statistics and geometric characteristics of the displacement patterns, and train a random forest for classification. We also use random forest regression to explore the estimation of associated physical parameters.

The synthetic dataset used is generated from the Okada elastic model. In this model, the deformation source is a rectangular dislocation described by physical parameters. The resulting classes are well separable and the model achieves good performance, but considering simplified assumptions: a north-south fracture, a blind fracture and no atmospheric noise. The next step is to improve robustness under more realistic conditions. Perspectives include the test of others algorithms and feature selection strategies, before moving to real data and exploring deep learning approaches as complexity increases.

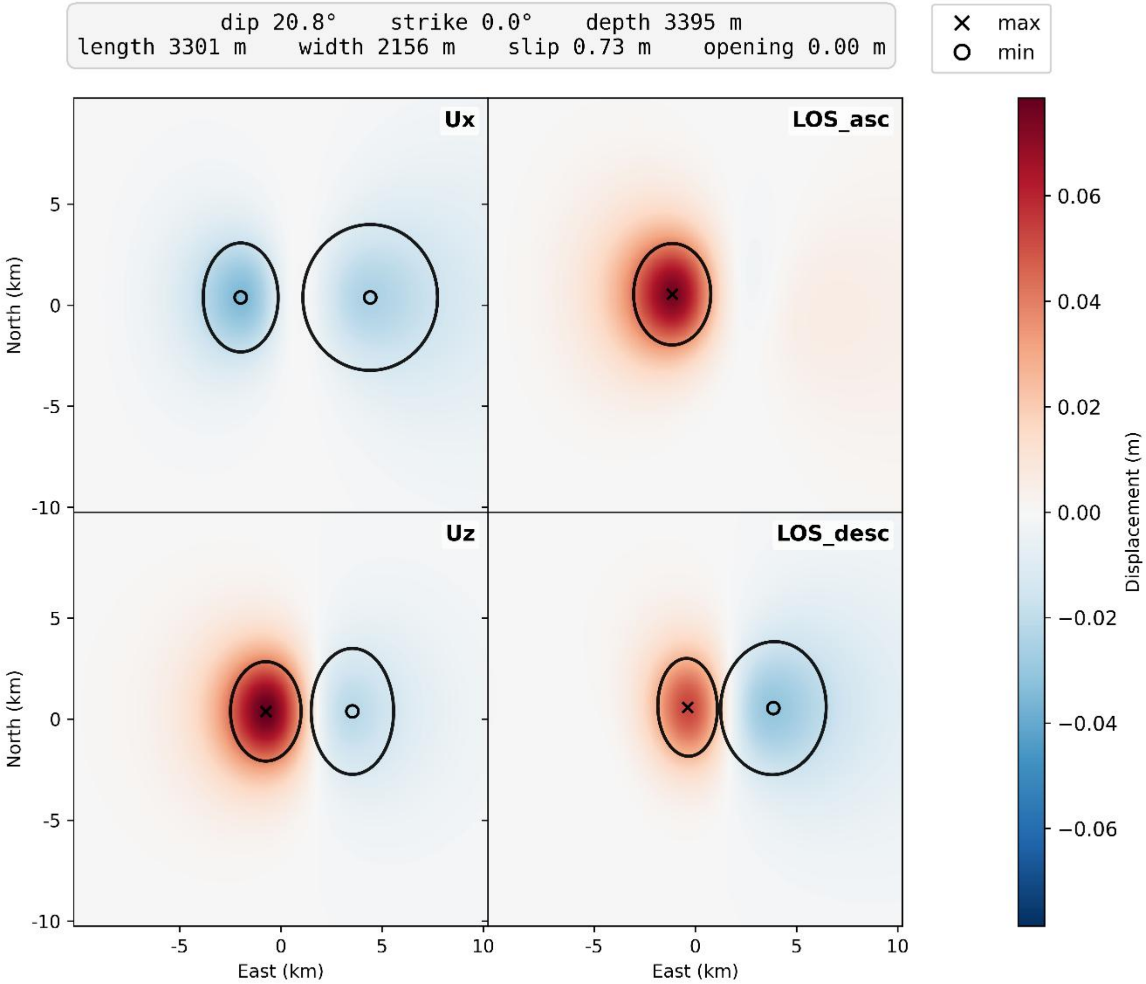

Figure: Feature extraction from synthetic reverse fault displacement fields

Mineralogy

Grégoire Demure

Experimental monitoring of the Antigorite + Brucite dehydration reaction at subduction zone conditions.

***Authors**: Demure Grégoire (ISTerre, ESRF, France), Rosa Angelika (ESRF, France), Brunet Fabrice (ISTerre, CNRS, France), Malvoisin Benjamin (ISTerre, France), Garbarino Gaston (ESRF, France), Jelavic Stanislav (ISTerre, France), Lanson Martine (ISTerre, France), Legros Emma (ISTerre, France), Auzende Anne-Line (ISTerre, France)*

Subduction zones represent the main geodynamic context where fluids and surface elements are brought in the earth's interior. The subducted slab carries water contained in different type of rocks. Among these rocks, serpentinites are the main water carrier (Schmidt and Poli, 1998). They contain both serpentine (either lizardite - Liz and or antigorite - Atg - mainly) and brucite - Brc which contain 13% and 30% water in weight respectively. When subducting, they dehydrate, forming other hydrated phases or dry phase and free fluids linked to arc volcanism ((Pagé et al. 2019). Furthermore, detection of low frequency earthquakes (LFE) and slow sleep events (SSE) are interpreted as a result of these fluids' migration (Bouchon et al. 2022). In subduction zones, the main dehydration reaction is supposed to be the antigorite breakdown (atg-out), occurring above 600 ºC (Hilairet et al, 2006). However, the serpentine + brucite reaction which occurs at lower T compared to atg-out can also release free fluids (Legros et al, 2025). This reaction was poorly investigated so far, thus the objective of this project is to produce experimental data in order to better understand the parameters controlling the reaction. In that aim, we monitored this reaction in-situ using Diamond Anvil-cells to reproduce subduction zones conditions combined with in-situ X-ray diffraction at ESRF. We complement these with piston-cylinder experiments to identify mineral textures and composition of quenched samples. Preliminary results show that the dehydration reactions occur between 511°C at 1.0 GPa and 550 ºC at 2.0 GPa depending on the mineral assemblage. Under these conditions, brucite is highly soluble in the fluid before reaching the reaction. The reaction including lizardite occurs earlier than antigorite indicating that the nature of the serpentine plays a crucial role. Furthermore this reaction's kinetics follows an Avrami low, meaning nucleation of olivine during dehydration.

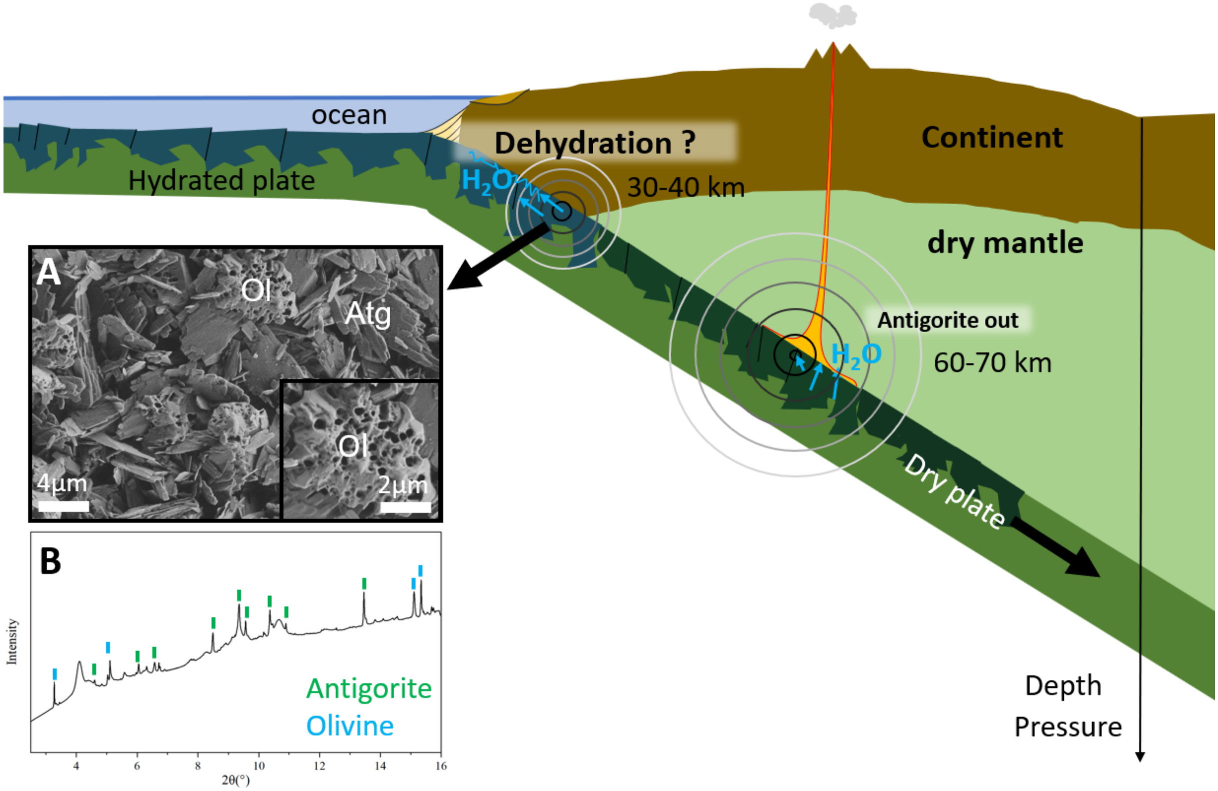

Figure: A: SEM image of dehydrated sample; Atg = Antigorite; Ol = Olivine. B: In-Situ diffraction pattern of dehydrated sample during experiment at the synchrotron.

Paula Dörfler

pH and carbonate anions availability decide LDH vs. Fe(III)-brucite formation from Fe(II)-brucite at ambient PT conditions

***Authors**: Paula Dörfler (ISTerre, France), Benjamin Malvoisin (ISTerre, France), Bruno Lanson (ISTerre, France), Martine Lanson (ISTerre, France), Fabrice Brunet (ISTerre, France), Angelika Rosa (ESRF, France)*

The low-T (< 150 °C) alteration of serpentinites is of primary importance for natural CO2 storage and H-generation under conditions where life may exist. While missing in most hand-collected or dredged oceanic samples, (Fe-bearing) brucite is abundant in cores of oceanic serpentinites retrieved from depths > 200 m [1]. This Fe-brucite, (Mg,Fe(II))(OH)2, is one of the most RedOx and T-reactive phases, its small grain size, often ranging between 20-100 nm, increasing further its reactivity. For example, oxidation into Fe(III)- brucite occurs within days at T < 150°C in the laboratory [2]. If anions are present, (Fe, Mg)-LDH may form from the oxidation of Fe(II)-brucite. Both CO3- and Cl-containing LDH are observed in many serpentinite samples, with abundances up to 10 wt%.

In this study, the reactivity of synthetic ferroan brucite was investigated through time-resolved oxidation experiments in synthetic and lab air at 21 °C, with and without anions. Based on XRD, we analyzed the reaction progress and derived the Fe(III)/Fe(tot) in brucite as well as the extent of LDH formation. Using SEM, TGA with coupled FTIR evolved gas analysis, Raman spectroscopy, and UV–vis spectrophotometry, we further describe the resulting phases as well as their formation mechanism.

Synthetic ferroan brucite oxidation reached a near-maximum reaction progress after 5 days in lab experiments when no anions were present. In-situ synchrotron XAS experiments in diamond anvil cells showed a decreasing Fe-O bond length during the isostructural oxidation. In the presence of CO32- anions, full conversion to LDH was observed after 1 day under ideal conditions at pH 10.5. SEM-observed grain sizes suggest that the oxidation proceeds in solid state for Fe(II)-brucite via H-diffusion, whereas LDHs form via dissolution-reprecipitation.

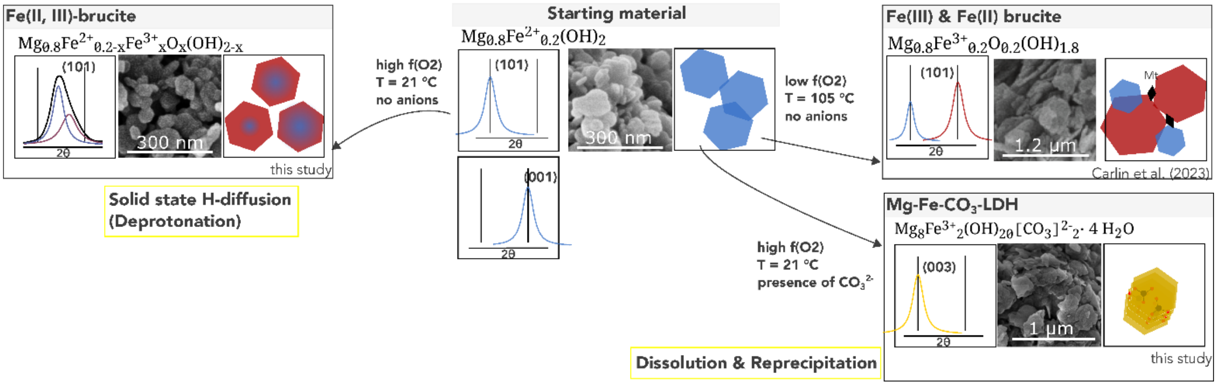

Figure: Reaction paths of Fe-containing brucite: If no anions are present, Fe(II)-brucite oxidizes via solid-state diffusion at T = 21°C and high f(O2) conditions, and dissolution-reprecipitation at T= 105 °C and low f(O2). If anions, i.e., CO32- are present, LDH form (T = 21 °C and under high f(O2) conditions).

Mateo Esteban

Neo-Archean komatiites as probes of the early Earth mantle

***Authors**: Mateo Esteban (ISTerre, France), Alexander V. Sobolev (ISTerre, France)*

Komatiites are ultramafic volcanic rocks derived from the most magnesian melts on Earth (over 18 wt% of MgO). Although the spatial and temporal distribution of komatiite is highly uneven, it is common in Archean and Proterozoic greenstone belts, with few confirmed Phanerozoic occurrences (e.g., Gorgona Island, Iran). Komatiites have the highest degrees of partial melting and are thus considered the closest estimate of the mantle among volcanic rocks. All of the above made komatiites of particular interest to constrain the chemical and thermal evolution of the Earth's mantle. After decades of komatiite research, the dominant model for their origin implies extensive peridotite melting in deeply rooted high-temperature decompressing plumes. However, ever since their discovery, the initial water content of komatiite and consequently their source temperature have been debated.

We analysed more than 300 olivine-hosted melt inclusions from a 2.69 Ga old flow of komatiites in the Belingwe greenstone belt (Zimbabwe). Natural melt inclusions were experimentally re-homogenised and analysed for major, minor & trace elements composition (EPMA and LA-ICP-MS), H2O content (Raman spectroscopy), and Sr-isotopes signature (LA-ICP-MS). Host olivine crystals were also characterised chemically.

Preliminary results show that these komatiites derived from a highly magnesian parental melt yielding 25.2 wt% of MgO and 0.3 wt% of H2O. New estimates translate to a minimal melting temperature of the source of 1709 oC at 4.8 GPa. This exceeds the contemporary ambient mantle temperature by a hundred degrees and thus further reinforces the mantle plume origin of these komatiites.

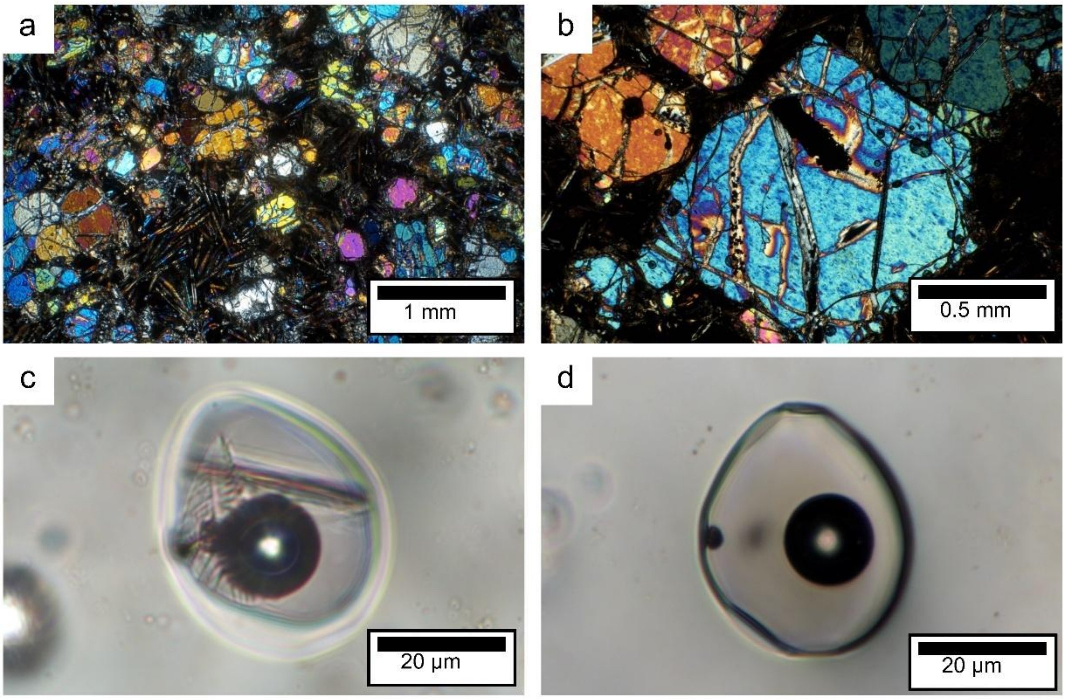

Figure: Photomicrographs of thin sections and a melt inclusion from Tony's flow komatiites. (a) and (b), thin section XPL images of sample zv10. Olivine grains are sepentinised only at the grain boundary and isolated fractures. (c) shows a partially crystallised natural melt inclusion from sample zv58. (d) is the same inclusion after the high-temperature re-homogenisation.

Maureen Gunia

The Variscan non-subduction oceanic basin at continental margin of the Chamrousse ophiolite (Western Alps)

***Authors**: Maureen Gunia (ISTerre, France), Carole Cordier (ISTerre, France), Emilie Janots (ISTerre, France), Adrien Vezinet (ISTerre, France), Julien Leger (ISTerre, France), Stephane Guillot (ISTerre, France), Alexis Plunder (BRGM, France), Valentina (ISTerre, France), Alexander Sobolev (ISTerre, France)*

Ophiolite complexes are rare oceanic lithosphere remnants that are evidence for suture zones in mountain belts. Ophiolite palaeo-geodynamic setting can be reconstructed from isotopic and elementary signatures of ophiolite rocks, with subduction-unrelated (mid-ocean ridge MOR, plume, and continental margin) and subduction-related (supra-subduction, volcanic arc) types (Dilek and Furnes, 2011; Pearce et al., 1984). The large diversity of geochemical fingerprints in these rocks are first controlled by the mantle source and melting conditions. The European Variscan cycle spans over 200 Ma and involves the opening and subsequent closure of three main oceans, leading to the collision between Laurussia and Gondwana during the Carboniferous (from 360 to 300 Ma)(Franke et al., 2017; Matte, 2001; Stampfli et al., 2013). Understanding Variscan ophiolites as the one of Chamrousse (External Crystalline Massif of Belledonne, Alps) is crucial for reconstructing the palaeo-geography of the Variscan belt. Despite by the global convergence context, by characterising its melt source through new zircon chemical investigations, we propose a geodynamic opening model independent of any subduction influence: Through these low U/Yb, Nb/Yb and Th/Yb ratios coupled with highly radiogenic initial Hf isotopes (ca. +12), the mafic-ultramafic complex of Chamrousse demonstrates an oceanic origin from a chemically depleted mantle source. This signature precludes any enriched mantle source or crustal contamination during magma ascent. This oceanic basin preserved a rifted margin architecture. To the west, the Cambro-Ordovician bimodal Séchilienne unit reflects the Cambro-Ordovician rifting of the North-Gondwana margin. To the east, the Devono-Dinantian Rioupéroux-Livet-Gavet formation represents the coeval continental basin of the Chamrousse basin. We propose that the Chamrousse basin initiated from a continental break-up (ca. 365 Ma) and evolved as a short-lived magma-poor oceanic basin (360 – 345 Ma) by lithospheric detachment faults exhuming gabbroic bodies within mantle rocks which induced the pervasive syn-magmatic deformation, prior to the final assembly of Pangea.

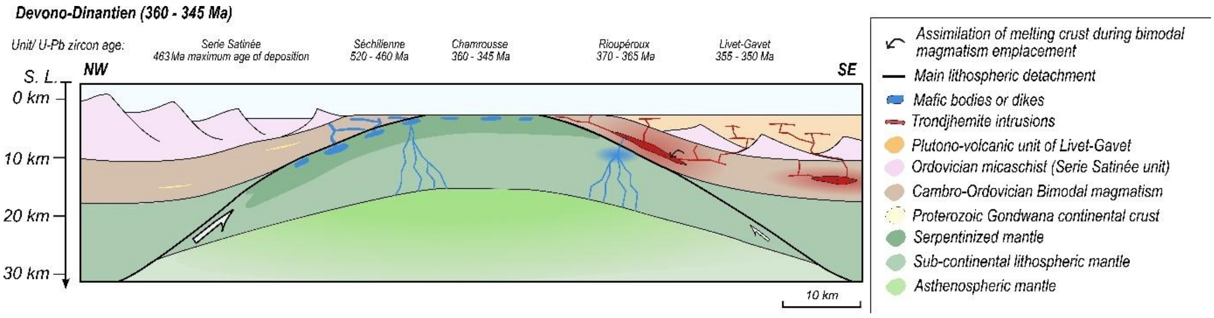

Figure: Paleo-geographic evolution of the Chamrousse oceanic basin within a magma-poor rifted margin. Melts from the ascending depleted asthenosphere emplaced as basaltic dikes and gabbroic bodies into the serpentinised mantle and, more locally, basaltic dikes in the westward adjacent Séchilienne unit. Within the eastern margin of the oceanic basin, the volcano-sedimentary basin recorded by the synchronous Livet-Gavet unit develops.

Emma Legros

Petrological characterization and thermodynamic modeling of the serpentine + brucite dehydration reaction in the Mount Avic (Aoste Vallée, Italian Alps) and Zermatt-Saas (Swiss Alps) meta-ophiolites: Mineral products, fluid production and Fe-Mg mobility

Authors: *Emma Legros (ISTerre, UGA), Anne-Line Auzende (ISTerre, UGA), Fabrice Brunet (ISTerre, UGA), Benjamin Malvoisin (ISTerre, UGA)*

Aqueous fluids in subduction zones play a key role in deep water and element cycling, seismicity, mantle wedge hydration, and magma generation. Serpentinites, containing up to ~ 13 wt.% H2O, are the main carriers of water into subduction and are expected to dehydrate above 600°C. It has been showed that brucite, containing ~ 30 wt.% H2O, is also an important hydrous component of subducted oceanic mantle. Consequently, the simplified reaction antigorite + brucite = olivine + H2O (R1) is highly relevant to deep subduction processes.

To investigate R1, we combine (i) petrological observations from ultramafic units of Alpine meta-ophiolites belonging to the former Piemont-Ligurian oceanic lithosphere (Zermatt-Saas Units; Mount Avic, Italian Alps, and Theodul Glacier, Swiss Alps), which experienced R1 conditions during Alpine subduction, and (ii) thermodynamic modelling using Perple_X to constrain fluid production and element mobility as a function of pressure-temperature (P-T) conditions, oxygen fugacity and bulk-rock composition.

Modelling with an updated thermochemical database shows that R1 produces olivine and magnetite minerals while releasing larger amounts of fluid than previously expected within a narrow temperature range (<10°C), implying relatively high dehydration rates in the slab. The released fluid is predicted to be highly magnesian (>1 mol/kg), with MgOaq as dominant aqueous species (Legros et al., 2025). Magnetite abundance increases with PT conditions, and its composition varies with bulk-rock chemistry, particularly the Fe3+/FeTot ratio and associated oxygen fugacity. During R1, magnetite becomes Mg-rich, consistent with Mg-rich fluid release.

These predictions are supported by petrographic observations, including brucite-microveinlets crosscutting metamorphic olivine veins in Zermatt-Saas serpentinites, indicating strong Mg segregation, and by the magnetite high and heterogeneous distribution in Mount Avic serpentinites. Finally, the P-T conditions of R1 closely match those of low-frequency earthquakes in the Mexican, Nankai and Cascadia present-day subduction zones, supporting R1 as a potential trigger of seismicity.

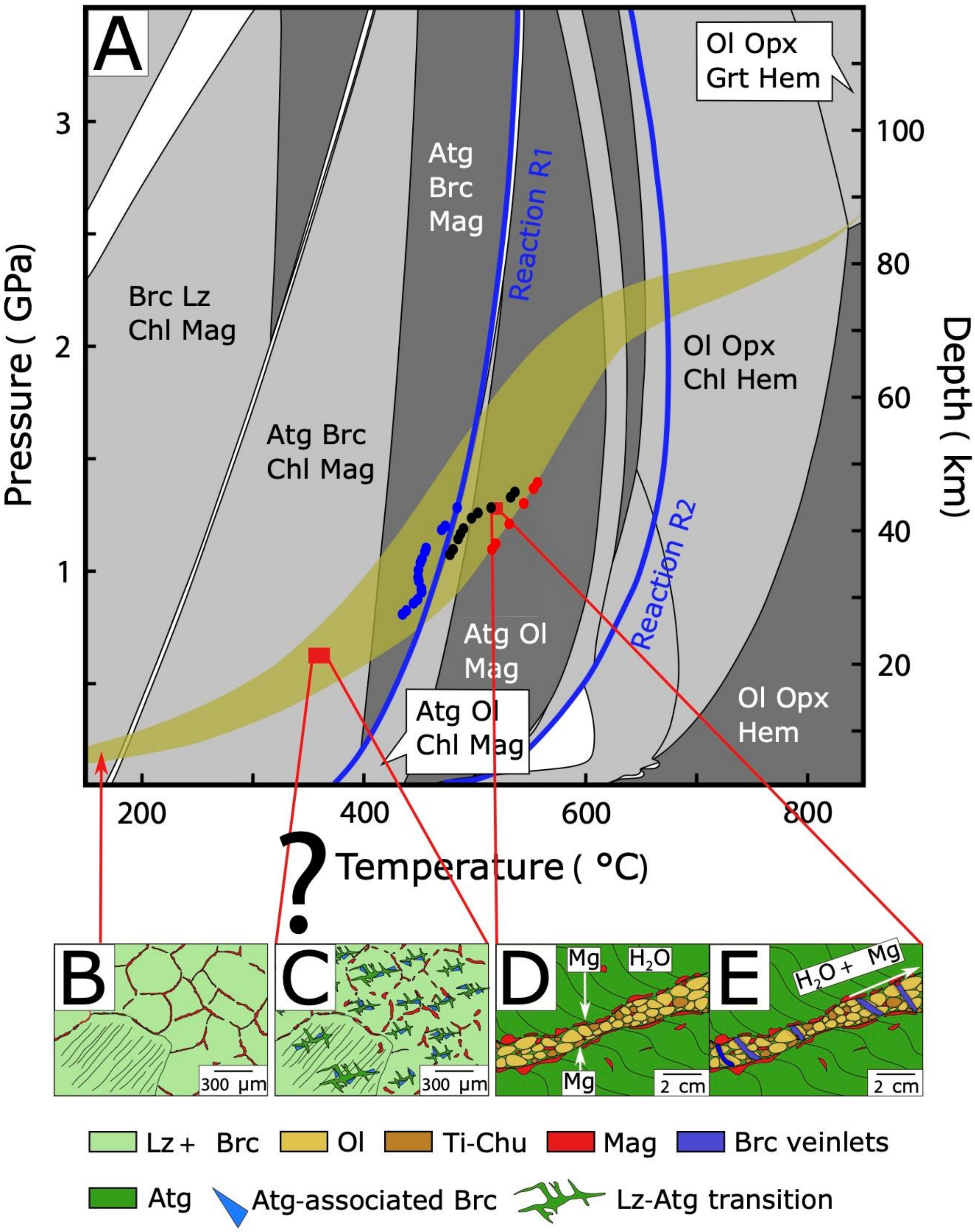

Figure: A: Simplified pseudosection of stable mineralogical assemblages (R1: Atg+Brc=Ol+H2O; R2: Atg-out). Yellow path is geotherm in actual subduction. Red, blue and black dots provide P-T conditions of LFEs in subduction zones of Cascadia, Nankai and Mexico respectively. B: Peridotite completely serpentinized, Lz+Brc mixture is the main mineralogical assemblage. C: Lz to Atg+Brc transition. D: Serpentinites partial dehydration and Ol+TiChu vein formation. E: Brc vein formation.

Flavien Perotto

Geo-inspired separation of rare earths by hydrothermal means : experimentation and modeling

***Authors**: Flavien Perotto (ISTerre, France), Fabrice Brunet (ISTerre, France), Hugues Cabane (Cristal'Innov, France)*

Rare Earth Elements (REE) are of both strategic and economic importance to Europe but there is a high risk of supply chain disruption, particularly due to China's monopoly on their production. REE, and in particular neodymium (Nd) and dysprosium (Dy), are present in permanent magnets from which they could potentially be recycled. However, their separation is complex and traditionally involves numerous steps and toxic solvents. Natural hydrothermal systems are known to be capable of selectively sorting chemical elements diluted in the Earth's crust.

In the frame of the present PhD project, we are investigating a geo-inspired method for separating REE from NdFeB magnet powders under hydrothermal conditions through a combined numerical modeling (COMSOL) and experimental strategy. The method is expected to be cleaner than the current The work carried out so far focused on the thermal and hydrodynamic numerical modeling of pilot-scale reactors. It showed that when filled by water, even small-scale horizontal cylindrical reactors (~5mm diameter) are traversed by a rather fast convection loop when submitted to differential heating. Heat transfer in such reactors was previously thought to be driven by heat conduction only.

Numerical simulations performed on different reactor geometries and under various boundary conditions showed that the apparition of the convection loop was resilient to the presence of obstacles on its course. The simulations also showed that key parameters, such as reactor inclination and water filling rate, strongly influence the shape and velocity of the convection loop, hence the temperature field inside the convecting fluid. Implementation of the effect of hydrodynamics on chemical mass transfer (dissolution/transport/precipitation) is in progress.

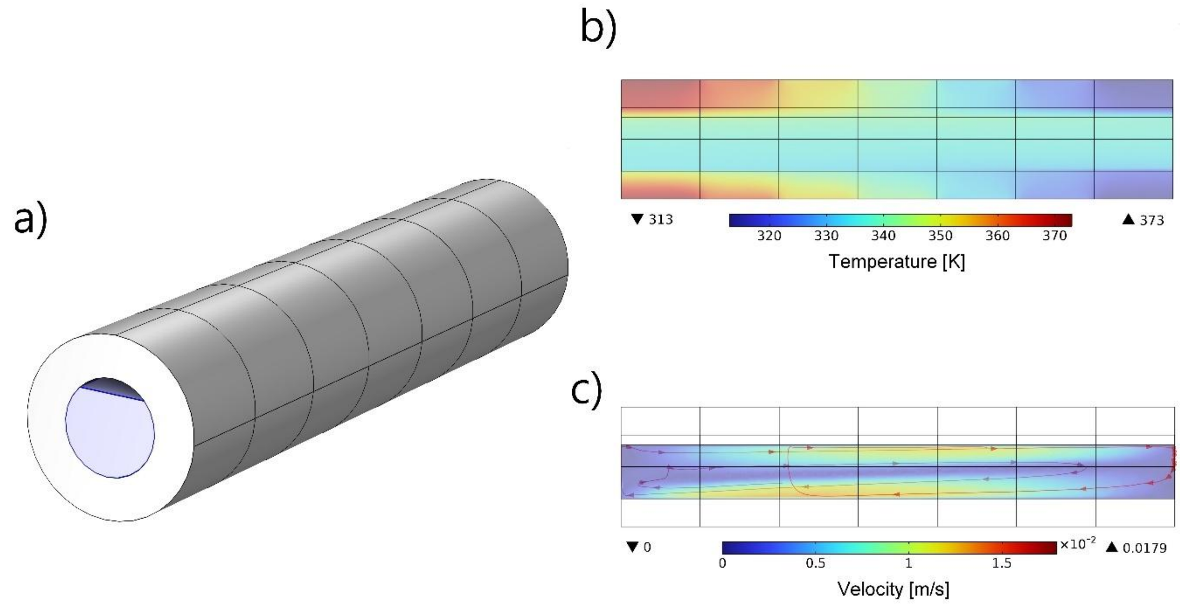

Figure: a) 3D Geometry of the pilot-scale autoclave. The 7 different heating areas are visible. b) 2D slices of computed temperature field in the reactor at t = 1250s and for an external temperature gradient of 373-313K. c) 2D slice of the velocity field in the same conditions, an example of particle trajectory is represented by the red line. The arrows on the line are separated by equal travel time.

Ivan Vujević

Redefining the Metrological Limits of Hydrogen Adsorption in Geological Materials: Implications for Underground Energy Storage

Authors:

Ivan Vujević (ISTerre, France), Valerie Magnin (ISTerre, France), Stanislav Jelavić (ISTerre, France), Rémy Guillet-Nicolas (LCS, ENSICAEN, France), Denys Grekov (IMT Atkantique, GEPEA, France) , Patricia de Rango (Laboratoire de Cristallographie, France), Eric Lewin (ISTerre, France), Yan Yao (ISTerre, France), Frédéric-Victor Donzé (ISTerre, France), Laurent Truche (ISTerre, France)

Hydrogen adsorption on natural minerals influences hydrogen mobility in deep geological environments, including underground hydrogen storage (UHS) systems and nuclear waste repositories. However, at ambient reservoir temperatures (>20 °C) and the specific surface areas typical of geological materials (10–50 $m^2.g^{-1}$), expected H_2 uptake often approaches the detection limits of conventional volumetric instruments. In this regime, cumulative uncertainties from void-volume calibration and sequential measurement propagation can produce apparently smooth Langmuir-type isotherms whose uptake values remain weakly constrained and may be overestimated. Inter-instrument comparison further shows that calibration-driven offsets in conventional single-cell instruments can become comparable to or larger than the true adsorption signal for low-capacity geomaterials, with implications for the interpretation of reservoir-scale storage capacity estimates.

Here, we present a high-pressure, dual-cell differential volumetric apparatus designed to resolve adsorption signals up to 100 bar. By measuring only the pressure imbalance between matched sample and reference cells, the instrument suppresses common-mode thermal and mechanical perturbations. Coupled with full uncertainty propagation and real-gas corrections using a multiparameter Helmholtz equation of state, this approach defines an empirical, mass- and pressure-dependent quantification threshold of 0.03 $mmol.g^{-1}$ at 100 bar. Benchmark measurements on reference materials and Callovo–Oxfordian (COx) claystone demonstrate that H_2 excess uptake in these geomaterials remains at or near this metrological limit. For COx, we constrain a metrologically defined upper bound of 0.04 $mmol.g^{-1}$ at 100 bar and 20 °C, approximately one order of magnitude below several previously published values.

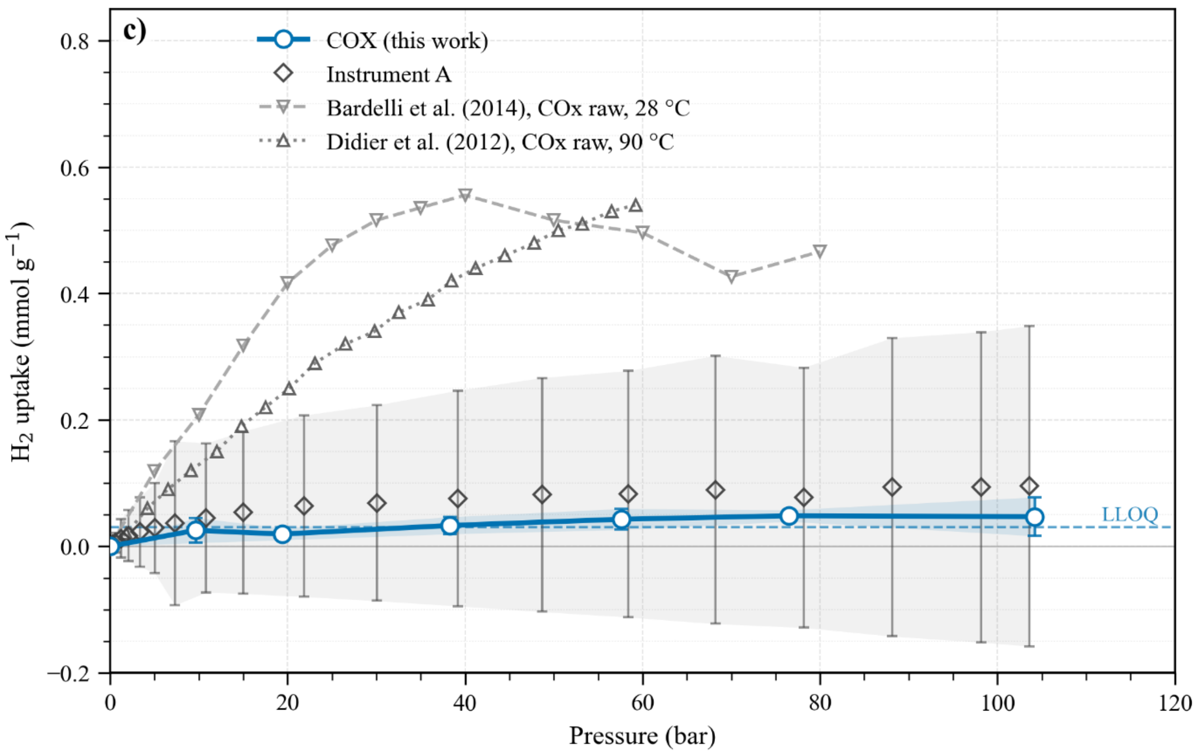

Figure: H2 adsorption isotherms on reference materials measured with the dual-cell differential apparatus at 291–293 K (17–19 °C). c) Callovo–Oxfordian claystone (COx), for which measured excess uptake remains near the quantification threshold. Although a slight positive trend is observed at higher pressures, the signal remains within the propagated ±2σ uncertainty envelope, limiting statistical confidence in a resolvable adsorption signal under the tested conditions. Published data from Didier et al. (2012) and Bardelli et al. (2014) are shown for comparisonunder their reported conditions. Uncertainties for these latter measurements are not reported here because available data are insufficient to robustly evaluate them. Note on Quantitation: The dashed line represents the Lower Limit of Quantitation (LLOQ). This limit is sample-specific and pressure-dependent, derived from the ratio of instrumental resolution (empirical uncertainty floor) to the available sample mass.

Seismic Cycle And Transient Deformations

Arthur Aymon

Fluid-rock interaction and deformation mechanisms in serpentinite-hosted strike-slip fault : insights from the Geyve ophiolite (North Anatolian Fault, Turkey)

***Authors**: Arthur Aymon (ISTerre, France), Julia de Sigoyer (ISTerre, France), Benjamin Malvoisin (ISTerre, France)*

Because of their particular rheological properties, serpentinites play a key role in active tectonics. Since these rocks can deform viscously until very low-pressure conditions, they are considered to promote weakness along major strike-slip faults, with implications for seismic risk. In the serpentinized Geyve ophiolite (Middle branch of the North Anatolian fault), active strike-slip deformation manifests instead as discrete fault planes cutting through serpentinite and filled with carbonates. This contrasts with what has been described for similar lithologies, raising questions about the mechanisms underlying the formation of these fault gouges as well as the coupling between fluid-rock interaction and deformation. This study addresses this issue combining field mapping, petrographic observations, microstructural and geochemical analyses. Field structural analysis reveals that deformation appears heterogeneously distributed and spatially associated with ophicarbonate rocks. Microscopic analyses of fault mirrors reveal a drastic grain-size reduction towards principal slip zones. Two main processes are identified: (i) cataclasis of serpentine aggregates (mainly lizardite) and (ii) development of a carbonate-talc matrix with variable degrees of carbonate cementation. In weakly-cemented gouges, micrometric dolomite and aragonite crystals display a strong shape-preferred orientation and a homogeneous grain size. In pervasively-cemented gouges, carbonate cement exhibits concentric compositional zoning in Mg and Ca suggesting variations in fluid composition. These observations indicate that mechanical grain-size reduction is accompanied by progressive carbonation of the protolith resulting in a soapstone-like matrix composition. Variations in cementation degree — controlled by either fluid availability or gouge maturation — may play a key role on the rheological behavior of the fault. Dolomite-talc matrix may accommodate deformation by grain-boundary sliding, promoting stable sliding whereas extensive carbonate cementation increases the mechanical strength of the fault, potentially modifying its seismic behavior. This preliminary study highlights the critical role of syn-kinematic mass transfer and fluid-rock interaction in controlling both the mineralogical evolution and the mechanical properties of serpentinite-hosted fault zones.

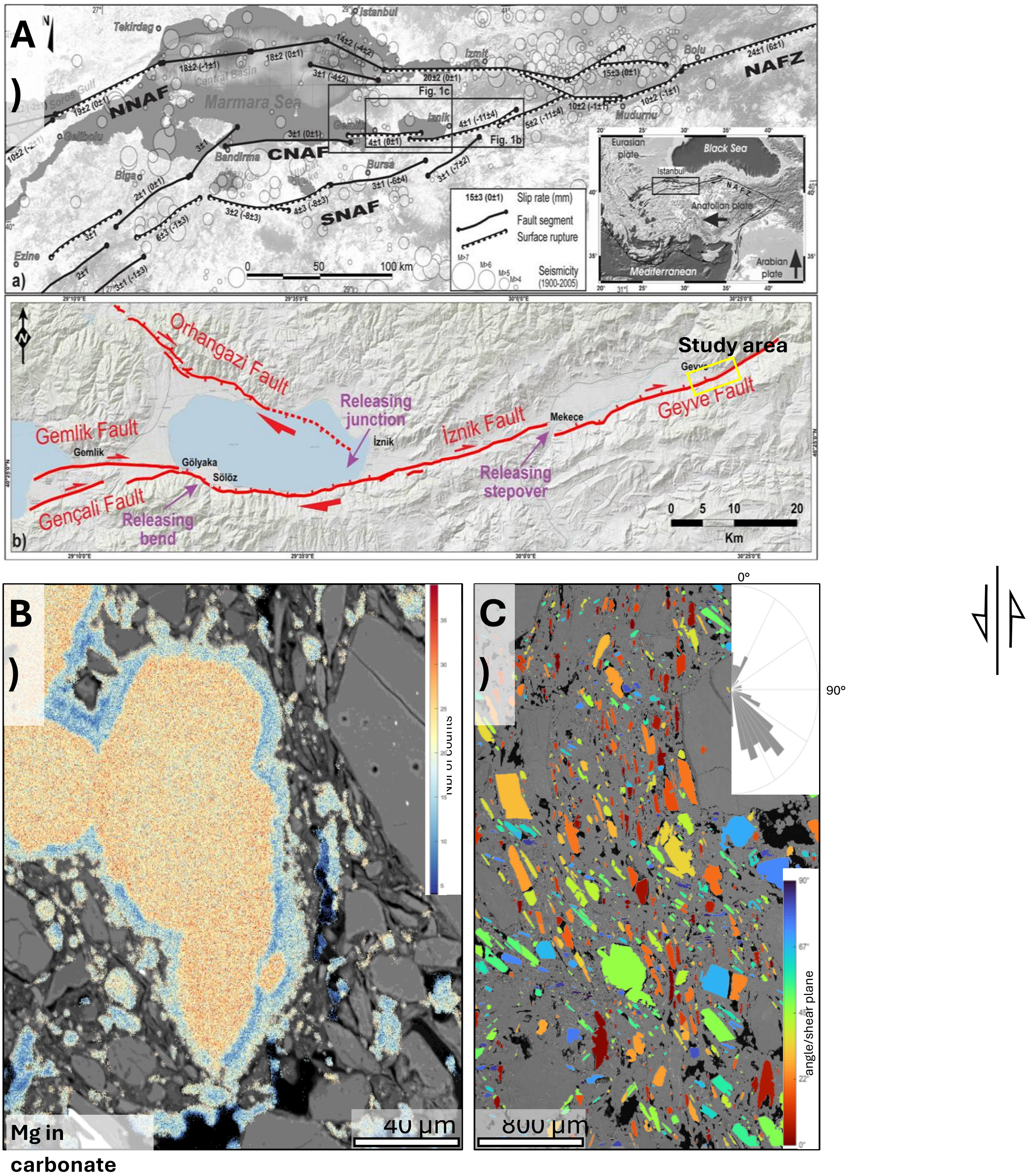

Figure: A) Map of active faults of the North Anatolian Fault Zone with its three branches and seismicity location; enlarged view on the Middle Branch with the study area location (modified from Civico et al., 2021; Murru et al., 2016). B) and C) Microscopic views of typical fault gouges B) Compositional map of carbonates. C) Orientation map of aragonite crystals with rose diagram.

Diego Cardellini

b-value variability in the 2018-2024 Noto Peninsula swarm: catalog completeness independent evidence for systematic spatiotemporal variations

Authors: *Diego Cardellini (ISTerre, France), Blandine Gardonio (ISTerre, France), Mathilde Radiguet (ISTerre, France)*

Between 2018 and January 2024, a long swarm of almost 150k earthquakes culminated in a Mw 7.6 mainshock on the Noto Peninsula. The sequence began in a compact deep source and propagated over 6 years to shallower, wider parts of the fault zone, long enough to observe the evolution of the system in real time. We track the swarm spatio-temporally without Mc bias, using two b-value estimators related to catalog completeness, b-positive (van der Elst, 2021) and b-Bayesian (Laporte, 2025). Spatially, b-positive increases with depth in the five sub-regions of Hirose et al. (2024), from about 0.85 at 5-10 km to 1.17 at 14-20 km. b starts above 1.3 in 2018, falls to nearly 0.80 in late 2020, rises sharply in 2021, and fluctuates around 1.0 with increasing variance up to the mainshock. Hydraulic diffusivity analysis (Shapiro, 2003) results in D = 0.24 m^2/s for the 2020-2022 sub-sequence (M ≥ 1.3). The diffusion is strongly directional with the highest diffusion towards the NW (D = 0.29 m^2/s), near zero diffusion towards the S and E (D < 0.06 m^2/s), consistent with fluid moving along the fault strike, rather than radially. The volume of the fluid involved is estimated following Danré et al. (2023). These results are consistent with fluid migration along permeable fault zone, although the data do not allow us to distinguish between a single continuous and repeated episodic injections.

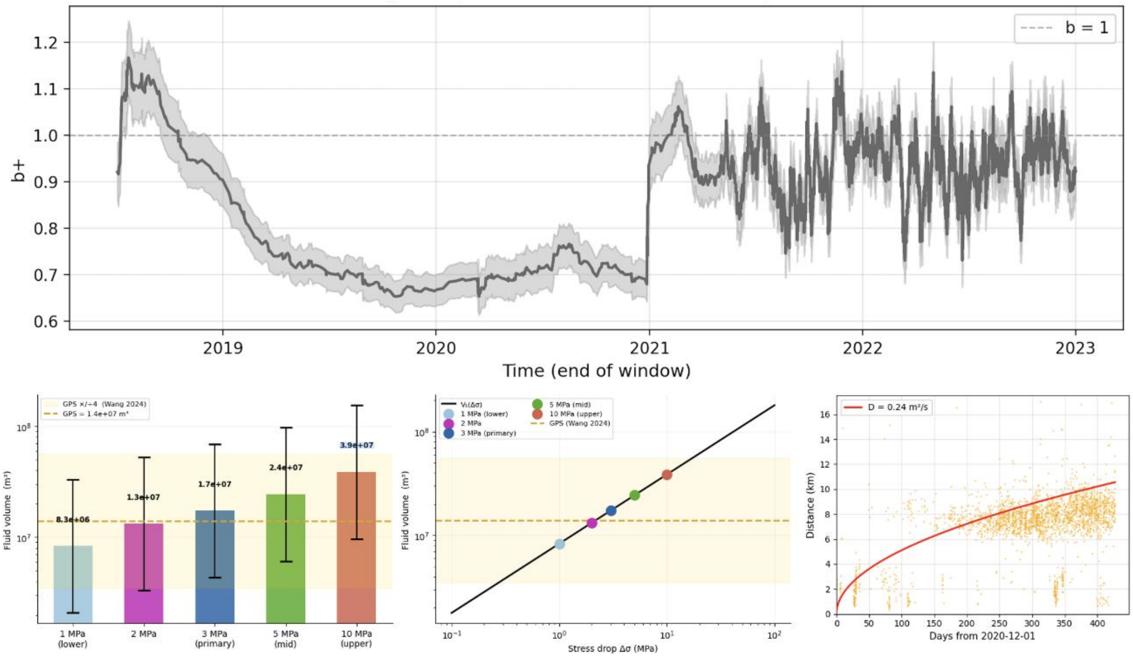

Figure: Seismological analysis of the Noto swarm (2020–2022), Japan. (top) Temporal evolution of the b+ value (van der Elst 2021) computed on a running window of 500 events (Mc = 0.1). The sharp increase at the swarm onset (December 2020) from b+ 0.7 to b+ 1.0 could be consistent with fluid-driven seismicity. (bottom left) Estimated fluid volume injected during the swarm using the method of Danré et al. (2023), for stress drops between 1 and 10 MPa. The dashed line indicates the GPS-derived volume estimate (Wang 2024). (bottom center) Fluid volume as a function of stress drop Δσ; the GPS constraint is satisfied for Δσ between 2–3 MPa. (bottom right) Pore-pressure diffusion front (Shapiro 2003) fitted to the spatiotemporal migration of seismicity (D = 0.24 m^2/s).

Estela Juana Centeno Moncada

High-resolution earthquake catalogue and structural organization of crustal seismicity in the Colca Valley, southern Peru (2015–2018)

Authors: *Estela Centeno-Moncada (ISTerre, France; Instituto Geofísico del Perú, Peru), Hugo Sánchez-Reyes (ISTerre, France), Hernando Tavera (Instituto Geofísico del Perú, Peru), Léa Pousse-Beltran (ISTerre, France), Caroline Chalumeau (ISTerre, France), Anne Socquet (ISTerre, France)*

The Colca Valley, in southern Peru, is characterized by an active crustal fault and persistent volcanic activity associated with the Sabancaya volcanic system. Historical earthquakes, including those at Maca (1991), Sepina (1992), and Ichupampa (2016), highlight the region's seismic potential. However, the spatial organization of cortical seismicity and its relationship to mapped fault systems remain poorly defined due to the limited resolution of regional seismic catalogs.

In this study, we present a high-resolution local seismic catalog for the Colca Valley covering the period 2015 - 2018, derived from continuous waveform data recorded by the local seismic network operated by the Geophysical Institute of Peru (IGP). Earthquake detection and association were performed using a fully automated workflow combining PhaseNet and PyOcto, followed by probabilistic earthquake location using NonLinLoc, source-specific station corrections (SSST), and relative relocalization using GrowClust3D.

The final catalog contains 13,360 earthquakes and reveals a highly heterogeneous spatial distribution of seismicity throughout the valley. Seismic clusters define elongated alignments that generally coincide with mapped crustal fault systems, especially along the Ichupampa fault zone, where the greatest release of seismic energy is observed. Additional clusters are observed near the Hualca Hualca and Sabancaya sectors, although with a more diffuse spatial organization.

Temporal analyses also indicate alternating periods of background seismicity and clustered activity.

These observations provide new constraints on the structural organization of cortical deformation in the Colca Valley and establish a seismotectonic framework for future studies focused on fault interaction, volcanic processes, and active deformation in the Colca-Sabancaya region.

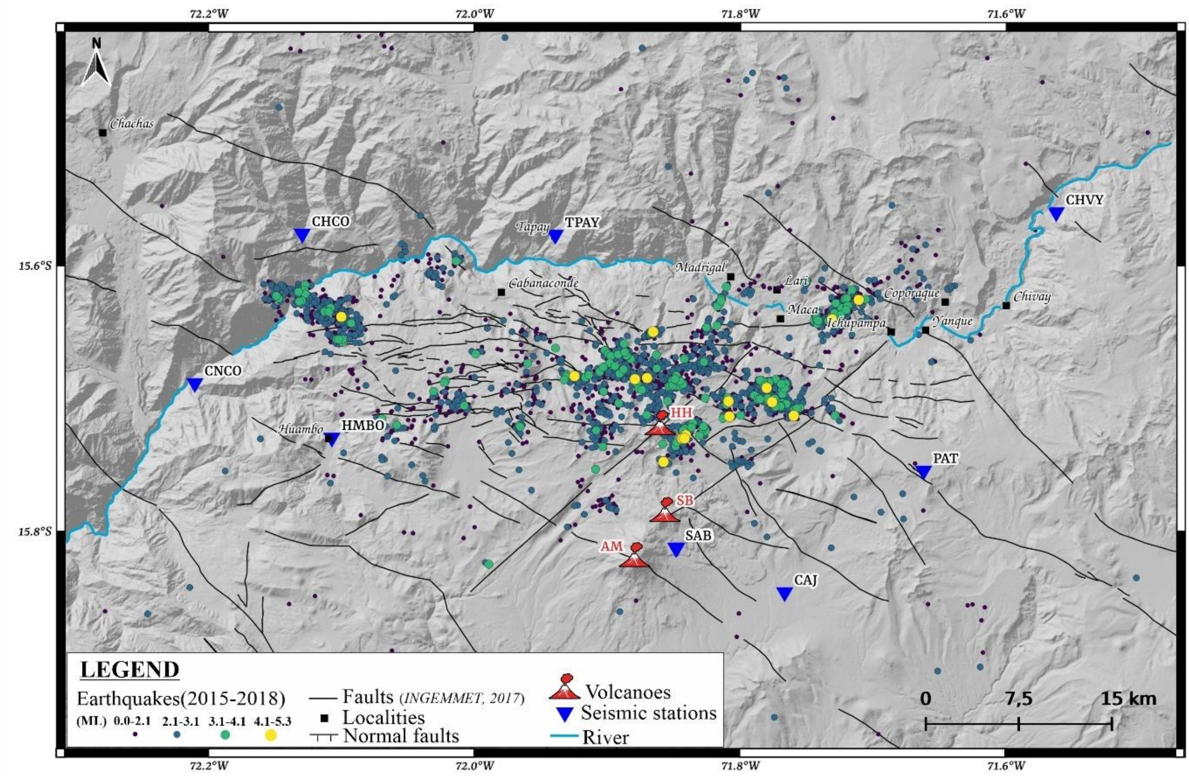

Figure: Spatial distribution of relocated seismic activity in the Colca Valley, southern Peru, during the period 2015–2018. Events are color-coded according to their local magnitude (ML). Cortical faults (black lines) are sourced from the database of the Geological, Mining, and Metallurgical Institute (INGEMMET), while blue triangles indicate stations in the local seismic network operated by the Geophysical Institute of Peru (IGP). The volcanoes Ampato (AM), Sabancaya (SB), and Hualca Hualca (HH) are also shown. The distribution of seismicity reveals clustering patterns and alignments that indicate strong structural control associated with the major cortical fault systems.

Lucile Costes

Rake-changing repeaters : a new class of co-localised similar earthquakes with both correlated and anti-correlated waveforms

***Authors**: Lucile Costes (ISTerre, France), David Marsan (ISTerre, France), Blandine Gardonio (ISTerre, France)*

Repetitive rupture of the same asperity has been documented in various tectonic settings through the observation of highly correlated waveforms from co-located earthquakes. These events, known as repeaters, are of particular interest because they provide key constraints on small-scale fault processes. In fewer cases, highly similar earthquakes exhibiting polarity inversions at all recording stations have been identified. These so-called anti-repeaters are thought to rupture the same asperity with an inverted focal mechanism. To our knowledge, no intermediate case involving rupture of the same asperity with a change in slip direction (rake) has been reported.

In this study, we search for such events within the aftershock sequence of the M7.1 Miyagi-Oki earthquake (26 May 2003), in the northeastern Japan subduction zone. This intermediate-depth intraslab sequence (70 km depth) exhibits a high seismicity rate and is well recorded by a dense seismic network. Using data from the 17 closest seismic stations, we compute waveform coherence, cross-correlation and anti-correlation for both P and S waves of event pairs. We identify 40 pairs of highly similar earthquakes displaying polarity inversions at several (but not all) stations. After performing relative hypocenter relocation, we retain thirteen co-located pairs with high-quality waveform similarity and polarity inversion. By comparing measured amplitude ratios with synthetic radiation pattern ratios, we invert the rake change for each event pair.

At this stage, the physical mechanism responsible for this newly identified class of similar earthquakes, that we name ‘rake-changing repeaters’, is uncertain. A change in rake between successive ruptures of the same asperity likely reflects a highly localised modification of the stress field. It could be driven by transient pore-fluid pressure variations or stress perturbations induced with nearby moderate slip. The identification of rake-changing repeaters opens new perspectives for investigating the complexity of local faulting processes at depth.

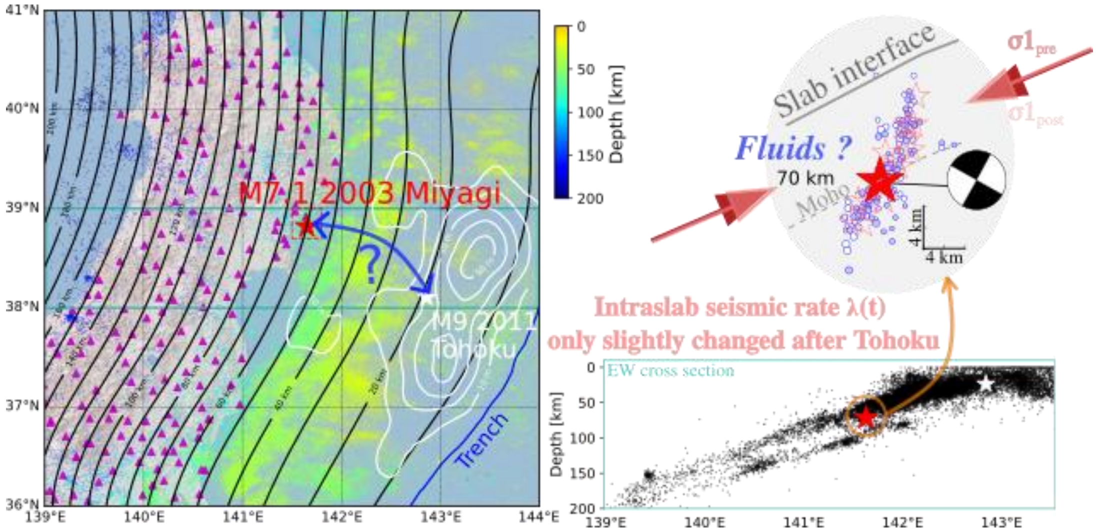

Figure: Rake-changing repeaters. (Top) P-wave waveforms of two rake-changing repeaters at two stations, exhibiting correlation and anti-correlation, respectively. (Bottom) Bloc diagram of a fault, showing the slip vectors of the two events, corresponding to a rake change of 40°. The implications of such characteristics are illustrated with a scheme.

François Faure

Multi-Modal Remote Sensing Segmentation of Geomorphological Objects with Deep Learning and Self-Supervision

***Authors**: François Faure (ISTerre, France), Swann Zerathe (ISTerre, France), Laurence Audin (ISTerre, France), Lorena Rosell-Guevara (Instituto Geológico, Minero y Metalúrgico INGEMMET, Perú), El Amira Cerine Bencheikh (ISTerre, France), James Holligsworth (ISTerre, France), and Sophie Giffard-Roisin (ISTerre, France)*

Mapping geomorphological objects is a major source of information for geological studies and natural hazard management. However, manual mapping requires time and expert knowledge. Recent advances in deep learning have led to numerous supervised techniques, but they remain limited to small geographic areas and rely mainly on optical imagery. The lack of digital elevation model integration and the need for large amounts of labelled data (often scarce in geomorphology) limit their performance. We thus study the capabilities of self-supervision and foundation models for large-scale mapping, based on Sentinel-2 red, green, blue, and infrared channels, as well as the TanDEM-X digital elevation model. We focus on active fault scarps, paleo-landslides, and active river channels in southern Peru and northern Chile. We created three new datasets, one for each object, which are employed to fine-tune and test different self-supervised models (GeomorPM, Copernicus-FM, TerraMind) against a benchmark supervised architecture (Residual U-Net). The results show that remote sensing foundation models can capture geomorphological features. We illustrate that self-supervision improves mapping quality compared to standard supervised approaches, especially when labelled data are scarce. The fine-tuned TerraMind model, adapted for each of the three objects, outperforms the Residual U-Net, GeomorPM, and Copernicus-FM, and demonstrates strong potential as a pre-mapping tool. We finally highlight the critical role of multimodality, particularly DEM data, for geomorphological segmentation tasks. Extending our method to new regions and objects, as well as understanding the geomorphological and deep learning factors influencing the detection performance are part of the PhD ongoing work.

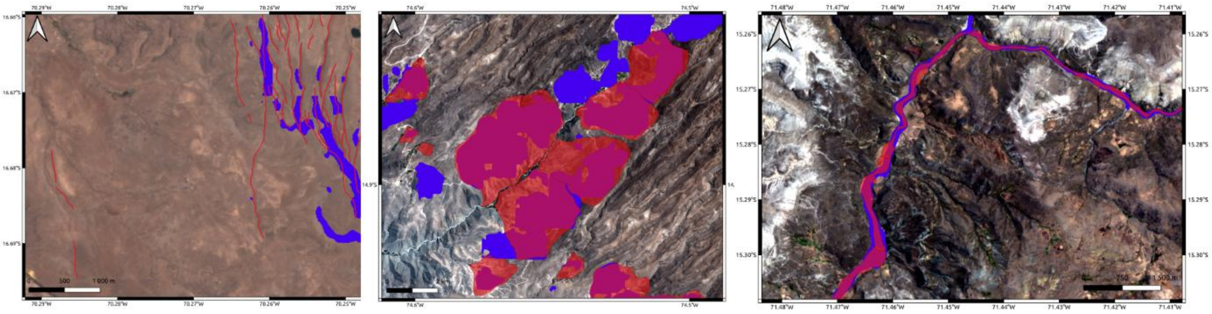

Figure: Segmentation results of active fault scarps (left), paleo-landslides (center), active river channels (right) with TerraMind-UPerNet model. Red: ground-truth (what should be detected, human manual mapping). Blue: prediction (what is detected by the model). Background image: Sentinel-2 RGB

Maaike Fonteijn

Bridging geodynamics and earthquake cycles in the central Apennines (Italy)

***Authors**: Maaike Fonteijn (ISTerre, France), Alexander Koelzer (Department of Earth Sciences, The Netherlands), Erwan Pathier (ISTerre, France), Anne Socquet (ISTerre, France), Ylona van Dinther (Department of Earth Sciences, The Netherlands)*

The Central Apennines undergo a large-scale extension with normal-faulting earthquakes of up to Mw ~7. These earthquakes occur on a complex fault network and are strongly clustered in space and time. Present-day deformation may therefore not be representative of long-term tectonic loading and seismic hazard. Furthermore, the tectonic drivers of extension and seismicity, as well as the presence of slab detachment beneath the Central Apennines, remain debated. We used 2D seismo-thermo-mechanical modeling with a visco-elasto-plastic rheology to address these questions. We show that the slab is detached, and that relative Adriatic plate motion is responsible for 50 % of the extension and eduction of subducted upper crust for 40 %.

We extend this modeling approach by introducing an invariant rate-and-state friction formulation and adaptive time stepping. This allows for the simulation of fully dynamic earthquake sequences within the same geodynamic framework. Faults are initiated as weak zones to localize deformation. Nevertheless, faulting can occur everywhere in the model depending on stress and strength conditions.

We simulate sequences of large normal-faulting earthquakes and aseismic slip events over ~20 kyr in a complex normal-fault network. Rupture on one fault transfers stress to adjacent faults and can trigger aseismic slip on nearby faults. These interactions govern where subsequent earthquakes occur. More than half of the total fault slip occurs aseismically.

We furthermore assess the variability of interseismic surface velocities between and within interseismic periods. Preliminary results show variability of several mm/yr in interseismic surface velocities. Some interseismic periods are relatively quiet and show little dispersion in velocities, whereas others exhibit larger velocity variations related to aseismic slip.

Our new modeling approach allows for the first time to simulate earthquake sequences within a self-consistent geodynamic framework. This enables a direct link between long-term tectonic loading and short-term geodetic and seismological observations.

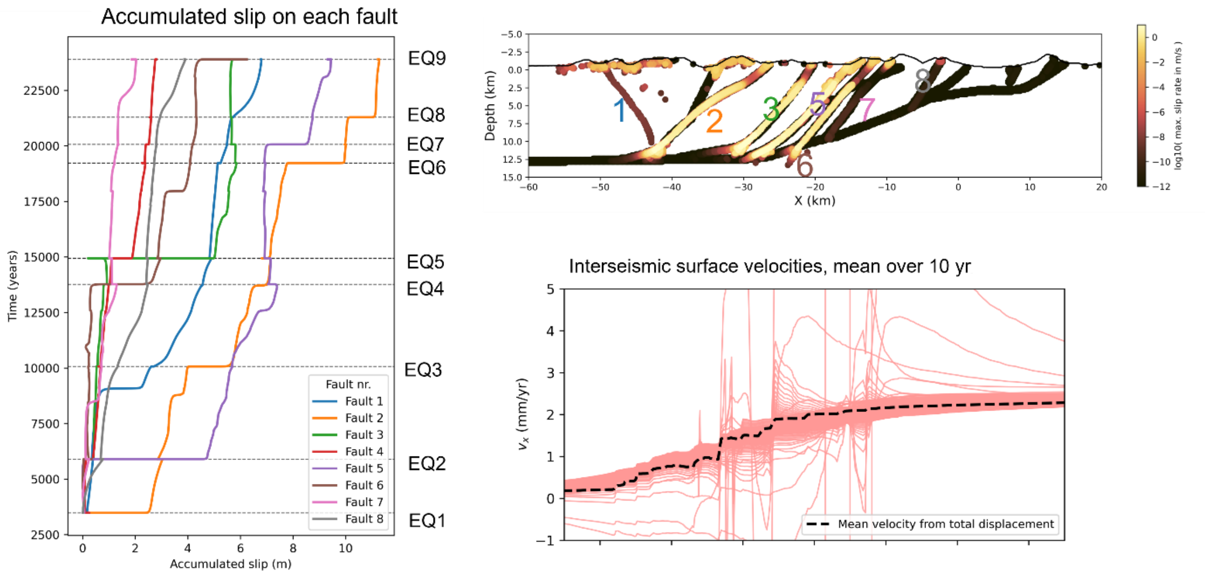

Figure: Simulated sequence of 8 normal-faulting earthquakes. a) Accumulated slip on each fault, demonstrating fault interaction. b) Maximum slip rate and corresponding fault numbers of fig a). c) Interseismic surface velocities of interseismic period 6, averaged over 10-year windows, illustrating the variability in surface velocities within one interseismic period.

Tom Hinton

Fault zone imaging of continental earthquakes: Bayesian inversion of near-fault geodetic data

***Authors**: Tom Hinton (ISTerre, France), Théa Ragon (ISTerre, France), James Hollingsworth (ISTerre, France), Mai-Linh Doan (ISTerre, France)*

Faults are commonly modelled as planar structures, but field and seismic observations show that faults are surrounded by a “damage zone” up to several hundred metres wide, in which the rock is fractured and its effective shear modulus is reduced. This damage zone influences near-fault surface deformation, and could influence the rupture mechanism – yet it is neglected in slip inversions, potentially biasing estimates of slip distribution and shallow slip deficit.

Recent developments in satellite coverage and optical image correlation processing now provide high-resolution images of near-fault surface displacement caused by major continental earthquakes – data that was previously inaccessible due to InSAR decorrelation near the fault. Can this near-fault geodetic data be used to image the damage zone around a fault?

We model surface deformation using 2D analytical solutions for a fault with compliant zone of reduced shear modulus (after Segall 2010). We use Bayesian slip inversion to solve for the distribution of slip on a fault, while also solving for the damage zone width and shear modulus. Far-field InSAR and GNSS constrain slip distribution at depth, and then near-fault optical data resolves the shallow slip and damage zone. Synthetic inversion tests demonstrate that the damage zone signal reaches 2–6% of total coseismic displacement, concentrated within 1–2 damage zone widths of the fault. This signal is resolvable for optical data noise levels up to ~3–4% and resolution improves with denser near-fault sampling.

Synthetic resolution tests place clear constraints on what can and can’t be resolved, providing context for previous literature results. Imaging the full along-strike length of the fault zone would allow us to study the relationship between fault zone and rupture mechanism. Our ongoing case study is the 2019 Ridgecrest doublet.

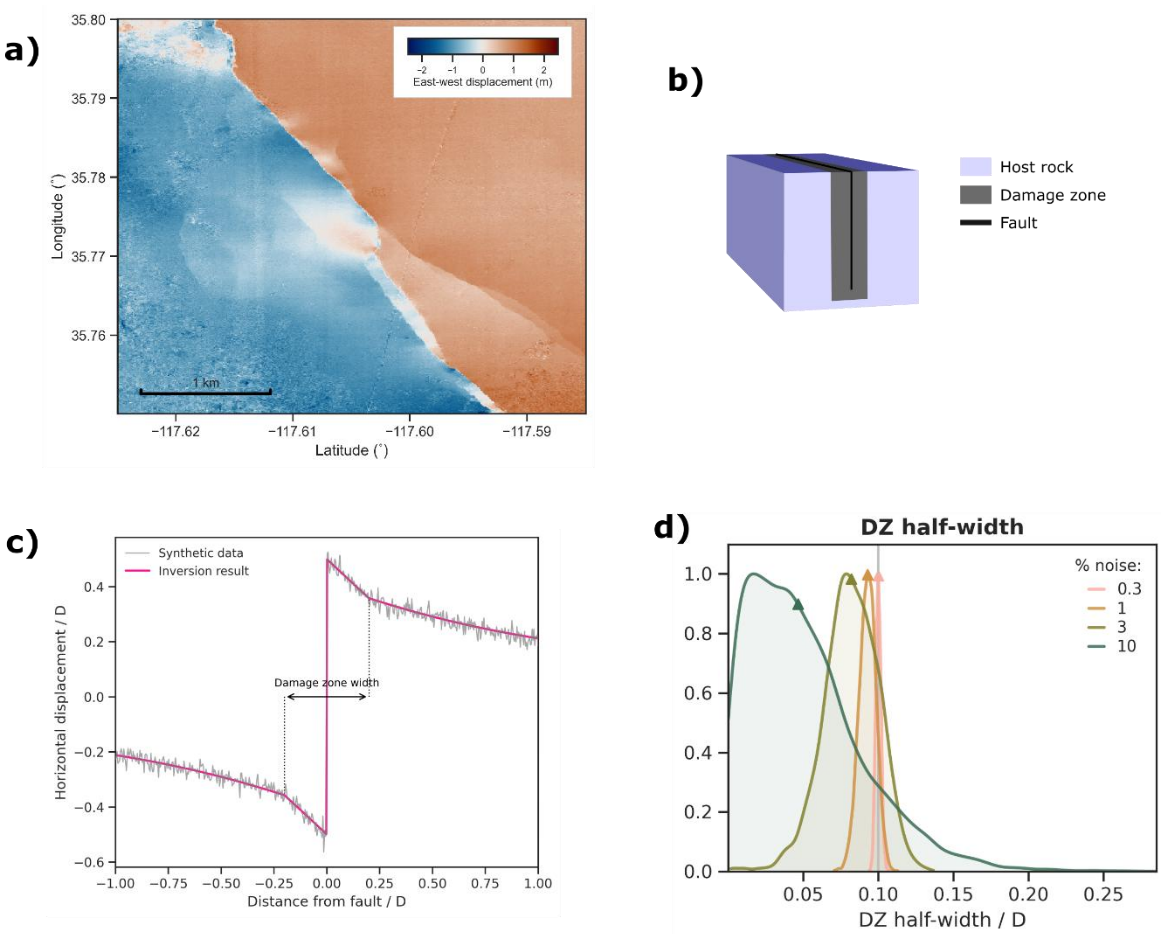

Figure: (a) Optical N-S displacement map for the Ridgecrest 2019 earthquake doublet; (b) fault zone model; (c) surface displacement profiles across a fault with a compliant fault zone and strike slip motion; (d) posterior distributions of the damage zone half-width parameter after a Bayesian inversion of synthetic data with different levels of Gaussian noise.

Cecilia Martinelli

Characterizing near-field displacements for surface-rupturing earthquakes using optical image correlation

***Authors**: Cecilia Martinelli (ISTerre, France), James Hollingsworth (ISTerre, France)*

Understanding how active fault systems accommodate deformation during large earthquakes requires a detailed knowledge of the surface co-seismic displacement field. Recent advances in very high-resolution satellite imaging, coupled with Optical Image Correlation (OIC) techniques, provide a powerful approach to document surface deformation in very high spatial detail. Unlike InSAR, OIC remains coherent close to surface ruptures, and thus provides constraints on the near-field displacement. Consequently, OIC techniques have found utility in documenting the degree of co-seismic displacement accommodated on and off the fault, as well as the fault zone width (FZW). Such measurements provide valuable insight into the mechanics of shallow crustal faulting, with important implications for Seismic Hazard Assessment.

The correlation approach used to retrieve the displacement field can bias the displacement result by spatially smoothing the displacement field (artificially widening FZW), and producing inaccurate results near discontinuities. Recent approaches typically estimate FZW with a strain thresholding approach, which maps the transition between elastic and inelastic deformation where strain exceeds 0.5%. However, a 0.5% strain threshold may also be sensitive to rheology, rupture speed, image resolution, etc. Therefore, it remains unclear to what extent we can trust estimates of off-fault deformation and FZW based on OIC.

In this study, we quantitatively explore sources of correlator bias using satellite imagery resampled to contain known synthetic earthquake displacements. We then compare outcomes of different OIC algorithms (MicMac, COSI-Corr, ASP, MicroFlow - a new deep learning-based correlator) on different optical datasets (Pleiades, WorldView, SPOT, ADS80) spanning the 2019 Ridgecrest earthquake. We retrieve estimates of FZW and slip localisation, and assess how different algorithms and data can bias interpretations of near-field deformation. This work highlights both the potential and limitations of OIC for measuring the complexity of the ruptures in a fault system and how such data can be used for improving measurement robustness and interpretability of near-field deformation processes for future earthquake studies.

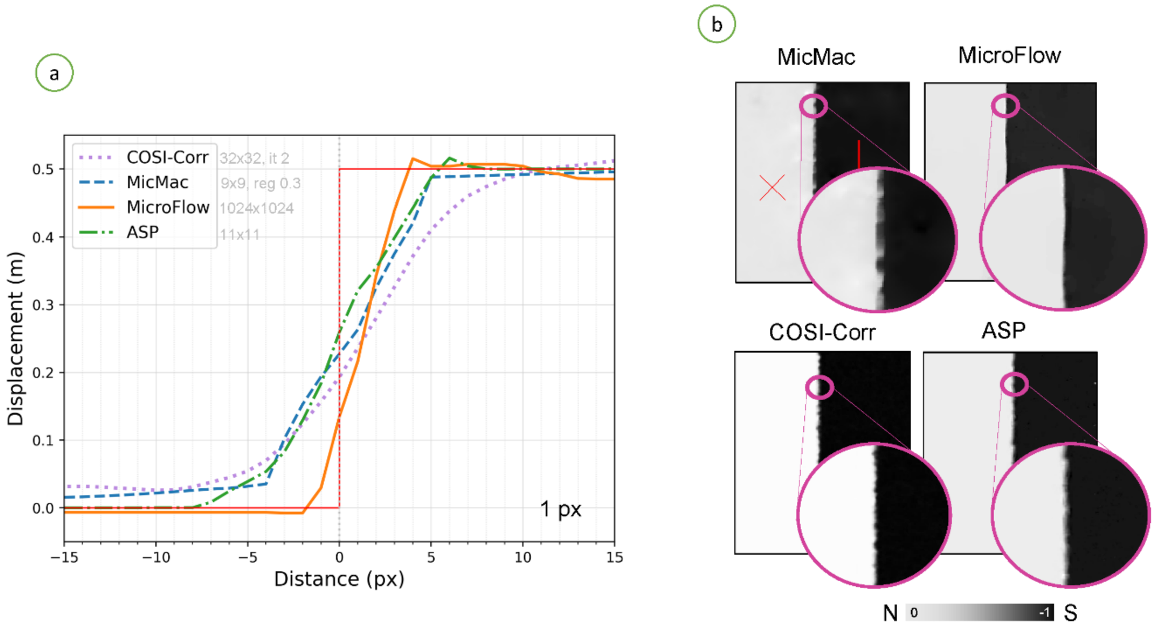

Figure: Comparison of displacement profiles and fault sharpness obtained with different image-correlation methods. (a) Displacement profiles extracted across a synthetic 1 px displacement discontinuity for four correlation approaches: COSI-Corr, MicMac, MicroFlow, and ASP. The red dashed line indicates the applied step displacement of 0.5 m (equal to 1 px). MicroFlow reproduces the sharpest displacement gradient, while COSI-Corr produces a smoother transition across the fault. (b) Corresponding displacement maps showing the fault discontinuity for each method. Insets provide a zoom on the fault zone to highlight the sharpness and spatial diffusion of the displacement gradient

Batul Nemr

Accounting for earthquake interactions in a probabilistic seismic hazard assessment for the Levant Fault System

***Authors**: Batul Nemr (ISTerre, France), Céline Beauval (ISTerre, France), Marlene Brax (CNRSL, Lebanon), Yann Klinger (IPGP, France)*

This study focuses on the Levant Fault system (LFS), a 1200-km strike-slip fault connecting the Red Sea to the East Anatolian fault. We aim to understand how using earthquake simulators may improve PSHA there. We use the physics-based simulator MCQsim (Zielke and Mai 2023) to produce long rupture catalogs that replace traditional fault-based source models. We use slip rates and fault geometry as in El Kadri et al. (2025), represent the system with 49 sections extending down to 17km depth, and mesh them into small triangular elements. Each element is assigned a slip rate, static and dynamic friction, and strength properties. Between earthquakes, the faults are loaded with backslip. We generate a 200,000-year rupture catalog with magnitudes up to Mw7.6, consistent with reported historical seismicity. At the scale of the fault system, the long-term magnitude-frequency distribution follows a Youngs and Coppersmith characteristic shape. Rates in the moderate magnitude range M<6 are larger than observed in the instrumental period, even when accounting for variability in time. Rates in the upper magnitude range are within the uncertainty of observed historical rates. On the long-term, 7% of the moment rate budget is not accommodated by earthquakes, compatible with a system that is thought to be entirely locked. In fact, analyzing the total slip rate per element shows that this unspent budget occurs on short fault sections due to artificial tapering of slip at the edges for modeling. Participation rate maps show that moderate events are distributed homogeneously along the fault system, while M7+ events are uneven along the main strand, likely due to geometrical reasons. We show that the fit with scaling relationships strongly depends on how earthquake dimensions are estimated from slip distributions. We combine the ruptures with a ground-motion model, and propagate the uncertainties identified up to the hazard levels. Further work is required to understand how results depend on uncertainties on input parameters, as well as why ruptures currently do not jump over major discontinuities, limiting the maximum possible earthquakes.

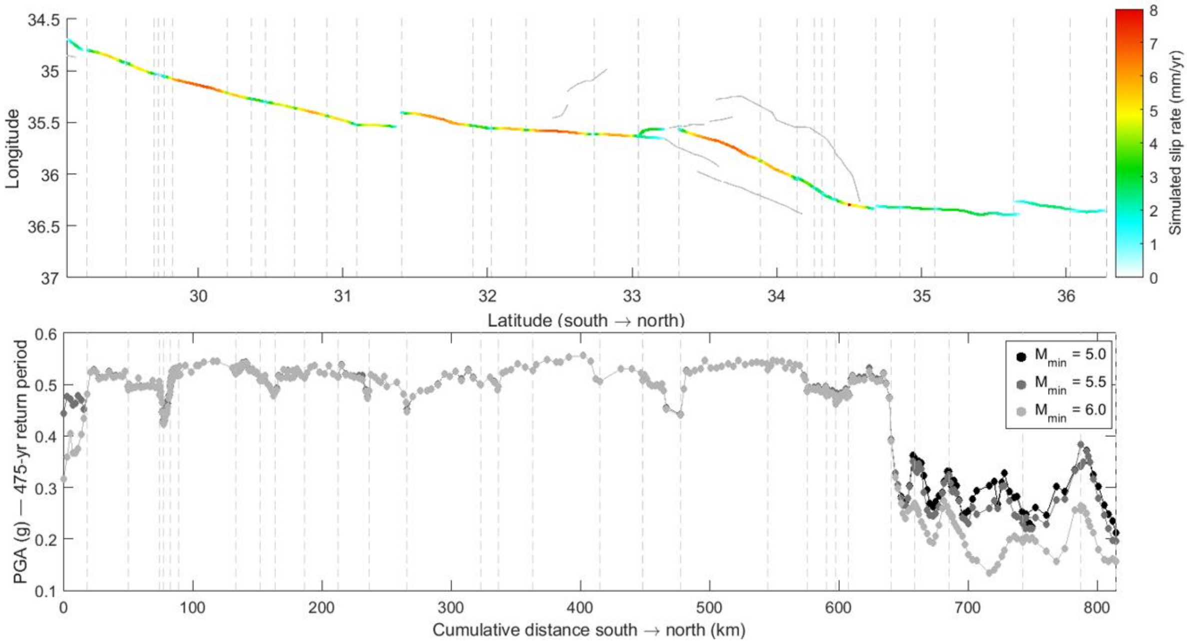

Figure: Seismic hazard profile along the LFS. Top panel: Cumulative slip rate released along the surface trace. Bottom panel: PGA values vs cumulative distance from the South, at 10% trimming (*to define a rupture plane), for different Mmin. PGA at 475-years return period, Vs30=760 m/s, Chiou & Youngs (2014) ground-motion model.*

Tectonics, Relief And Basins

Yannick Boucharat

Dynamic topography atop the Caribbean double subduction

***Authors**: Yannick Boucharat (ISTerre, France), Laurent Husson (ISTerre, France), Diane Arcay (Géosciences Montpellier, France), Nestor Cerpa (Géosciences Montpellier, France)*

Understanding the link between subduction dynamics and surface topography in subduction zones is essential for biogeographic reconstructions. Here we focus on the Caribbean Plate, overriding plate of the Pacific subduction zone to the west and the Atlantic subduction zone to the east. In this study, we test different processes that may control vertical velocity variations in the upper plate using thermo-mechanical models in simple Cartesian configurations. In particular, the isolation of the upper mantle by the two subducting slabs could cause variations in dynamic topography. We quantify these variations to decipher their contributions at the surface, to later reconstruct the paleogeography using more complex models, allowing us to establish a link with the biodiversity of the Caribbean during the Cenozoic era. We show here that the total convergence velocity of the facing slabs and the rheology of the upper plate control upper mantle dynamic pressure, and thus dynamic topography. A weak rheology of the upper plate and low velocities allow slab rollback, leading to continuous depression of the upper mantle and surface subsidence, whereas strong rheology and fast velocities anchor trench positions, leading to slab folding at the mantle transition zone and cyclic overpressure and underpressure, resulting in cyclic uplift and subsidence. Such process could have allow successive emersions and drownings of terrestrial pathways in the Caribbean, controlling terrestrial flora and fauna migrations across the Lesser and Greater Antilles.

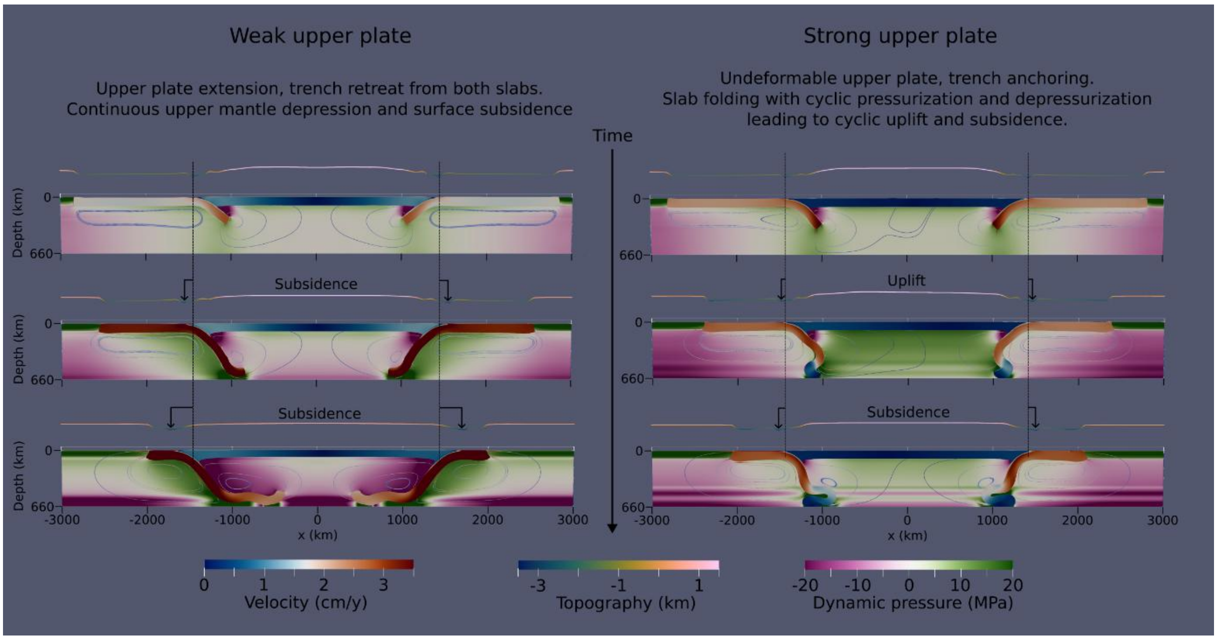

Figure: Mechanical subduction modelling of two facing slabs with a weak upper plate (left panel) and a strong upper plate (right panel). Thin dashed lines represent the initial trench position, associated arrows highlight trench migration. Streamlines represent the velocity vector field.

Anna Duhoux

Long-term orogenic and topographic evolution of the Western Alps: combining geo-thermo-chronological and modelling approaches

***Authors**: Anna Duhoux (EDYTEM, ISTerre), Yann Rolland (EDYTEM), Stéphane Schwartz (ISTerre)*

This thesis aims to help bridge the gap between geological data and large-scale palaeogeographical models in the western part of the Alpine belt, in order to better understand its long-term polyphase evolution. Combining structural geology, geochronology, thermochronology and thermo-mechanical modelling allows us to propose plausible deformation sequences and topographic evolution through time.

Sampling and structural characterisation, across and along-strike of the belt, provide additional geological constraints on the evolution of the western Alps. The fieldwork area currently includes the Chablais region (deformed Subalpine units and Préalpes nappes), the Rocheray External Crystalline Massif and its overlying flysch units, as well as the Chenaillet ophiolite and underlying Schistes Lustrés. All these units recorded several distinct tectonic events that contributed to the building of the Western Alps. The resulting data are therefore key for constraining future thermo-mechanical simulations.

The first modelling phase was designed as preliminary work to constrain the Pyreno-Provencal structural and topographic inheritance before the onset of Alpine collision sensu stricto. It also aims to reconcile diverse geological evidence across southeastern France by simulating the lithospheric behaviour of the linkage zone between the Pyrenean and Valaisian domains during Cretaceous tectonics. Our results show that “en-échelon” rifting, followed by rapid inversion and subsequent slow convergence, successfully reproduces first-order geological observations. The preferred model displays similar magnitudes of extension in both the Pyrenean and Valaisan/Vocontian segments, i.e. significant Cretaceous burial of the Pelvoux Massif followed by its exhumation, together with continuous subsidence within the Vocontian Basin. It also preserves a poorly deformed and topographically stable linkage zone, consistent with the Durancian Isthmus inferred from Provence geology. Finally, the model highlights the importance of the inherited Variscan crustal structure, mainly its high thermal state, in controlling subsequent deformation.

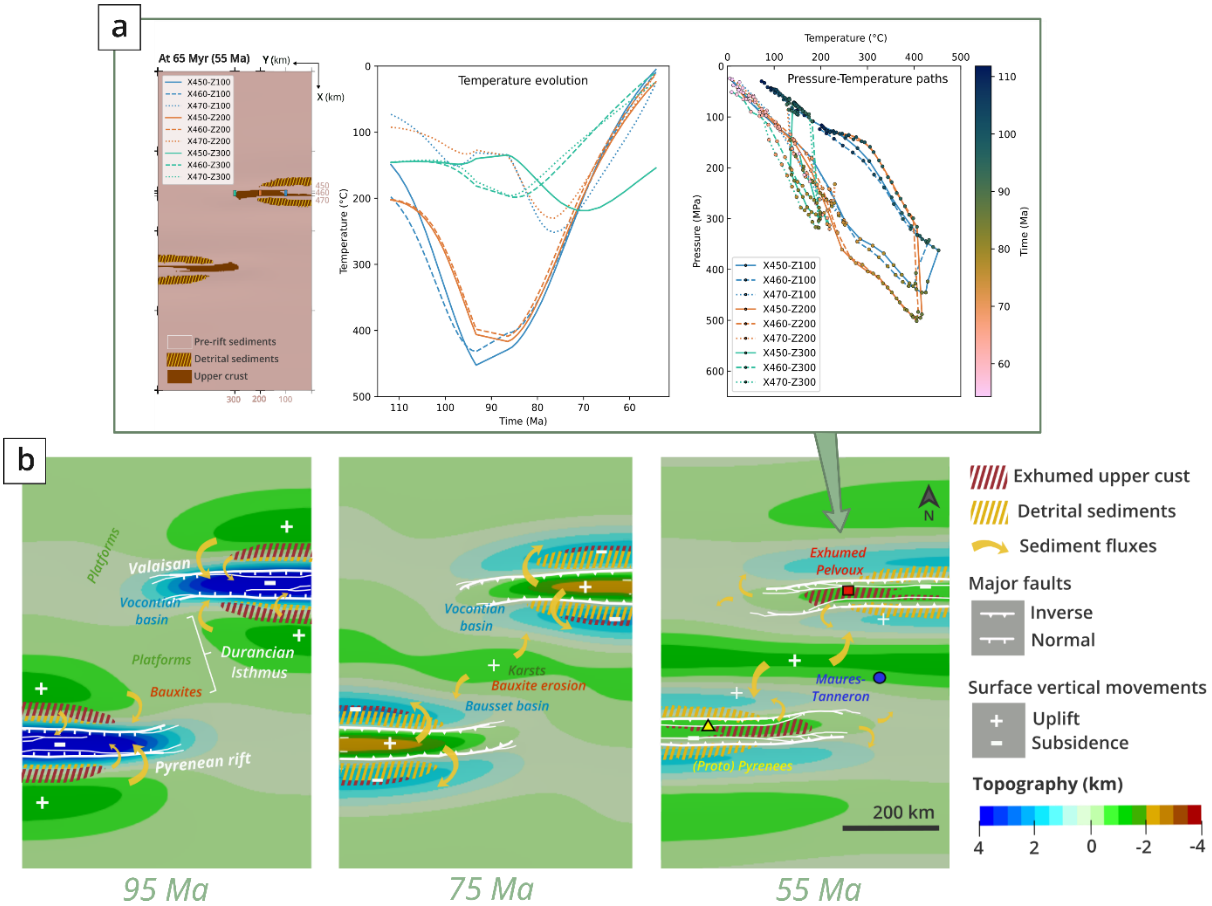

Figure: Pyreneo-Provençal modelisation results: linkage between Pyrenean and Valaisan domains during Cretaceous. (a) Passive markers positioning, temperature evolution and P-T-t paths for the Pelvoux Massif units. (b) Palaeogeographical and geological interpretation of the preferred model.

Bastien Féaud

Post-glacial geomorphic response, erosion dynamics and sediment transfer in the Eastern Pyrenees

***Authors**: Bastien Féaud (ISTerre, France), Pierre Valla (ISTerre, France), Romain Delunel (EVS, France), Magali Delmas (UPVD, France), Julien Carcaillet (ISTerre, France), Benjamin Lehmann (ISTerre, France), Marie-Edmée Torcheboeuf (UPVD, France), Nouméa Paradis (ISTerre, France)*

Mountain landscapes have been deeply shaped during the Quaternary by glacial–interglacial cycles. In the context of current climate change, quantifying alpine erosion remains challenging due to the complex interaction of geomorphic processes across varying timescales. This work aims to better constrain the transient geomorphic response and sediment transfer in alpine catchments, particularly since the Last Glacial Maximum (LGM, ca. 20 ka), using terrestrial cosmogenic nuclides (TCNs) 10Be and 26Al as proxies for erosion processes. We focus on the Ariège and Têt catchment (Eastern Pyrenees), high-relief areas with diverse lithologies and extensive Quaternary glacial imprints. Modern river sediment samples were collected along the main river and their tributaries, covering contrasting lithologies, topo-climatic conditions, and glacial coverage during the LGM. This dataset is complemented by lateglacial sedimentary archives and fluvio-glacial terrace deposits from the downstream foreland in the Ariège catchment.

26Al/10Be ratios in modern river sediments are mostly consistent with surface exposure and minimal burial or recycling, indicating relatively simple sediment transfer dynamics. Measured 10Be concentrations in modern river sediments are 2 to 5 times higher than in lateglacial and fluvio-glacial sediments, suggesting effective glacial erosion that partially reset the TCN signal, followed by a post-glacial adjustment towards an "interglacial" signal. Catchment-averaged denudation rates derived from 10Be show high spatial variability (33 to 294 mm/ka), with a significant correlation between denudation and mean catchment slope. This suggests that topography exerts a primary control on present-day erosion patterns, while other climatic or lithological parameters play a secondary role.

Our work contributes to a better understanding of the sensitivity of alpine landscapes to climate forcing and associated changes in geomorphic processes over glacial-interglacial oscillations, using TCN approach for quantifying erosional processes, sediment production and transfer in mountainous environments.

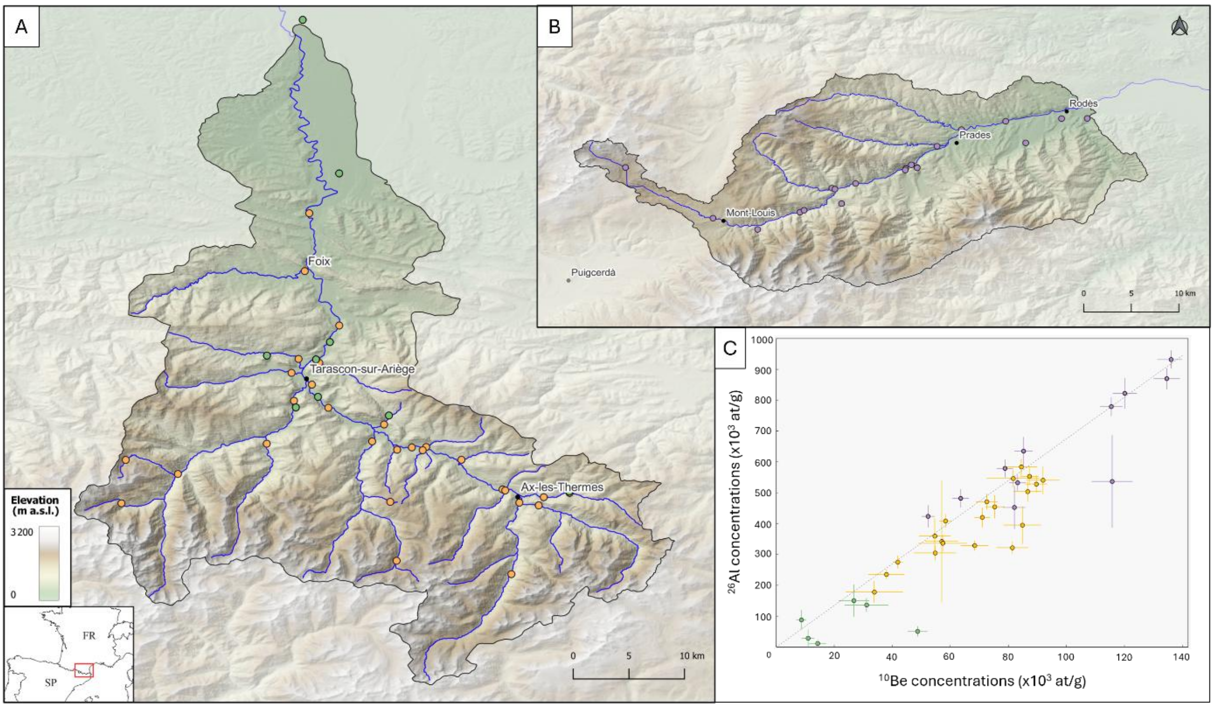

Figure: Samples locations in the Ariège (A) and Têt catchments (B). Modern river sediment samples are represented in orange (Ariège) and purple (Têt), while Lateglacial/Fluvio-glacial deposits are represented in green. C: Relationships between 26Al and 10Be concentrations for all samples. The dashed grey line represents the surface production ratio (6.75:1), and samples are colored as in panels A and B.

Martin Huraut

Chronostratigraphy in the Miocene Digne-Valensole basin (SE France): Magnetostratigraphy and U-Pb dating of fossil oysters.

Authors: *M. Huraut (ISTerre, France), J. Léger (ISTerre, France), D. Bienveignant (ISTerre, France), A. De Leeuw (ISTerre, France), A. Villand-Jacquet (ISTerre, France), W. Krijgsman (Dep. Of Earth Sciences, The Netherlands), M. Krasnoperov (Dep. Of Earth Sciences, The Netherlands)*

The sedimentary records of the Digne-Valensole Basin provide an excellent window into the tectonic and climatic history of the Alpine foreland during the Miocene. However, this basin lacks a robust chronostratigraphic framework because it lacks volcanic ash and fossils of stratigraphic interest. The present study presents new chronostratigraphic data based on two methods: magnetostratigraphy and U–Pb dating of calcite of oyster fossils.

The marine molasse of the Digne Basin yielded U–Pb ages for 12 stratigraphic levels. The paleomagnetic study, meanwhile, is based on the analysis of 260 samples distributed over 800 m of sedimentary thickness. The interval studied corresponds to the transition from marine to continental molasse, and the results of this study suggest that the transition is dated to around 13.8 Ma (Langhian–Serravallian transition, Middle Miocene). This date corresponds to a major climatic event: the Mid-Miocene climatic transition (mMCT), that follow the Middle Miocene Climate Optimum (mMCO).

U—Pb dating of oyster fossils remains an emerging application of the U–Pb method. Magnetostratigraphy thus appears to be a method that allows 1) the validity of U–Pb ages to be assessed, 2) the section to be dated at higher resolution, and 3) dating to be extended to continental sediments.

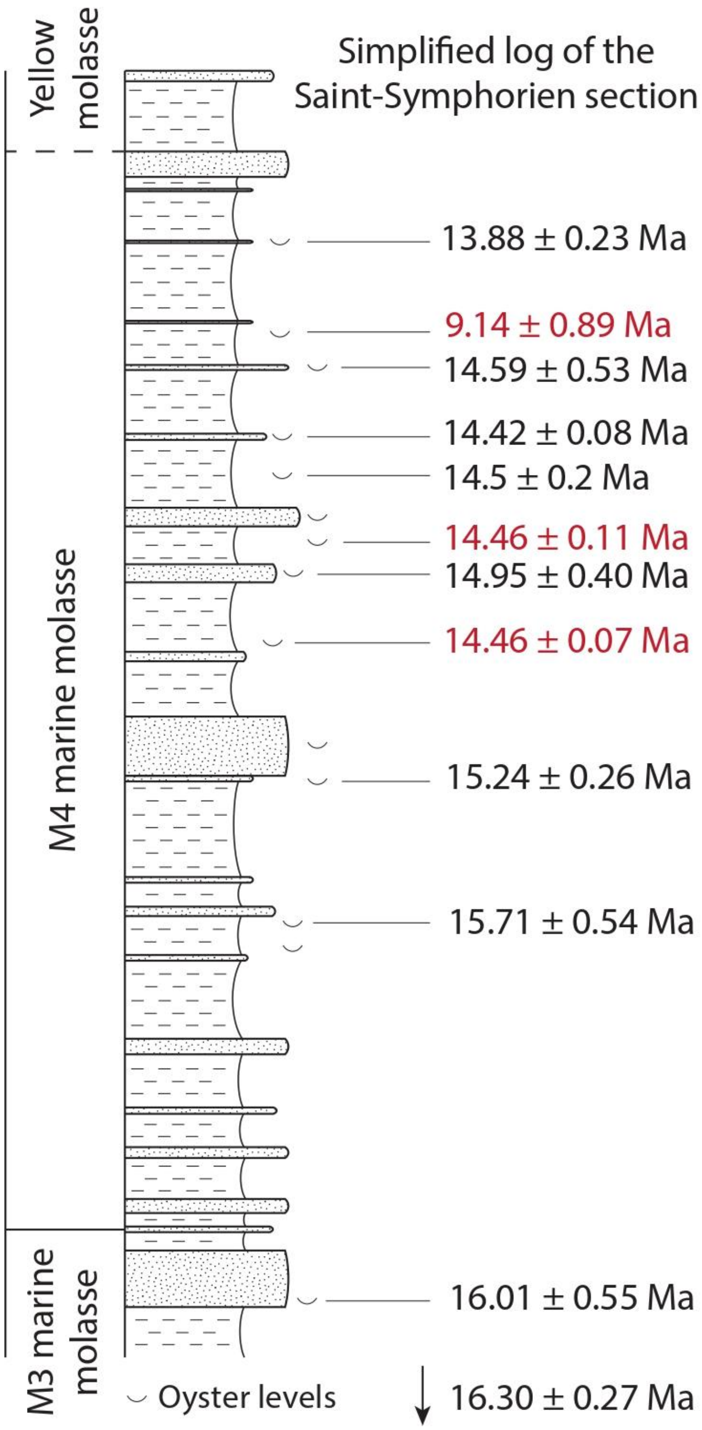

Figure: U-Pb ages of oyster calcites in the Saint-Symphorien section, Digne-Valensole basin, SE France.

Marcelline Péan

Reconstructing ice sheet fluctuations in Terre Adélie (East Antarctica): a cosmogenic nuclides perspective

***Authors**: Marcelline Péan (ISTerre/Edytem, France), Yann Rolland (Edytem, France), Pierre Valla (ISTerre, France)*

The contribution of the East Antarctic Ice Sheet (EAIS) to future global sea level rise and climate change remains a major source of uncertainty in climate projections. To reduce this uncertainty, we propose new reconstructions of EAIS fluctuations in Terre Adélie and investigate their relationship with oceanic forcing mechanisms. Previous works provide geomorphic and chronological evidence that the ice sheet extended to the continental shelf break during LGM (Last Glacial Maximum; ~20ka). However, its response to the major climate and oceanic transitions following the LGM remains poorly constrained.

Here, we combine paired in situ cosmogenic nuclide exposure age (10Be-26Al) from inland and coastal nunataks and with beryllium isotopes measurements from marine sediments cores. Exposure ages from inland nunataks indicate long-term ice-free conditions, with apparent exposure ages reaching ~150 ka, whereas coastal sites document significant ice-sheet thinning after ~20 ka. In the Archipel Pointe Géologie area, erratic boulder exposure ages together with marine beryllium isotope records constrain the final phase of regional deglaciation around ~ 15 ka. Marine sediment records further suggest enhanced intrusions of Circumpolar Deep Water (CDW) onto the continental shelf since ~14.5 ka, supporting a strong oceanic control on ice-sheet retreat. These phases of deglaciation coincide with major climatic events, including the Antarctic Cold Reversal (ACR) and Meltwater Pulse 1A (MWP-1A), highlighting both the sensitivity of the EAIS margin to coupled ocean-climate forcing.

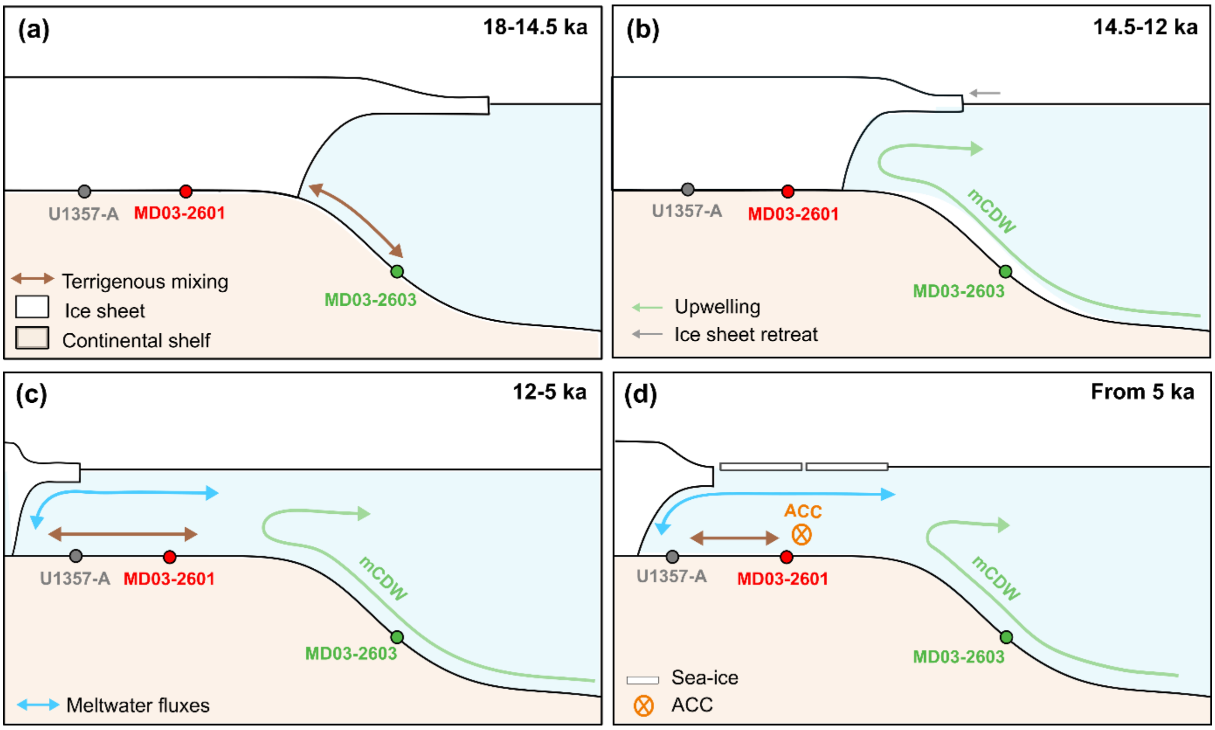

Figure: Conceptual synthesis of the main retreat episodes of the East-Antarctic ice-sheet (EAIS) since the Last Glacial Maximum, in the Adélie Land basin. The model illustrates the main variations in the marginal position of the EAIS in response to ocean circulation, in particular modified Circumpolar Deep Waters (mCDW) and onset of the Antarctic Coastal Current (ACC). (a)-(d) panels are sectional views of the EAIS and Adélie Land basin during the key-time periods discussed in the text. The meltwater input (blue lines), terrigenous mixing (brown lines), ACC (Antarctic Coastal Current; orange line), and CDW (Circumpolar Deep Waters; green line) are inferred from multi-proxy records from proximal and distal sediments presented in this study.

Vincent Polin

Investigation of coastal dynamics in French Guiana and human settlements using sedimentological and geomorphological studies

Authors: *Vincent Polin (ISTerre, France), Pierre Valla (ISTerre, France), Cécile Gautheron (ISTerre, France)*

French Guiana has a wide coastal area open to the Atlantic Ocean, combining the ancient coastal plain of Coswine (Upper Pleistocene) and the recent coastal plain of Demerara (Holocene), separated by an erosional ridge. A global transgressive sedimentary sequence on the Guiana shield, dating back to the Upper Pleistocene, demonstrates successive phases of marine transgressions and regressions since the Marine Isotopic Stage 5 (130-74ky). With its humid equatorial climate with dry seasons and its gently rolling coastal relief, the coastal zone represents a suitable settlement area. However, traces of settlement are sparse and relatively recent: no late Pleistocene remains (12ky maximum) have yet been identified. This absence could be explained by sea-level fluctuations, which significantly impact the area if land above water. Moreover, the proposed chronological framework for the development of the Coswine-Demerara sequences is still largely debated and is not spatially homogeneous. With climate change and the current sea levels rise, coastal habitats are more and more subject to chronic flooding, in addition to increased coastal erosion, leading to growing vulnerability for communities.

Our study aims to better understand the recent dynamics (120ky to present) of preservation and erosion of deposits along the Guyanese coastal fringe, from a morphogenetic and sedimentologic perspective, focusing on cheniers, rocky headlands and marine floodplains. We employ multiproxies analysis to characterize these dynamics and quantify the coastline evolution, using morphometric data (high-resolution LiDAR), sedimentologic data (filed crops/logs, grain size distribution) and ^{14}C, OSL, and cosmogenic nuclides dating (on rocky headlands). The field mission of October 2025 provided new data on the Demerara Plain, particularly the coastal areas of Corossony, the Guiana Space Centre, and Kamouyeneh-Macouria, in connection with a dry savanna area within the Mont Grand Matoury Nature Reserve. Our preliminary results demonstrate intrinsic variability in this plain, characterized by significant heterogeneity in the sedimentary record, with distinct erosion and depositional morphologies.

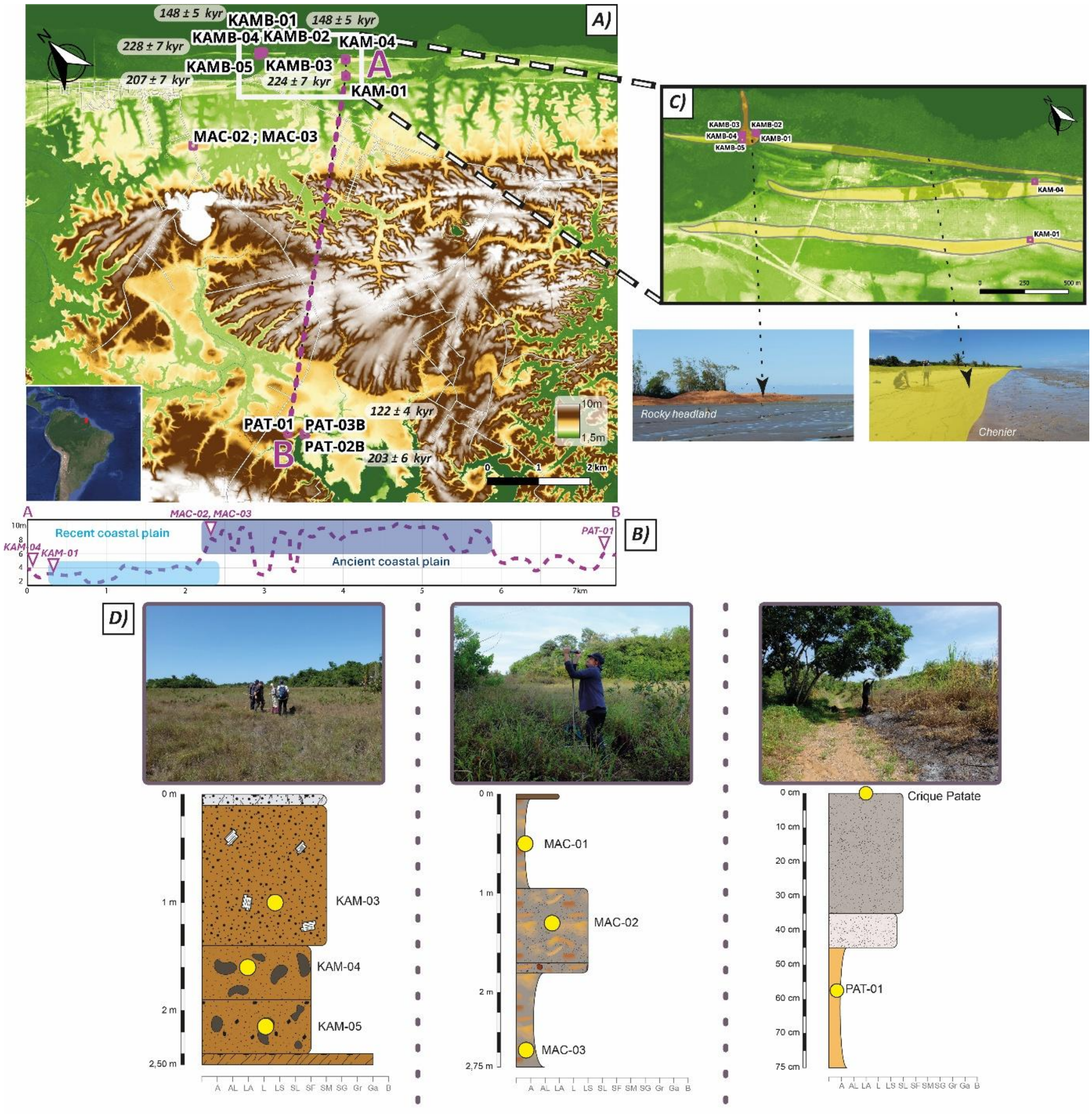

Figure: A) DTM (Digital Terrain Model) of the study zone (RGE ALTI®) with samples collected in October 2025 and the exposure age calculated from ^{10}Be concentration measurements on rocky headlands; elevation profile AB is shown in B), demonstrating a clear difference in elevation between the recent and ancient coastal plains. C) Zoom on the Kamuyeneh coastal area, with cheniers (sandbanks accumulated on a deposit of marine clays along the coastline) highlighted in yellow and rocky headlands in orange, with photos of the two morphologies. D) Three cores done in October 2025 with a photo of the sampling site, the log with OSL samples and the grain size distribution. Unimodal curves indicate alluvial or marine deposits, while polymodal curves indicate weathered deposits.

Quentin Portal

Lateglacial glaciers dynamics in the Mont Blanc foreland (Northern French Alps): model-data coupling in the Arve Valley

***Authors**: Quentin Portal (ISTerre, France), Christian Crouzet (ISTerre, France), Jean-François Buoncristiani (EPHE, Biogéosciences, France), Tancrède Leger (Institute of Earth Surface Dynamics, Switzerland), Guillaume Jouvet (Institute of Earth Surface Dynamics, Switzerland), Julien Carcaillet (ISTerre, France)*

Despite several studies (Coutterand, 2010 and references theirin) over the past decades, the chronology of glaciers advances at the Last Glacial Maximum (LGM) and subsequent retreat during the Lateglacial period in the Northern French Alps remains poorly constrained, as data are still too scarce and sometimes contradictory. In this area, the interactions between major glaciers, such as the Rhône and Arve glaciers in the north and Isère glacier in the south, represent major challenges for reconstructing post-LGM glacial dynamics. We present a new framework for understanding Lateglacial glacial dynamics in the Arve Valley, integrating 18 new 10Be exposure ages from glacially-transported boulders, with revised geomorphological mapping based on LiDAR-derived DEMs.

Our results indicate that the deglaciation of the Arve Valley initiated with a phase of glacial thinning around 17.6 ka BP. The Arve glacier subsequently thinned progressively but persisted in the downstream sector of the valley until the end of a readvance phase at 15.9 ka BP. Then, the glacier retreated by over 30 km within 300 years, before withdrawing toward the Mont-Blanc massif ahead of the Younger Dryas readvance.

To further refine our understanding, we confront 10Be exposure ages with numerical simulations of the deglaciation at 200 m resolution using the Instructed Glacier Model (IGM, Leger et al., 2025). This will enable us to analyse possible deglaciation rates and spatial patterns in the Mont Blanc foreland, as well as the influence of key parameters such as geography, topography, and climate.

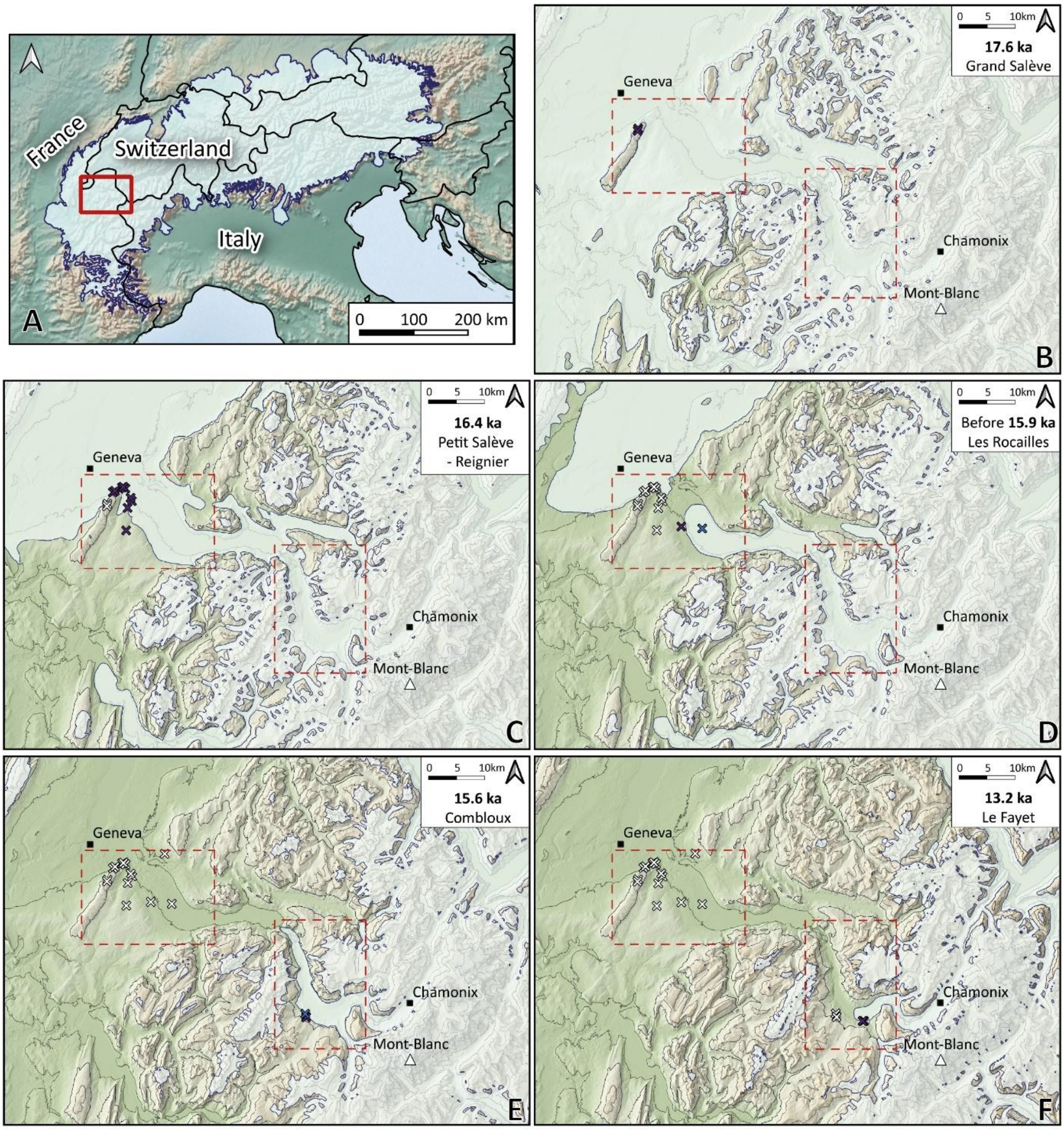

Figure: A) The study area in the global context of the Alps. LGM extension of glaciers are from Leger et al. 2025 and references therein. B to F) Schematic reconstruction of the dated deglaciation steps in the Arve Valley. Red rectangles delineate the sampling areas. Coloured crosses show sampled boulders which allowed to provide exposure ages for each retreat stadial.

Raphaël Tournier

African paleogeography since 30Ma : setting boundary conditions for climatic, physiographic and biodiversity models.

Authors: *R. Tournier (ISTerre, France), L. Husson(ISTerre, France), S. Prat (HNHP, MNHN, France), J-R. Boisserie (CFEE, Ethiopie), D. Barbon (UAR 3330 Savoirs et Mondes Indiens, Inde), N. Bellahsen (ISTEP, France), C. Doubre (EOST, France), R. Pik (CRPG, France), T. Salles (School of Geosciences, Australia), P. Sepulchre (LSCE, France), C. Tiberi (Geosciences Montpellier, France)*

The African continent has undergone major Cenozoic transformations, including the formation of the East African Rift System and the opening of the Red Sea and the Gulf of Aden. The impact of these transformations on the various components of the Earth system over time—climate, hydrographic networks, and the dispersal and evolution of biological species—raises multiple questions.

In this context, we aim to reconstruct the paleogeographic evolution of continental Africa over the past 30 million years using a multi-layered modelling approach. First, the integration of several geodynamic components (including mantle-driven dynamic topography, the history of crustal tectonics, plate tectonic motions, and volcanic eruptive dynamics) allows us to produce an elevation model for Africa since 30 Ma that is continuous in space and time. This elevation model is then used as a boundary condition for climate simulations, followed by physiographic simulations, generating a more comprehensive and coherent representation of past environments.

The simulation outputs reveal the sensitivity of climate reconstructions to topographic boundary conditions, as well as temporal variations in hydrographic networks. These new topographic, climatic, and physiographic constraints provide improved calibration for future eco-evolutionary studies on the African continent.

We then evaluate the spatial and temporal accuracy of these reconstructions by confronting them with field-based evidence. This assessment identifies the scales at which the models are most robust, informing which interrogation can be explored with confidence. It also highlights where the reconstructions are consistent with geological, paleoenvironmental, and paleontological data, and where their precision may require further refinement.

Looking ahead, the objective is to continuously update these maps and simulations, which will also be used to investigate the dispersal and evolutionary changes of Cenozoic faunal communities in Africa, notably early hominids. This whole study offers a coherent spatio-temporal context for evaluating links between the different components of the Earthsystem.

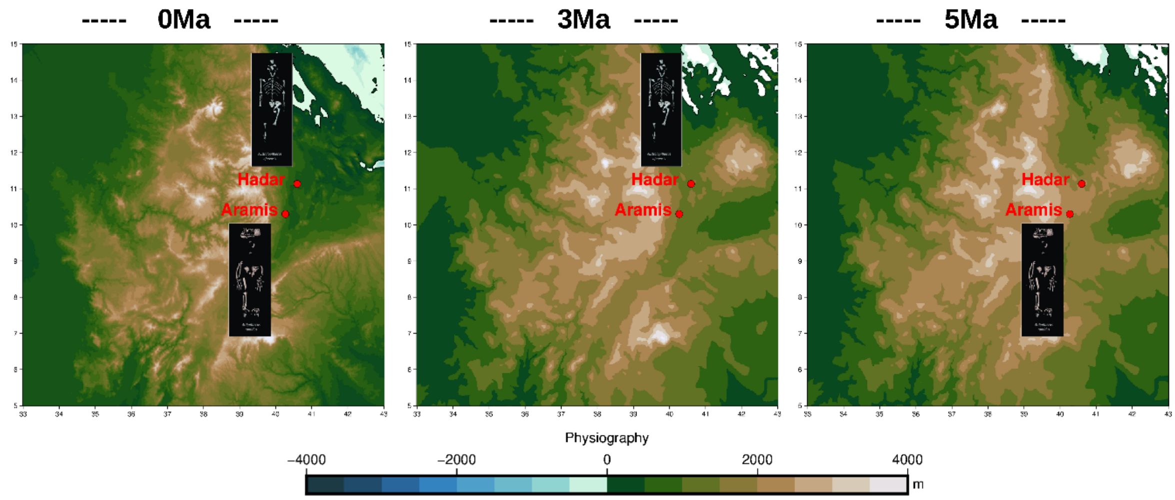

Figure: Physiographic reconstruction of the Afar region at 0, 3, and 5 Ma, showing the locations of the Hadar and Aramis hominin fossil sites, corresponding to Australopithecus afarensis ("Lucy") at 3 Ma and Ardipithecus ramidus ("Ardi") at 5 Ma. Reconstructions suggest that the region was significantly more elevated than at present, with estimated paleoaltitudes of ~1500–2000 m.

Millary Agung Widiawaty

Mangrove and coral reef interplay: insights from geological, geomorphological and oceanic factors in Indonesia

***Authors**: Millary Agung Widiawaty (ISTerre, France), Gino de Gelder (ISTerre, France), Laurent Husson (ISTerre, France)*

Mangroves and coral reefs are critical ecosystems in tropical coastal zones, yet the local environmental and geological settings that govern their distribution and development are often poorly known. This study investigates the spatial distribution and characteristics of these ecosystems in Indonesia, with a focus on the island of Sumba, by examining the underlying geological, geomorphological, and oceanic-climatic controls. We integrate geospatial big data from multiple sources, including thematic maps, field surveys, and optical and radar satellite imageries. Analytical methods include swath profile analysis, coastal transects, and geological interpretation to identify key environmental drivers. Preliminary results reveal that mangroves are predominantly associated with sedimentary and intertidal environments, where salinity, wave energy, temperature, tidal dynamics, and the presence of river estuaries shape their occurrence. In contrast, coral reefs are primarily found in clear-water marine environments characterized by suitable bathymetry, low sediment input, stable sea-surface temperatures, and moderate hydrodynamic conditions. Notably, both mangrove and reef distributions are controlled by the regional geological history: tectonic uplift and Quaternary sea-level fluctuations have controlled the staircase coastal morphology around Sumba Island, which is the main factor influencing reef and mangrove accommodation space. These findings offer critical insights for the conservation, management, and rehabilitation of coastal ecosystems in Indonesia.

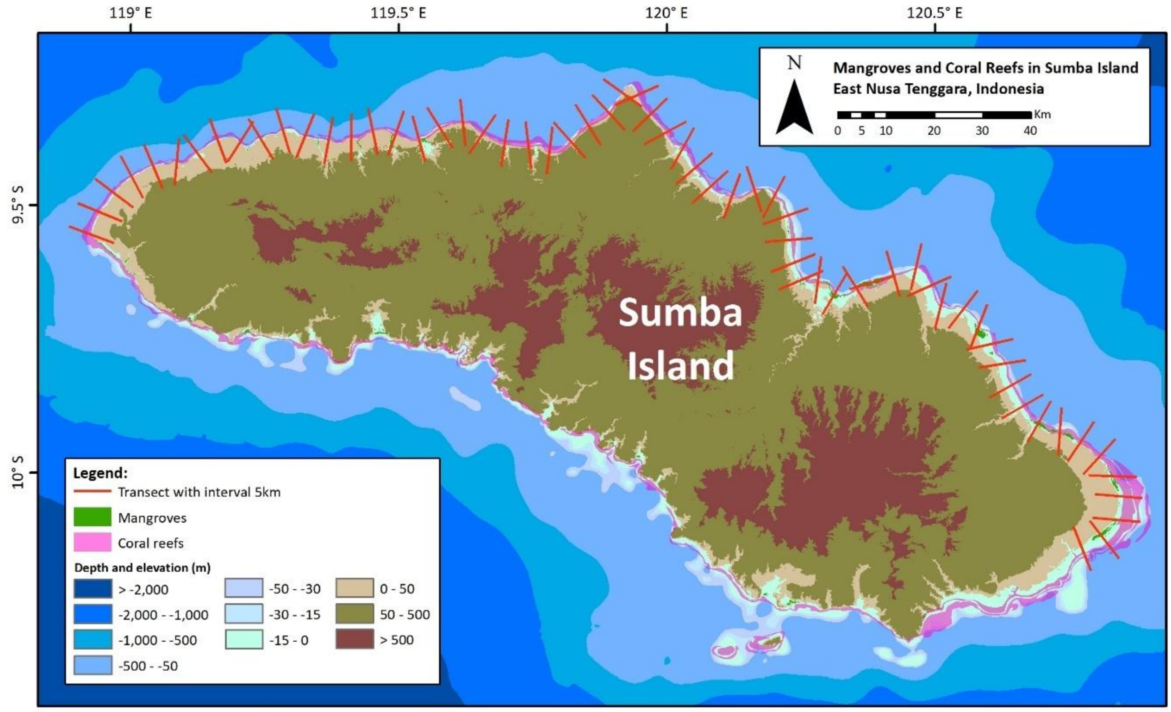

Figure: Mangroves and coral reefs on Sumba Island, East Nusa Tenggara, Indonesia, showing the study area in northern Sumba with a 10 km land-to-sea transect.

Waves and Structures

Valentin Cassayre

Multi-component time-frequency polarization-based full waveform inversion: application on the 3D SEG/EAGE Overthrust model

***Authors**: Valentin Cassayre (ISTerre, Grenoble and ITES, Strasbourg), Romain Brossier (ISTerre, Grenoble), Ludovic Métivier (ISTerre, Grenoble and LJK, Grenoble), and Serge Sambolian (ITES, Strasbourg)*

Physical models of the subsurface can be estimated using information carried by seismic waves propagating through the Earth. These waves are generated by earthquakes and recorded by seismic stations in the context of seismology and generated by artificial sources are recorded by dense arrays of geophones on land or by ocean-bottom nodes on the seafloor in the context of geophysical exploration. For both applications, recording multi-component seismic becomes standard practice.

Full-waveform inversion (FWI) is one of the highest-resolution methods available for estimating subsurface physical properties from seismic data. However, typically only the vertical components are used in the inversion. When not discarded, the different components are usually inverted independently, ignoring the inter-component correlation held by this vectorial recording. Polarization emerges naturally to address this limitation as the relationship between particle motion recorded along different directions.

In this work, we propose a polarization-based objective function adapted for three-component (3C) FWI. The method extends previous two-component method defining the misfit function as a polarization mismatch in the time-frequency domain. To improve robustness, a time-frequency weight based on recorded energy was added to reduce the effect of regularization for low energy signals.

The proposed formulation is evaluated on a realistic three-dimensional synthetic model and compared with conventional inversion strategies. The results illustrate the robustness of the polarization based objective function, and highlight its ability to exploit the additional information contained in multi-component seismic data.

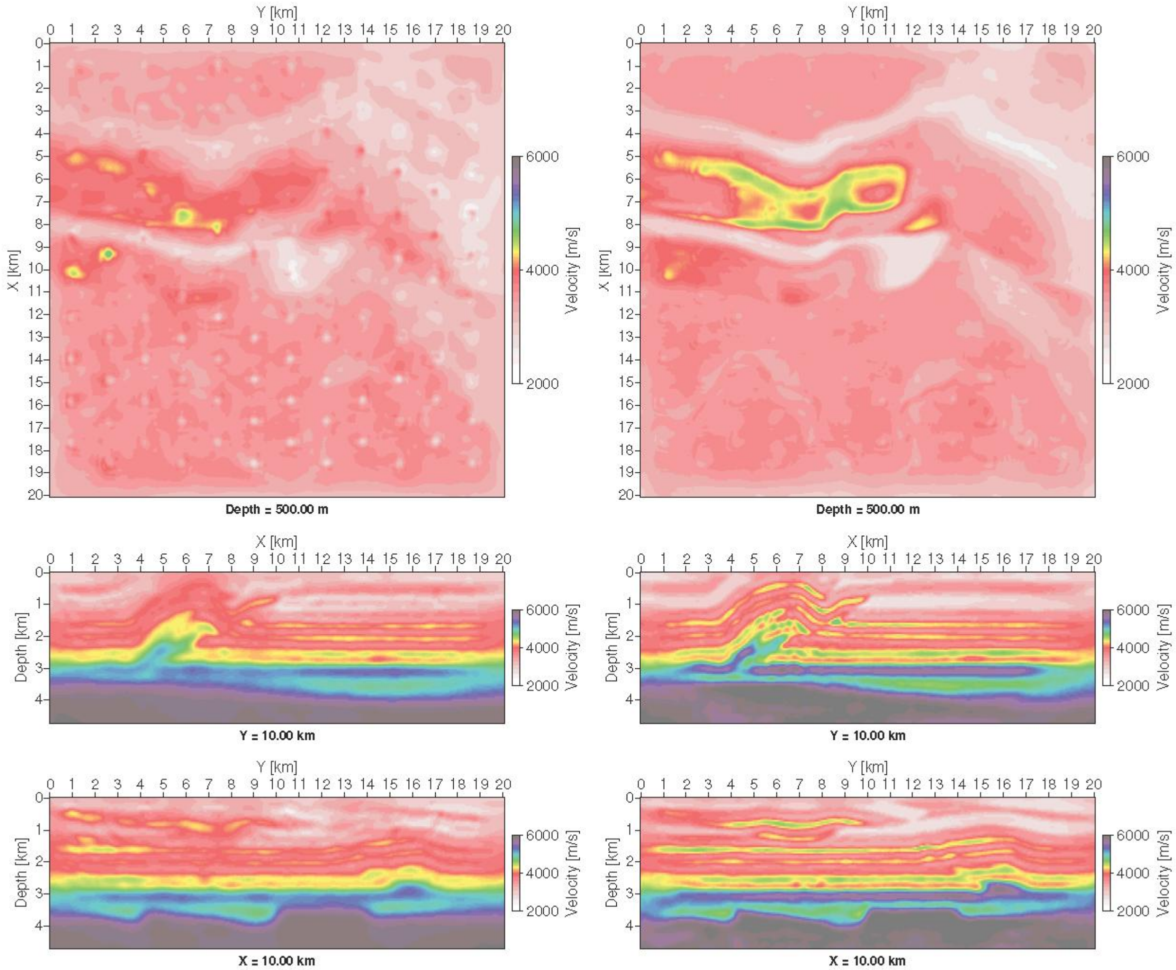

Figure: Final P-wave velocity model obtained through 50 iterations of conventional multi-component L2 FWI (left) and the proposed 3C polarization-based FWI (right). Slices at constant depth (top), Y (middle) and X (bottom). Synthetic dataset generated using an acoustic modeling on the 3D EAGE/SEG Overthrust model (P-wave and density). Initial model is a smoothed version of the true P-wave velocity with a constant density. Only the P-wave velocity was inverted.

Lena Castel

Bayesian inversion of passive seismic data for imaging and site response assessment: application to a dense network of sensors in the Rhône valley, France.

***Authors**: Lena Castel (ASNR, France - ISTerre, France), Laurent Stehly (ISTerre, France), Céline Gélis (ASNR, France), Christine El Khoury (ASNR, France)*

The aim of this thesis is to numerically predict site effects in a sedimentary basin with 1 month of ambient noise recordings.

The study site is located above a well-studied part of the Messinian canyon in the Rhône valley near the Tricastin nuclear power plant (see Fig. 1a). The dataset at our disposal (DARE project) is composed of 1 month of continuous noise recordings from 400 three-component nodes located in a 12 by 10 km grid (blue dots on Fig. 1a). Forty-nine broadband stations were also installed in the area to record earthquake ground motion for about 8 months. They have been used to compute the standard spectral ratio (SSR), empirical measurements used to estimate site effect.

In this work, we use pre-existing ambient noise correlations. Firstly, we will build a probabilistic 3D tomographic velocity model of the area using a Bayesian ambient noise surface wave tomography (ANSWT). In comparison with classical ANSWT, Bayesian ANSWT allows us to better image the main impedance contrasts, e.g., the one between the bedrock and sedimentary units. These impact the wave propagation within the basin and therefore the ground motion amplification. In addition, we evaluate the interface and velocity uncertainties. Secondly, we will model the ground motion in each of the deterministic 3D velocity models (derived from the probabilistic model). These modeled ground motions will then be used to estimate the numerical SSR and its uncertainty, which will later be compared to the empirical measurements, allowing us to discuss the potential and limits of Bayesian ANSWT in geologically complex media.

So far we have computed around 83 000 correlations and the group velocity measurements displayed on Fig. 1b and 1c show a good agreement with the expected geological structures. We are currently in the process to adapt the code to retrieve multiple group velocity measurement per frequency per correlation, those multiple measurements will later be used in the Bayesian ANSWT.

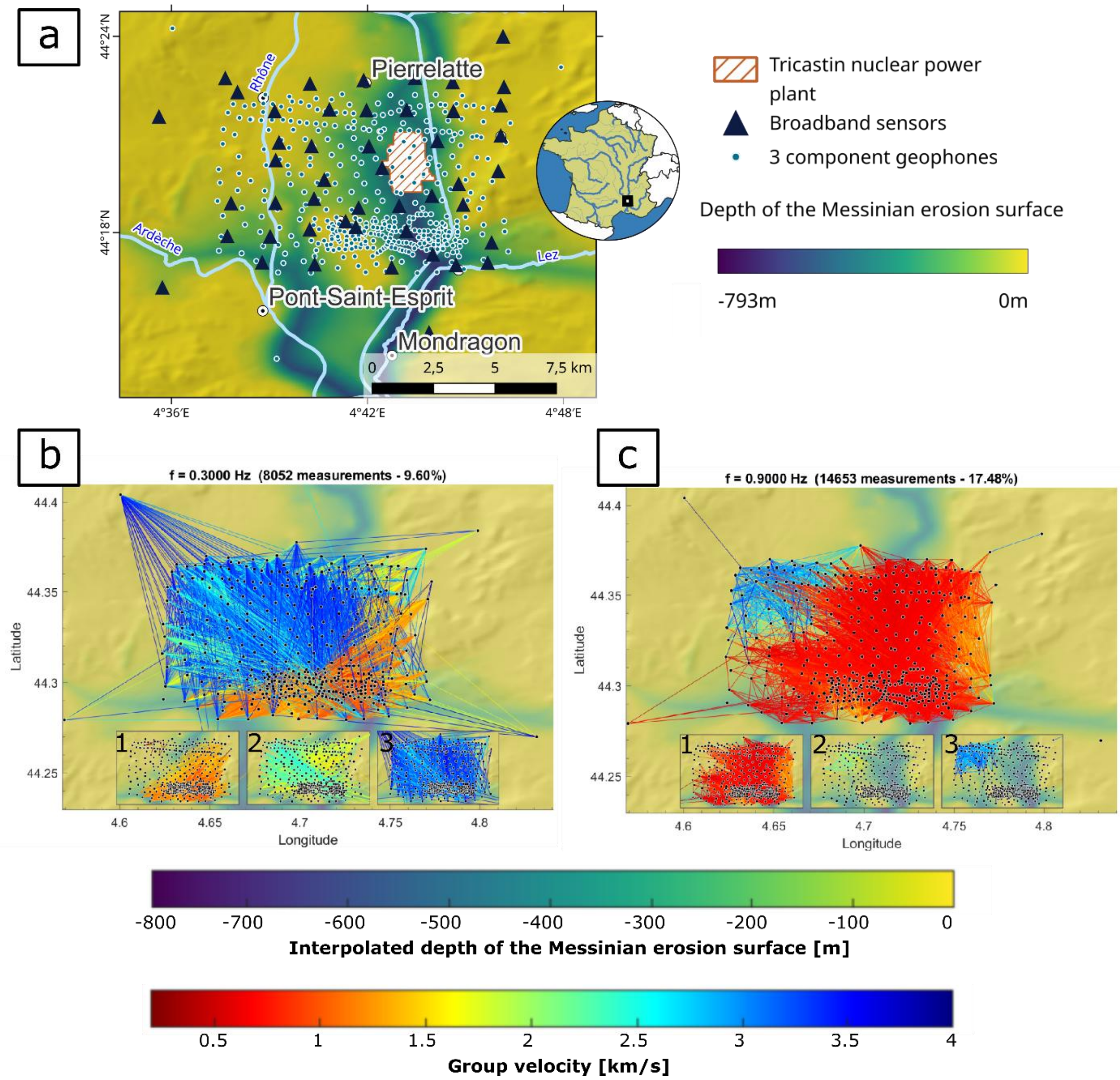

Figure: Figure 1a is the map of the study area with location of the nodes used for the Bayesian ambient noise surface wave tomography (light blue circles). Black triangles represent the broadband stations used to compute the SSR (Lavoué et al., 2024). Sub-figure 1b and 1c are maps of group velocity measurements at different frequency after quality control, for paths selected at 0.3Hz and 0.9Hz, respectively. The insert maps on both Fig. 1b and 1c display selected path in the following group velocity ranges: insert 1 [0 , 1.3[km/s ; insert 2 [1.3 , 2.0[km/s ; insert 3 [2.0 , 4] km/s. The background on all the sub-figures is an interpolation map of the canyon depth is taken from Do Couto et al. (2024).

Marie Gärtner

Unsupervised encoding of seismo-volcanic signals of a full eruptive cycle at Piton de la Fournaise (2014-2023)

***Authors**: Marie A. Gärtner (ISTerre, France), Reza Esfahani (ISTerre, France), Michel Campillo (ISTerre, France), Nikolai Shapiro (ISTerre, France)*

Active volcanoes generate a wide variety of seismic signals that are linked to different physical processes. These seismo-volcanic signals provide valuable insight into the state and dynamics of a volcano's plumbing system. However, their complexity and variability make it challenging to link these signals to underlying physical processes.

Here we present an unsupervised machine learning workflow to extract statistically significant features directly from continuous seismic recordings. Our approach is based on a deep scattering network, a lightweight convolutional neural network with fixed wavelet-based kernels, that provides robust and interpretable representations of complex signals across multiple scales. Since this method does not rely on prior information like catalogs and labels, it enables the exploration of the full complexity of the seismogram and allows for a more comprehensive characterization of volcanic activity.

We apply our methodology to a decade of three-component seismic data (2014 to 2024) recorded at Piton de la Fournaise on La Réunion, France, one of the most active volcanoes in the world. Using data from multiple stations of the permanent network, we analyze the most recent complete eruption cycle and identify distinct patterns in the continuous seismic signal that are associated with different phases of volcanic activity. Furthermore, we are able to detect signal patterns that are not captured by the observatories' routine monitoring (Fig.).

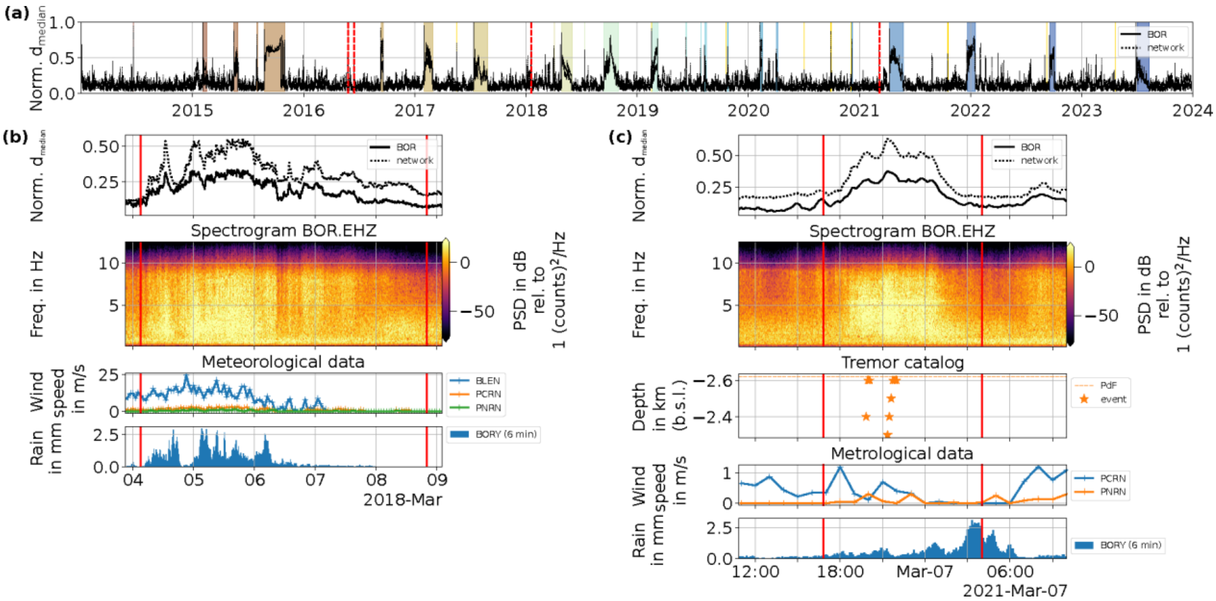

Figure: Example of the distance analysis we applied to the output of the deep scattering network at station BOR and the median of all analysed stations (network). We show the distance to the median (dmedian), defined as the distance of each sample from the median over the analysed time period (a). Local maxima indicate time intervals in which the signal characteristics deviate from ambient noise, which is approximated by the median. b) and c) show two example time windows of signal patterns that were not identified by routine monitoring of the Observatoire Volcanologique du Piton de la Fournaise (OVPF). b) shows a tremor coinciding with a period of heavy rainfall and high wind speeds. c) highlights a local maximum capturing a potential inter-eruptive volcanic tremor.

Mathieu Herbelot

Contribution of Dense Seismic Arrays to the Characterization of Hydrological Dynamics in Karst Systems

***Authors**: Mathieu Herbelot (ISTerre, France), Stéphane Garambois (ISTerre, France), Laurent Stehly (ISTerre, France), Christophe Voisin (ISTerre, France), Aurélie Boura (Hydrosciences Montpellier, France), Véronique Léonardi (Hydrosciences Montpellier, France)*

A significant proportion of the world's water resources is stored in karst regions. To develop water management strategies adapted to karst hydrosystems under conditions of global change, it is essential to account for their specific characteristics, from infiltration zones to discharge points. This requires a better understanding of groundwater recharge, water storage within the karst reservoir, and transfer toward outlets. However, the structural heterogeneity of karst systems poses challenges for imaging and monitoring groundwater flow processes. Among the hydrological and geophysical methods used to study subsurface water dynamics, our project focuses on integrating innovative seismic monitoring techniques with interdisciplinary approaches within a multi-scale framework.

To address these challenges, our study investigates hydrological flows along preferential pathways within a karst environment recharging the Lez aquifer, a critical resource supplying drinking water to approximately 340,000 inhabitants in the Montpellier area.

As part of the PEPR OneWater K3 project, we conducted ambient seismic noise monitoring using a dense array of 100 velocimeters deployed over one month across a 200 m × 1 km area encompassing fault zones and localized karst features. These data are used for both imaging and monitoring, with the latter aimed at producing dynamic maps of seismic velocity variations derived from autocorrelations and cross-correlations between stations. These localized variations are then correlated with rainfall and hydrological observations. We aim to derive the hydrological properties controlling a synthetic model capable of reproducing seismic velocity responses to temperature and rainfall variations, with a spatial resolution highlighting distinct geological compartments. In a second step, the seismic network is used to detect seismic noise generated by fluid transfers, particularly within the most permeable zones.

Furthermore, the deployment of broadband seismic stations over four years is expected to provide insights into the long-term dynamics and seasonal variability of the Lez aquifer at a larger scale.

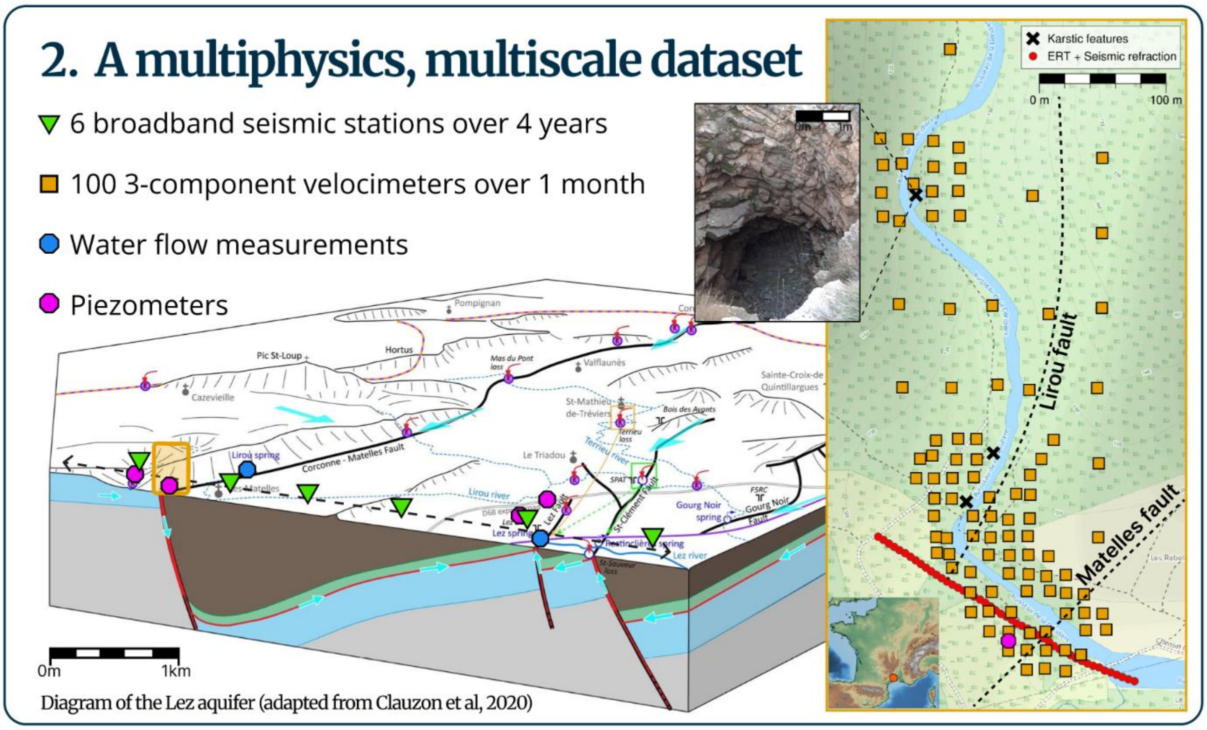

Figure: Multiphysics and Multiscale Investigation of the Hydrological Dynamics of the Lez springs.

Jonas Michael

Deep Learning Seismic Waveforms to Predict Sea Ice Properties

Authors: *Jonas Michael (ISTerre, Grenoble), Ludovic Moreau (ISTerre, Grenoble), Marielle Malfante (CEA, Grenoble)*

Accurate and continuous estimates of sea-ice properties are essential for understanding the dynamics of a warming Arctic.

In this context, seismic methods are promising tools for achieving high temporal and spatial resolution estimates of sea-ice thickness and mechanical parameters. However, current approaches rely on computationally expensive waveform inversions of icequakes, which prevents their application to real-time estimation of ice properties in the field.

To address this limitation, we explore replacing such inversions with convolutional neural networks (CNNs) trained on physically informed synthetic waveforms to infer sea-ice thickness.

The synthetic icequake waveforms are generated by a one-dimensional forward model for flexural waves in floating ice that accounts for ice thickness, mechanical properties, and source–receiver distance. Realistic source spectra are incorporated using a library of field data.

On synthetic waveforms, the networks recover ice thickness and source distance with low error, indicating that the learned relationship between waveform characteristics and physical parameters captures the dominant dispersive physics.

However, when applied directly to field icequake waveforms, the accuracy decreases, reflecting the limitations of using synthetic waveforms alone for training due to idealized model assumptions.

Based on additional tests, we outline strategies to improve CNN performance and robustness when applied to field data.

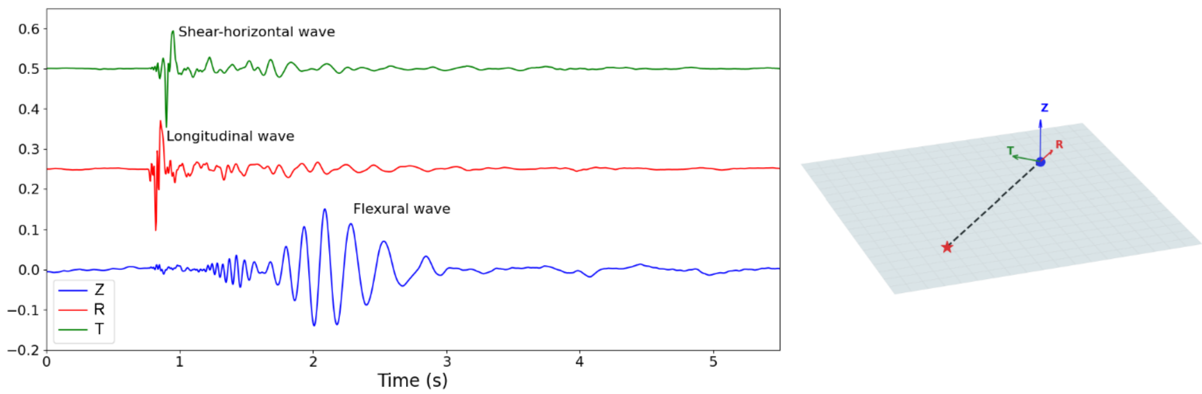

Figure: The different wavetypes (modes) encountered in floating sea ice. Note that the dispersion of the flexural mode may be used to infer ice thickness.

Laurens Oostwegel

Using the urban fabric and morphometrics to analyze the vulnerability of the built environment

***Authors**: Laurens J.N. Oostwegel (GFZ, Germany; ISTerre, France), Danijel Schorlemmer (GFZ, Germany; ETH, Zurich), Philippe Guéguen (ISTerre, France)*

Recently, increasingly detailed building footprint datasets that characterize the built environment are becoming available. The semantic information that is relevant for seismic risk assessment in these datasets is still incomplete. Enriching these datasets with more complete and accurate information increases our understanding of the built environment and reduces uncertainties in seismic risk assessment (Oostwegel et al., 2025).

We explore how the study of urban form can be used to enrich building footprints with properties relevant for seismic risk. Our method is based on the Urban Taxonomy (Fleischmann et al., 2025), a hierarchical framework that characterizes urban fabric through quantifiable metrics (morphometrics) derived from building geometry and street networks. Building plots are approximated by a Voronoi tessellation of building centroids, and building blocks are created by clustering buildings within a street network. Using these three levels of building geometries (single building, building plot, and building block), together with the street network, we compute 144 morphometric attributes. These serve as input features for an extreme gradient boosting algorithm.

Our initial results show that these morphometrics can predict building occupancy type and year of construction with accuracies of 94% and 55% respectively. These results raised the question whether morphometrics can serve as a proxy for vulnerability itself. We use the 2023 Kahramanmaraş earthquake sequence in Turkey as a case study, as post-earthquake damage observations have been recorded that provide ground truth at the building level. This allows us to train and evaluate a model that links urban fabric characteristics directly to observed structural damage.

Vulnerability remains a component of the risk chain that has high uncertainties. Even if we know the exact structural properties of a building, it is difficult to predict the level of damage according to shaking intensities. Mostly, we don’t even know the structural properties. As the building geometries are much more widely available, this method method has the potential to produce high-resolution vulnerability maps from openly available geodata alone.

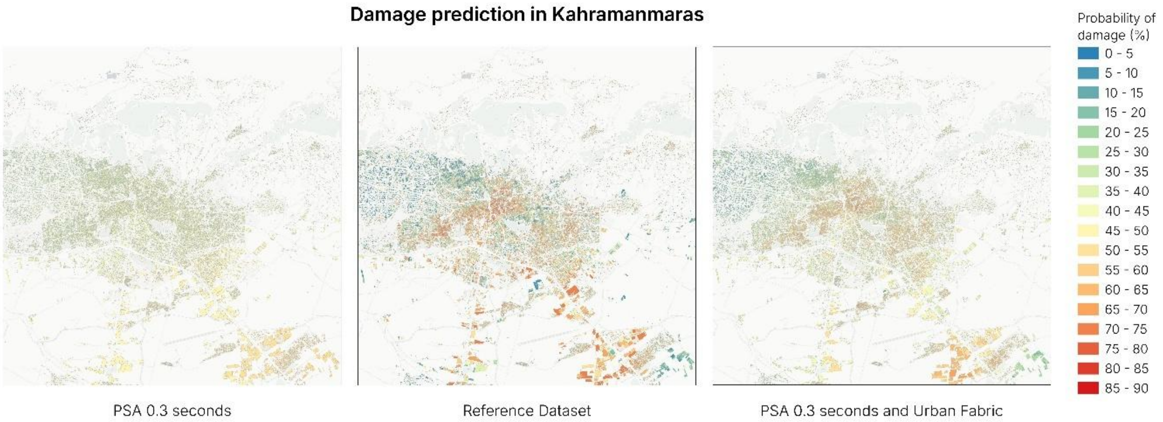

Figure: Prediction of the probability of damage after the Turkey sequence according to only PSA 0.3 (left) or PSA 0.3 and the morphometric attributes (right). The reference dataset is created with inSAR data by Ainscoe et al. (2025).

Piel Pawlowski

Study of the mantle transition zone by combining earthquake data and seismic noise data: application to the Alps and Massif Central

Authors: *P. Pawlowski (ISTerre, France), H. A. Pedersen (ISTerre, France, P. Boué (ISTerre, France, B. Tauzin (Mantle8, France ; LGL-TPE, France) and L. Tomasetto (ISTerre, France)*

Knowledge of the depth and detailed structure of the mantle transition zone's upper and lower boundaries, the so-called 410 km and 660 km discontinuities, enables us to constrain mantle temperatures and composition. At regional scale, P waves reflected on the discontinuities extracted by stacking seismic noise analysis provide additional information to that obtained by receiver functions. Initially (Poli et al., 2012), it was assumed that the waves extracted reflected, albeit in a non perfect wave, the so-called Green's function. We here show how these waves stem from long-range mantle phases which interact in the correlation function to enhance short-range reflections. We here show the impact on different temperature and compositions on the Green's functions and present a methodology on how to model the P wave reflections in a more realistic way, using different noise scenarios and global wave propagation. This opens up the possibility to explore the impact of different compositions and temperature models of the mantle on the P wave reflections, and further constrain their lateral heterogeneity in terms of realistic Earth models.

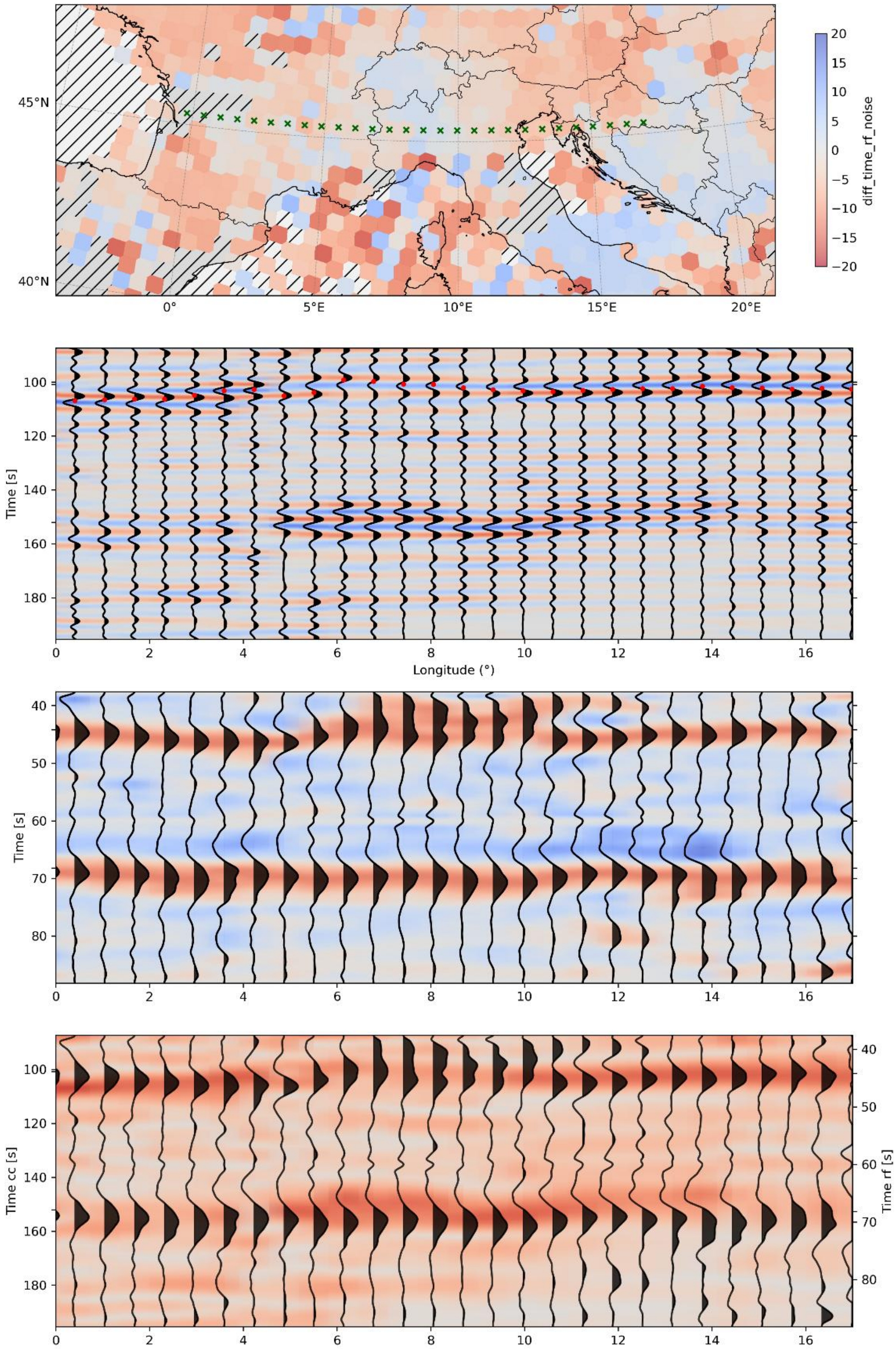

Figure: Observed arrival times of Pv410p in the noise cross-correlations functions. 2nd panel: Cross-correlations functions on the profile showed in first panel in green. 3rd panel: Receiver functions computed on the same profile showed as the concatenation of stack on P410s piercing points rf (~40 to 60s) and P660s piercing points cells rf (~60 to*

90s). 4th panel: Combination of receiver functions (background color) and noise correlations (black lines).

Leon Schreiner

Imaging Seismic Attenuation in Europe with a Multi-Method Approach

***Authors**: Leon Schreiner (ISTerre, France), Helle Pedersen (ISTerre, France), Nikolai Shapiro (ISTerre, France)*

Seismic wave attenuation is a critical parameter for understanding the Earth's crust, its heterogeneity, fluid presence, and tectonic processes. However, reliable 3-D imaging of attenuation remains challenging, as existing methods are often applied to specific depths and structures. This PhD project addresses this challenge by integrating multiple attenuation quantification techniques — quality factor Q from Lg waves, coda waves from seismic noise correlations, and ballistic waves from earthquakes — to develop a unified framework for crustal attenuation imaging in the greater Alpine region. We leverage the improved data coverage in Europe and aim to provide a comprehensive understanding of attenuation, with potential extensions to high-coverage areas.

To resolve attenuation, source and site effects must also be accounted for. While a global joint inversion is an option, it often suffers from trade-offs between the terms. Alternatively, source and site terms can be quantified pre-inversion. We implemented an approach to quantify site response relative to a reference by analysing the late coda wavefield of weak-motion recordings from European crustal earthquakes over the past 20 years. Exploiting the coda's properties (equipartition, isotropy, independence from source/path effects), we measure vertical and horizontal site terms across nine frequency bands (0.7–9.5 Hz) for 3,337 stations, covering both high- and low-seismicity regions. By combining these measurements with geological data and slope, we create continuous site term maps. This scalable and efficient method provides a transferable framework for regional studies and delivers a public database as a resource for the seismological and civil engineering community. After resolving the issue of trade-off between site term and attenuation in an inverse problem, the Lg wave quality factor Q can be constrained.

This work lays the foundation for the PhD's core objective: combining multi-technique approaches quantifying crustal attenuation at different depths and achieving 3-D attenuation imaging in broad and complex tectonic settings.

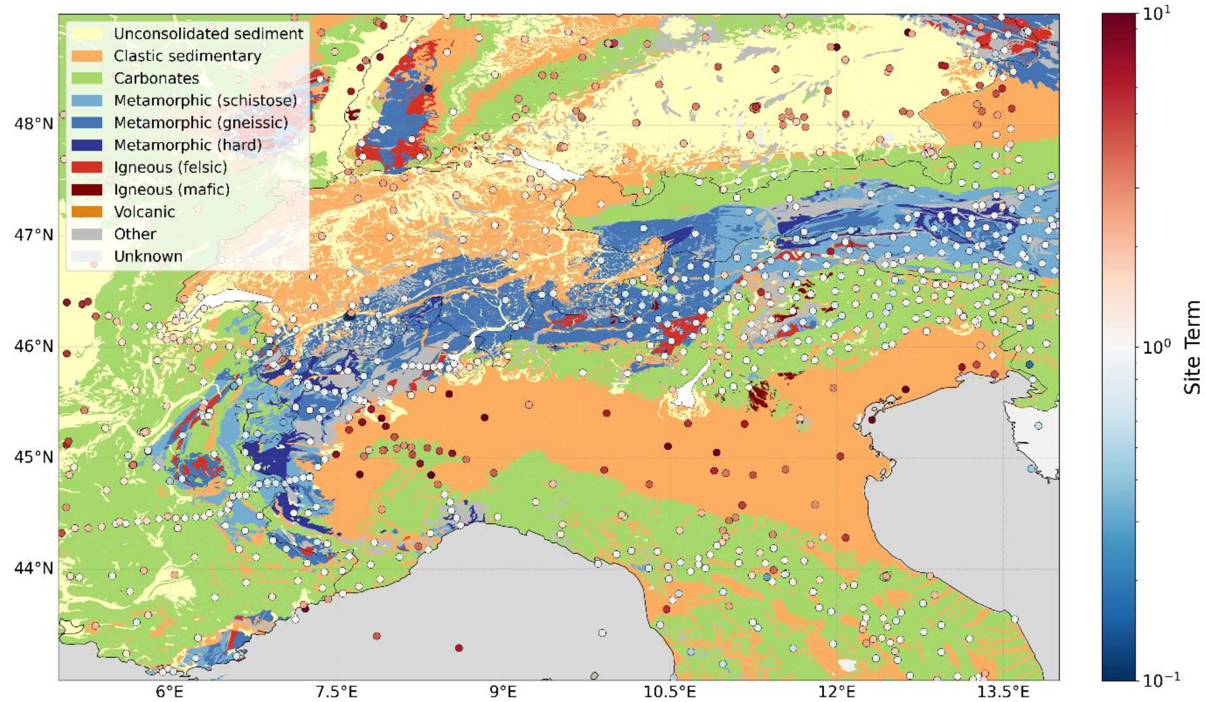

Figure: Site terms estimated from the coda-wave method at seismic stations in the Alpine region (at 1.0 Hz). The background shows surface lithology, which correlates well with the estimated site response: sedimentary basins exhibit strong amplification, whereas bedrock sites show weak or negligible amplification.

Gabin Simonet

Ambient seismic sources and velocity structure inversion from cross-correlation with membrane waves

Authors: *Gabin Simonet (ISTerre, France), Laura Ermert (ISTerre, France), Pierre Boué (ISTerre, France)*

Ambient seismic noise has been widely investigated over the past 20 years, particularly for Earth imaging applications. Several natural and anthropogenic processes induce seismic noise, among these, ocean gravity waves are dominant at specific frequencies. By recording seismic waves travelling along the Earth's surface and computing the cross-correlation between receivers, coherent wave propagation can be extracted. However, since noise sources depend on factors like ocean state, large variations of the ambient wavefield in amplitude, frequency content and directionality are observed both through space and time. It is therefore well known that the surface wavefield does not meet the criterion to retrieve the exact Green's function as the theory of interferometry would suggest.

While this is of major concern for ambient noise tomography, implying careful processing and selection of the data, cross-correlations can also help us describe the noise sources themselves. Several studies have investigated source imaging, and in the recent years ambient noise full waveform inversion has emerged. It aims to find both the best source model and Earth structure that would fit the observed cross-correlations. However, the computational cost of modelling seismic wave propagation increases exponentially with frequency, currently limiting applications to long periods.

In this project, we aim to model both Rayleigh and Love wave cross-correlations with the membrane wave assumption. Because the observed cross-correlations are dominated by surface waves propagating in two dimensions, full 3D Earth modelling is often unnecessary. A 2D sphere approximation, referred to as membrane, is sufficient to simulate cross-correlations while substantially reducing computational cost. To begin with, we aim to map seismic ambient sources at long period with a global-scale network. Then, we will model surface wave velocity in Europe using the Adria Array, a temporary network covering the Adriatic plate and its active margins in the central Mediterranean.

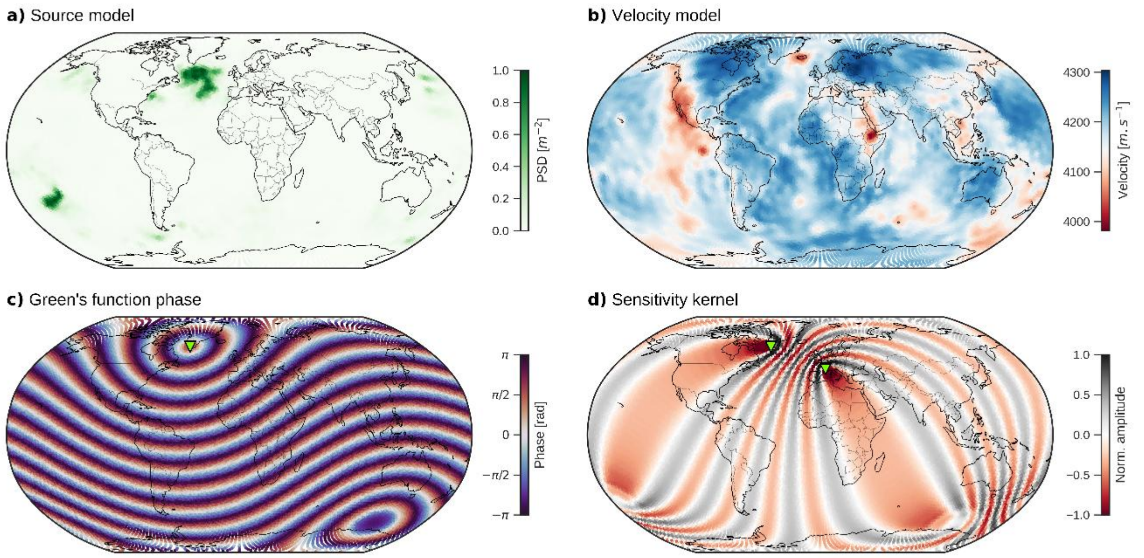

Figure: Example of synthetic cross-correlation maps between station G.SSB and G.IVI at 300s of period. a) Realistic seismic source model obtains from remote sea state observations. b) Rayleigh wave velocity computed from the global 3D velocity model S40RTS. c) Phase of the synthetic Green's function for station G.IVI at 300s of period. d) Source sensitivity kernel for a given amplitude measurement.

Margot Vignon-Livache

Multi-scale noise-based seismic imaging of the French Massif Central using data from the MACIV experiment

***Authors**: Margot Vignon-Livache (ISTerre, France), Nikolai Shapiro (ISTerre, France), Laurent Stehly (ISTerre, France), Anne Paul (ISTerre, France), Aurélien (Geological Survey of Denmark and Greenland, Geophysics and Sedimentary Basins Department, Denmark)*

Recording nearly 600 Myr of geological history from the end of the Proterozoic to the present day, the French Massif Central (FMC) is the largest area of exposed Variscan basement in Western Europe and provides key insights into continental crustal growth during the Proterozoic–Phanerozoic transition and the Variscan orogeny.

The FMC volcanic provinces, influenced by the European Variscan Belt and the European Cenozoic Rift System (ECRIS), represent a major example of European intraplate volcanism. The origin of the ECRIS remains debated: it may solely result from Alpine subduction or involve small-scale upper-mantle plumes. However, understanding the geology, tectonics, and volcanism of the FMC is still limited by the lack of accurate information on crustal and lithospheric structures.

Within the framework of the ANR MACIV project, the ISTerre, GET-IRAP, and LMV laboratories deployed seismic networks to cover the entire FMC, including 35 backbone stations, 65 broadband stations along three transects, and a dense array of 625 nodes installed for one month in the Chaîne des Puys and Cézallier–Monts-Dore volcanic regions in October 2025.

My PhD aims to build new high-resolution seismic models of the crust and lithosphere using ambient-noise seismic tomography. The primary goal is to better understand intraplate volcanism and the influence of pre-existing Variscan structures on the evolution of magmatic provinces. A further objective is to assess the volcanic hazards, and to provide structural information relevant for exploration of geothermal, water, and mineral resources.

Interstation cross-correlations were computed to retrieve Rayleigh and Love waves and measure phase and group velocity dispersion curves. These measurements are now used in 2D surface-wave tomography to construct velocity maps. Future work will involve depth inversion to derive 3D structural models of shear-wave velocity and radial and azimuthal anisotropies. Surface-wave-based methods will also be applied to the large-N arrays to probe the magmatic plumbing system and the level of activity beneath the FMC volcanoes.

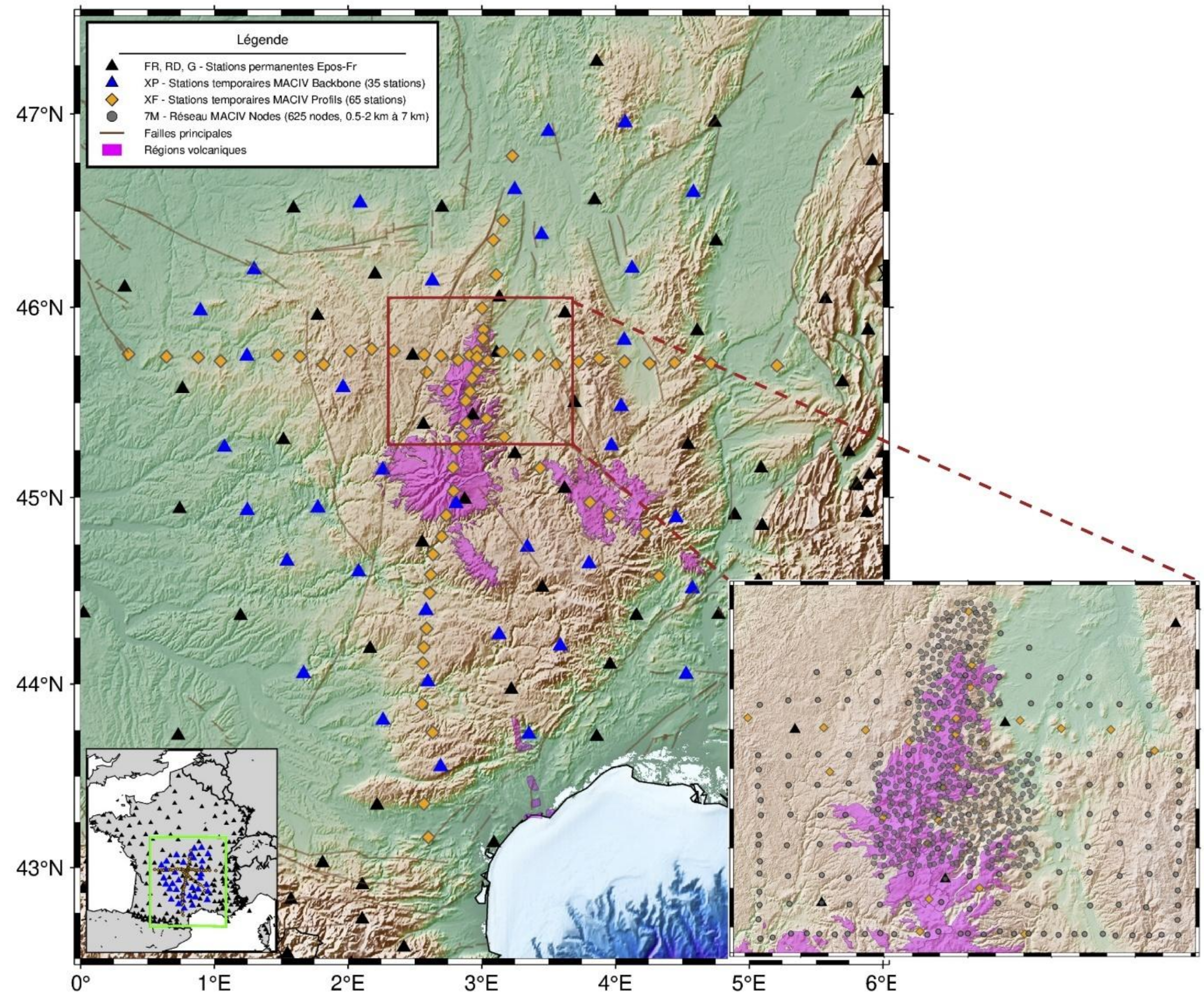

Figure: Map of the MACIV networks (C. Aubert).

IPhDC

2026

ISTerre PhD Congress